UNDERSTANDING THE MECHANISMS OF BLUE LIGHT IRRADIATION-INDUCED GROWTH REDUCTION OF PATHOGENIC *E. COLI*

By

Courtney A. Mitchell

Dissertation
Submitted to the Faculty of the
Graduate School of Vanderbilt University
in partial fulfillment of the requirements
for the degree of

DOCTOR OF PHILOSOPHY
in

Chemical Engineering
August 2016
Nashville, Tennessee

APPROVED BY:

Bridget Rogers, Ph.D. (chair)

Maria Hadjifrangiskou, Ph.D.

Scott Guelcher, Ph.D.

Matthew Lang, Ph.D.

TABLE OF CONTENTS

Page

DEDICATION iii

ACKNOWLEDGEMENTS iv

LIST OF EQUATIONS vii

LIST OF FIGURES viii

LIST OF SCHEMES x

LIST OF TABLES xi

Chapter

1. BLUE LIGHT IRRADIATON BACKGROUND AND INTRODUCTION 1
   - Background 1
   - Significance 4
   - Research plan 11
   - Research design 20

2. MATERIALS AND METHODS 23
   - Bacterial strains and culture conditions 23
   - Growth curves 23
   - *In vitro* light delivery to *E. coli* 24
   - Calculations for delivering wavelength, energy dose, and energy flux 25
   - Reduction determination 27
   - Viability assay 29
   - Persister assays 31
   - Biofilm assay 31
   - Motility assay 32
   - RNA extraction and qPCR 32
   - Singlet oxygen generation 36

3. BLUE LIGHT IRRADIATION INDUCES A VIABLE, PERSISTER-CELL LIKE STATE IN *ESCHERICHIA COLI* 38
   - Abstract 38
   - Introduction 39
   - Materials and methods 42
   - Results 46
   - Discussion 55

4. THE BLUE LIGHT SENSOR USING FLAVIN ADENINE DINUCLEOTIDE IS NEEDED TO REDUCE THE GROWTH OF UROPATHOGENIC *ESCHERICHIA COLI* AT 455 nm... 59
Abstract....59
Introduction 60
Materials and methods....63
Results 66
Discussion 72

5. DETERMINING THE ENERGY THRESHOLD FOR EFFECTIVE BLUE LIGHT IRRADIATION-INDUCED CYTOXICITY OF UROPATHOGENIC *ESCHERICHIA COLI* 75
Abstract....75
Introduction 76
Materials and methods....77
Results 79
Discussion....86

6. KINETIC ANALYSIS OF PHOTOSENSITIZER EXCITATION AND SINGLET OXYGEN FORMATION....90
Introduction 90
Mechanisms of BLI....90
Potential endogenous photosensitizers 91
Formation of singlet oxygen 92
Detection of singlet oxygen 93
Detection of singlet oxygen by Singlet Oxygen Sensor Green....94
Model....95
Jablonski diagram 96
Excited photosensitizers are likely absorbing multiple photons....100
Conclusion....103

7. CONCLUSIONS, WORKING MODEL, AND BROADER IMPACT 104

Conclusions 104
Working model for BLI reductions 107
Broader implications 108

REFERENCES 111

This work is dedicated to my grandparents, Curtis Mitchell, Sr. (1932-2013) and Vernice Mitchell (1936-2015), and my dear friend, Latasha DuBois (1989-2014). May you all rest in complete peace. Thank you all for watching over me during this process.

ACKNOWLEDGEMENTS

This journey to the Ph.D. has brought many challenges and learning experiences, but has more importantly given me the opportunity to meet, befriend, and collaborate with some amazing people. Without them, this work could not have been possible.

> We must never forget our teachers, our lecturers and our mentors. In their individual capacities have contributed to our academic, professional and personal development.
>
> —Lailah Gifty Akita

First, I would like to thank my mentor, Dr. Bridget Rogers for allowing me to work in her lab, even though my research interests were divergent from those of her lab. Bridget has provided amazing support, technical expertise, and helped guide my curiosity and passions for over four years. My co-mentor, Dr. Maria Hadjifrangiskou has provided unparalleled scientific support and expertise and welcomed me into her lab during my third year of graduate school. I am extremely grateful for the training and continuous support. Thank you to Dr. Jennifer Powers for contacting Bridget "by chance" and for connecting the two of us with Maria; you were pivotal in moving this work forward. Dr. Matthew Lang and Dr. Scott Guelcher, thank you both for serving on my Dissertation Committee and for providing me with great wisdom, feedback, and for guiding my ambitious goals.

To my collaborators, Dr. D. Greg Walker and Dr. Sarah Gollub, thank you for your insight and direction as a fresh-faced graduate student. You taught me to take advice early on.

Over the years, I have had amazing mentors. I am thankful they still guide and inspire me to this day. Thank you to David Mitnick and his wife, Doris for pouring into me since high school. One of the great advantages of attending an HBCU is that everybody you come in contact with has the potential to become an academic, professional or personal mentor. I am grateful to have all three in Dr. Ates Akyurtlu, Dr. Jale Akyurtlu, Dr. Morris Morgan, and Dr. Eric Sheppard. Thank you all for motivating me and pushing me past my comfort zone. You have provided me with amazing experiences, most of which are still impacting me. While my graduate school experience was not as nurturing as my undergraduate experience, I am thankful for the mentorship I have received from Dr. Don Brunson, Dr. Ruth Schemmer, and Burgess Mitchell. Dean Brunson, thank you for recruiting me and for always having an open door. Dean Schemmer, thank you for the invaluable career advice and trainings you provided me. Dean Mitchell, thank you for the opportunities you have given me to work with undergraduate students through mentoring and teaching and for always having an open door. I am also extremely grateful for the staff at the Bishop Joseph Johnson Black Cultural Center: Dr. Frank Dobson, Jeff King, and Jacqueline Grant. Thank you all for your encouragement and for the programming provided by the BCC.

> You can't change the world alone - you will need some help - and to truly get from your starting point to your destination takes friends, colleagues, the good will of strangers and a strong coxswain to guide them.
>
> —William H. McRaven

To the former lab members of the Rogers Lab: Dr. Bobby Harl, Marc Panu, and Dr. Ben Schmidt, thank you for your assistance and guidance and for being an ear during frustrating times in lab. Coming in to this work, I had minimal biology knowledge. Without the help, training, and expertise of the Hadjifrangiskou lab, this work would have not gone as far as it did. Thank you to Dr. John Brannon, Erin Breland, Spencer Colling, Allison Eberly, Kyle Floyd, Kirsten Guckes, Dr. Carrie Shaffer, Bradley Steiner, Himesh Zaver, and Ellisa Zhang for feedback and for not laughing at my simple questions; I have learned a lot from you. A lot of times undergraduate students are overlooked, but I am extremely appreciative to Rebecca Ebbott and Taryn Dunigan for their assistance with performing experiments for this work.

I am thankful for the ups and downs I have shared with the Chemical and Biomolecular Engineering incoming class of 2011. We have laughed together, cried together, studied together, and partied together, so thank you all for sharing this journey. Congratulations to those who have finished and for the remaining, you are so close to the end (I promise there is light at the end of the tunnel)! Thanks Dr. Dushyant Barpaga, Jana Black, Sonia Brady, Dr. Jessica Haley, Harris Manning, Tim Moore, Ethan Self, and Dr. Faizan Zubair.

Thank you to the amazing support staff whom are often overlooked, but make everything run smoothly. A special thanks to Michele Cedzich, Mary Gilleran, Sheri Kimble, Rae Uson. You all have made my days more pleasant with your smiles. Michele, you have made this journey so much better; thanks for being not only a great recruiter and travel partner, but also a great friend. I would also like to thank the housekeeping staff who checked up on me to ensure I was safe and fed during late nights in lab: Terrence, Ms. Gerdine, Rudy, Markele, and Mr. Nathan; you all are gems.

> "For I know the plans I have for you," says the Lord. "They are plans for good and not for disaster, to give you a future and a hope."
>
> —Jeremiah 29:11 NLT

Most importantly, I extend my extreme gratitude to My Creator. Thank you for this journey and for seeing me through and for the constant reminder that "the best is yet to come." This scripture encouraged me through this journey, especially when I wanted to give up. I am thankful for the people who continued to speak this scripture over my life. Thank you to my church family, Bethel World Outreach Church: Pastor James and Debbie Lowe, Bishop Rice and Jody Broocks, and the entire pastoral staff; to my direct leaders, Pastor Steve and Cindy Hollander; to the members (past and present) of the Engage Ministry Team; and to the MISFITS small group. You all encouraged me through your words and your prayers. A special thank you to The Mount church family under the leadership of Bishop Kim W. Brown and Elder Valerie K. Brown for continuing to cover me in thoughts and prayers while I was in Nashville. Thank you to my amazing prayer partners and sisters: Valerie Fomengia, Ashli McLean, Mama Kris McLean, Lorreann Moore, Amanda Paul, Rebekah Sharpe, Chatiqua Vaughn and Maxine Woodhouse. Thank you for going to war with me and on my behalf.

I have been blessed with some amazing friends who did not allow the ups and downs of this journey to negatively affect our friendship. Thank you to my friend of almost 20 years, DeQuan Smith; you are an amazing person inside and out and I am extremely blessed to have shared

these 19 years of friendship with you. Thank you to my lifelong friends: Andrea Taylor and Andria Chambers. Thank you to my friends since high school: Patrina Allen, Oscar Bazemore, Latasha DuBois, Janelle Hinton, Josh Lee, and Channel Vialet. Thank you to my friends from Hampton who walked the same journey with me and who served as a source of encouragement through this process: Rhonda Jack, Dr. Justin Morrissette McAlman, and Dr. Nellone Reid. Thank you to my OBGAPS friends for serving as an outlet from research. Thank you to Dr. Ami Agbabli and Dr. Ayeetin Azah for your consistency in friendship and prayers during my "home stretch." A special thank you to my best friend, partner-in-crime, and the world's greatest boyfriend, Chike Abana; you truly push me to be the best I can be. I would also like to thank our close friends, Dr. Valentine and Kenechi Chukwuma.

It takes a village to raise a child.
—African proverb

I extend a huge thank you to my village. These people include my immediate family, extended family, and my surrogate family. I would like to thank my maternal grandparents, Henry and Malissia Lee and my paternal grandparents, Curtis and Vernice Mitchell; my aunt Jennifer; my uncle Tamal; all of my great aunts and uncles; and my cousins. A special thanks to the constant motivation and encouragement of my cousins Keisha Graves, Isaiah Moore, Dr. Jevie O'Neill, and Chris Sivels. I want to extend a special thank you to my surrogate parents: Andy and Kris McLean, Loretta Ritenour, and Terry Wilson.

I am forever grateful and indebted to my immediate family: daddy; mommy; my siblings Kelly, Cayla and DJ, Kiara, and John; and my beautiful nieces Jayda, Payton, and Layla. Thank you all for your unwavering love and support. Thank you for being a shoulder to cry on. Thank you for the constant encouragement. Thank you for speaking life over me when I wanted to give up. You all are the reason I did this and continue to push forward. I love you all from the bottom of my heart and am thankful God blessed me with each and every one of you.

Research is not possible without funding. I would like to thank my funding sources: the National Defense Science and Engineering Graduate (NDSEG) Fellowship (grant 32 CFR 168a) awarded by the DoD and funded by the Air Force Office of Scientific Research; support from the Department of Education's Graduate Assistance in Areas of National Need (GAANN) Fellowship (grant P200A090323); and The National GEM Consortium Fellowship. Funding for this work was also provided by Vanderbilt University School of Engineering from Dr. Bridget Rogers and academic professional development funds to Maria Hadjifrangiskou.

Thank YOU for taking the time to read some or my entire dissertation.

LIST OF EQUATIONS

Equation **Page**

2.1. Irradiation time....26

2.2. Percent reduction in CFUs....27

2.3. Percent change in CFUs....27

2.4. Percent of cells killed....30

5.4. Energy per photon....81

6.1. Quantum yield of triplet state....99

6.2. Number of photons needed to interact with one electron....101

6.3. Total energy absorbed....102

6.4. Internal conversion leading to fluorescence and the energy decay by fluorescence....103

6.5. Internal conversion leading to the intersystem crossing, the intersystem crossing, and the vibrational relaxation/internal conversion leading to the lowest triplet electronic state....103

LIST OF FIGURES

Figure **Page**

1.1. Proposed mechanism of BLI....5

1.2. Schematic of bacterial electron transport chain and synthesis cascade of porphyrins and porphyrin enzymes....7

1.3. Growth curves of three different strains of *E. coli*....9

1.4. Percent reduction in CFUs for strains post-120 J/cm^2, 455 nm BLI....9

1.5. Percent reduction in CFUs for UTI89 and energy-deficient isogenic mutants, UTI89Δ*qseC*, and UTI89Δ*ubiI*....11

2.1. Viewing angles for LED lamps....24

2.2. Experimental flow for BLI experiments....25

2.3. Manufacturer's light parameters....26

2.4. Light source calibration curve....29

2.5. Workflow for ATP assay....30

3.1. Photosensitizers play a major role in the response to visible light exposure....31

3.2. Growth rate heterogeneity exists between *E. coli* strains....46

3.3. CFU reduction of different *E. coli* strains in response to BLI_{455} at different growth phases....47

3.4. Effects of BLI on preventing pre-formed biofilms....48

3.5. Percent reduction differences between CFUs on agar plate assay and glass slide assay....49

3.6. BLI_{455} is not completely bactericidal against *E. coli*....50

3.7. UTI89Δ*ubiI* contains more persister cells in stationary phase and exhibits higher tolerance to BLI....53

3.8. qPCR steady-state transcript levels of heme biosynthesis genes in UTI89, EC958, and UTI89Δ*ubiI*....54

4.1. Tolerance to BLI by mutants lacking blue light sensor is not due to defects caused by mutation 68

4.2. Percent reduction in CFUs at 420 nm and 470 nm 69

4.3. Viability of cells post-BLI 71

5.1. Percent reductions in CFUs at varying wavelengths, energy doses, and growth phases.....80

5.2. Percent reductions in CFUs of strain UTI89 at varying wavelengths, energy fluxes, and growth phases.....85

5.3. Percent reduction in CFUs of strain UTI89 at 420 nm, 240 J/cm^2 86

6.1. Red-shift of emission wavelength as a result of a red-shift in excitation wavelength.....93

6.2. Chemical structure of hypericin.....96

6.3. Jablonski diagram 97

6.4. Representation of spin multiplicities for electrons in singlet and triplet states 99

6.5. Jablonski diagram for the multi-photon interaction with a ground-state photosensitizer and subsequent singlet oxygen formation.....103

7.1. Working model for BLI-induced reductions in *E. coli* 108

LIST OF SCHEMES

Scheme **Page**

6.1. Type 1 (I) Reaction 94

6.2. Type 2 (II) Reaction 94

6.3. Formation of singlet oxygen from hypericin 96

LIST OF TABLES

Table **Page**

1.1. Aim 2. Variable parameters by study 20

2.1. Light source calibration 28

CHAPTER 1

BLUE LIGHT IRRADIATON BACKGROUND AND INTRODUCTION

BACKGROUND

Photodynamic therapy has been used to treat a range of conditions, including jaundice in neonates and bacterial infections [1-10]. The application of blue light as an antimicrobial strategy, especially in the wake of increasing antibiotic resistance, is appealing. However, previous studies elucidated differences on the responses of bacteria to irradiation with blue light (or blue light irradiation-BLI), ranging from a decrease in growth for some species, to stimulating proliferation in others [2, 11-15]. Studies evaluating the phototoxic effect of blue light on bacteria revealed that bacterial porphyrins, which are endogenous photosensitizers absorbing blue light, lead to the formation of reactive oxygen species (ROS) [2, 14, 16]. In turn, these ROS have a cytotoxic effect. Conversely, significant literature documents the ability of bacteria to sense and respond to blue light, via the use of BLUF (sensor of blue light using FAD) domain-containing proteins [17-33]. No studies to date have characterized the extent of photo-toxicity at different growth phases of the bacterial lifecycle of a single bacterial species. **The hypothesis for this work was that the growth phase of a given bacteria will influence its susceptibility to BLI.** To test this hypothesis, we:

Aim 1: Defined the longitudinal response of *E. coli* to 455 nm blue light irradiation (BLI).

The bactericidal effect of BLI at 455 nm (BLI_{455}) on a range of non-pathogenic to intestinal and uropathogenic *E. coli* isolates was evaluated. Assessment of bacterial viability post 120 J/cm^2 (total dose) BLI_{455} revealed that while significant reduction in colony forming units (CFUs) was

observed at all phases of growth and with all strains, growth was not completely inhibited. Subsequent analysis of a series of isogenic mutants revealed that mutants with a lower proton motive force exhibited higher tolerance to BLI. Based on these observations, **it was hypothesized that porphyrins associated with the *E. coli* electron transport chain are a target of BLI and that growth phase-dependent variability is a function of differential expression of genes encoding for porphyrin and porphyrin-containing enzymes.** To test this hypothesis it was:

(i) Determined whether electron transport chain components and other porphyrin-containing *E. coli* factors have growth-phase dependent changes in expression that may contribute to the altered susceptibility of *E. coli* to BLI, and

(ii) Determined the contribution of the BLUF domain-containing sensor, UTI89_C1346, in response to BLI. To accomplish this quantitative real-time polymerase chain reaction assays (qPCR) were performed to understand target key players in the cytotoxic cascade, BLUF signaling genes were mutagenized, an ATP release assay was used to determine if the photo-toxicity was lethal, and suppressor screens were completed to identify point mutations.

Together, these studies helped elucidate the mechanism and extent of BLI-induced cytotoxicity of *E. coli*.

Aim 2: Quantified the effects of exposure properties on *E. coli* growth.

At higher radiant exposures, blue light exhibits a broad-spectrum antimicrobial effect against both Gram (+) and Gram (-) bacteria. It has been shown that the higher the dose, the higher the cytotoxic effect, while at lower doses proliferation of bacterial growth has been observed [2, 11-15]. There is also a dependency on wavelength, in which shorter wavelengths are more effective

in killing bacteria [2, 12, 15, 34], as can be seen with UV inactivation. While studies have shown that there is a wavelength and dose dependency on cytotoxicity, there have been no studies that look at varying the rate of energy delivery or varying growth phases. **The resulting hypothesis was that 1) under similar exposure conditions, the relative reduction in post-exposure growth of *E. coli* irradiated during the exponential phase will be greater than that of *E. coli* irradiated during the stationary growth phase and 2) as compared to WT, proton motive force-deficient mutants will be less susceptible to the effects of the BLI parameters, until energy thresholds are overcome.** To test this hypothesis, a determination of photo-toxicity was made as a function of:

(i) Wavelength,

(ii) Total energy dose delivered, and

(iii) Energy flux.

These determinations were accomplished by exposing bacteria in exponential, transition, and stationary growth phases at different wavelengths; varying the total dose delivered; and changing the intensity/time of light delivered to modulate the energy flux (rate of energy delivery per area). Completing these studies helped determine if reduction of *E. coli* growth after BLI was more dependent on total energy delivered or the rate of energy delivery. This understanding provided insight into absorption and energy barriers. Both are critical in understanding the phototoxic mechanism.

Combined these studies provided further understanding of the mechanism of BLI-induced photo-toxicity on *E. coli* and provided direction to extend studies to other bacterial species.

SIGNIFICANCE

There is a significant need to combat antibiotic resistance.

A major research effort has been led to find alternative antimicrobial approaches to which, it is hypothesized, bacteria will not be easily able to develop resistance [2]. Antimicrobial resistance is becoming a factor in virtually all hospital-acquired infections and physicians are concerned that several bacterial infections soon may be untreatable [35]. The application of blue light as an antimicrobial strategy, especially in the wake of increasing antibiotic resistance, is appealing.

Blue light as an antimicrobial strategy, in the wake of increasing resistance, is appealing.

Photodynamic therapy employs visible light and has been used to treat photo-aged facial skin [36-39], acne [36-39], jaundice in neonates [40] and clinical bacterial infections [36, 37]. This has been successfully accomplished both through the use of exogenous photosensitizers, such as dyes, i.e. methylene blue [15, 41-44] and with endogenous bacterial photosensitizers present as porphyrins, flavins, cytochromes, NADH, etc. [2, 42, 43, 45]. Blue light (in the 400-500 nm range) irradiation (BLI) is attracting increasing attention due to its intrinsic antimicrobial effect without the addition of exogenous photosensitizers [2]. Several types of light sources, including fluorescence, halogen, xenon, and tungsten lamps and recently lasers, are accepted by hospitals as routine treatment methods or undergoing clinical trials [38]. However, LEDs are a strong alternative as light sources because they retain low energy consumption, improved robustness, small size, and relatively low price compared to other lasers or lamps [5].

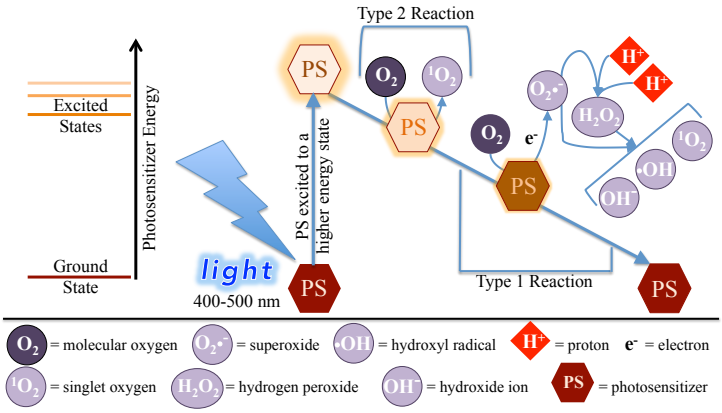

Figure 1.1. **Proposed mechanism of BLI.** Photosensitizers are excited upon light absorption and electrons are released to form ROS.

ROS is released after absorption of blue light by porphyrins.

It is a commonly accepted hypothesis that the phototoxic effect of BLI on bacteria, involves porphyrins, which are endogenous photosensitizers absorbing blue light, and lead to the formation of reactive oxygen species (ROS) [36-39]. In turn, these ROS, notably singlet oxygen, have a cytotoxic effect by reacting with organic compounds, which could range from protein to DNA damage [2, 39, 40, 42, 43, 45-55]. Lipovsky et al. suggest that after absorption of light, excited cytochromes (porphyrin-containing) cause electron transfer to molecular oxygen, which generates singlet oxygen [11]. Absorption of light by photosensitizers switches the molecules to an excited state [56, 57] as illustrated in **Figure 1.1**. As illustrated, the excited photosensitizer is relaxed to its ground state by a Type 1 or Type 2 reaction, depending on the energy level of the excited state. In a Type 1 reaction an excited photosensitizer reacts with ground-state molecular oxygen to produce different ROS in a multi-step reaction, ultimately leading to the formation of singlet oxygen, $^1O_2$; in a Type 2 reaction singlet oxygen is created directly [11, 13]. The type of ROS that is created is dependent on the availability of protons (H^+), oxygen (oxygen's state matters), and the energy level of the excited photosensitizer. Different ROS can be produced by the following Type 2 reactions.

$$O_2 + e^- \rightarrow O_2^{\cdot -} \qquad \textbf{Reaction 1.1}$$

$$2O_2^{\cdot -} + 2H^+ \rightarrow H_2O_2 + O_2 \qquad \textbf{Reaction 1.2}$$

$$2O_2^{\cdot -} + H_2O_2 \rightarrow OH^- + {\cdot}OH + {}^1O_2 \qquad \textbf{Reaction 1.3}$$

It must be noted that ROS are generated as a natural byproduct of the oxygen metabolism [54]. In fact, they are constantly produced and eliminated under normal physiologic conditions and have important functions in cell signaling, homeostasis, and clearance of microbial infections [54]. However, during times of environmental stress, such as intense BLI, ROS levels can increase dramatically leading to oxidative stress; oxidative stress can result in damage to cellular proteins, lipids, and DNA [11, 12, 50, 54, 58]. Alone, the products of **Reaction 1.1** and **Reaction 1.2** are not detrimental to the cell [11, 13, 54]. It is thought that bacterial toxicity is directly linked to singlet oxygen, either through excess energy from the Type 2 reaction or completion of **Reaction 1.3** in the Type 1 reaction [11, 13]. In order for **Reaction 1.3** to occur high energy (4 electrons per singlet oxygen, based on Type 1 reaction) input to the system is required in addition to protons, which are pumped through in the electron transport chain [59].

Porphyrins are key components in blue light absorption.

Porphyrins are photo-acceptors that are active in controlling metabolic pathways in bacterial cells [56]. They are synthesized during heme production (see **Figure 1.2**) and make up the prosthetic groups of cytochromes [45, 60-65]. Reduction in bacterial growth has been seen in a porphyrin content-dependent manner, i.e. the more porphyrin that is exposed to blue light, the more reduction in growth is observed [11, 12, 64, 65]. From literature searches, it is reported that different bacteria produce specific porphyrins in abundance and are more readily photosensitized by those specific porphyrins [2, 16, 39, 44, 45, 61-67]. Endogenous porphyrins typically absorb blue light around 400 nm, the Soret Peak, but vary by specific porphyrin [11, 56, 63, 65].

Porphyrinogens are porphyrin enzymes (as seen in **Figure 1.2**) and undergo rapid oxidation under air to become porphyrins; a mutant that accumulates porphyrinogens consequently also contains corresponding porphyrins [60, 64, 65].

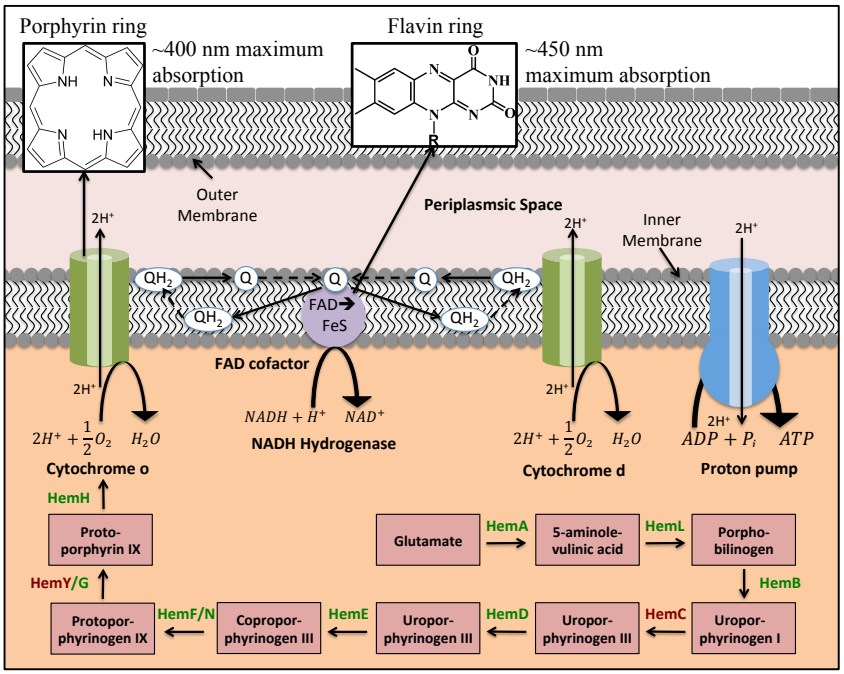

Figure 1.2. Schematic of bacterial electron transport chain and synthesis cascade of porphyrins and porphyrin enzymes.

The electron transport chain houses porphyrin-containing cytochromes and involves FAD as an electron acceptor.

Proton motive force is produced when proton pumps actively release protons (H^+) from the cytoplasm to the intermembrane space (between the inner and outer membrane) and create a proton gradient (**Figure 1.2**). The proton pumps are found in the inner membrane and require energy from electrons for initiation of this process in the electron transport chain to begin. NADH and $FADH_2$ serve as electron donors, while ubiquinone (labeled "Q" in **Figure 1.2**) and porphyrin-containing cytochromes (**Figure 1.2**) serve as both electron acceptors and mobile electron carriers in the electron transport chain [59].

BLUF is a known blue light sensor in bacteria.

In some bacteria there are proteins that harbor a blue light sensing FAD (flavin adenine dinucleotide-a redox cofactor like NADH) domain, called BLUF (blue light sensor using FAD). Significant literature documents the ability of bacteria to sense and respond to blue light, via the use of these BLUF domain-containing proteins [2, 17, 23, 28, 32, 53, 60, 68, 69]. Specifically, *Escherichia coli* (*E. coli*) senses blue light via the BLUF-EAL protein BluF (YcgF) [27, 28]. The BLUF domain is at the N-terminal and the EAL domain is at the C-terminal [19, 25]. BLI induces a short-lived flavin excited state, which extracts an electron from the conserved tyrosine forming a transient semi-quinone biradical [32].

BLUF photoreceptors have been shown to regulate lifestyle decisions, for example biofilm formation and virulence [53, 70]. The BLUF domain binds flavins non-covalently and uses their isoalloxazine ring structure as a pigment to absorb blue light [53]. The FAD component in BLUF has an absorption maximum near 450 nm [17, 23, 53, 68, 69]

Not all bacteria respond to blue light the same.

Certain wavelengths of light can promote bacteria growth, while certain wavelengths of light can inhibit and kill bacteria [12, 37]. There is also a dose-dependent response that follows the Arndt-Schultz Law, stating that weak stimuli increase physiologic activity, moderate stimuli inhibit activity, and very strong stimuli abolish activity [71]. This increased stimuli can come in the form of increased energy (dose) [71] or an increase in the rate of energy delivery. There is an energy barrier that must be surpassed to attain a reduction in activity, or in this case, reduction in growth. In a study examining the effects of BLI on a Gram (+) and Gram (-) species as a function of energy dose and wavelength, Guffey and Wilborn showed that at a lower wavelength (405 nm), both Gram (-) *Pseudomonas aeruginosa* and Gram (+) *Staphylococcus auteurs* decrease in

an energy dose-dependent manner [34]. However, at 470 nm, this dose-dependent increase was only seen with the Gram (+) species [34]. At the higher wavelength, 470 nm, both bacterial species were reduced less by BLI than at 405 nm. While the dose-dependent trend does not hold for *P. aeruginosa*, there was a greater reduction in colonies when compared to the respective energy doses of *S. aureus*. From this study, *P. aeruginosa* was shown to be more susceptible to BLI than *S. aureus*. In general, Gram (-) species are less susceptible than Gram (+) [2, 43, 51, 63].

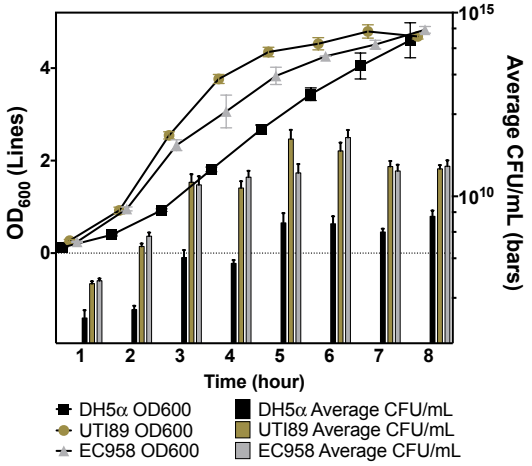

Figure 1.3. Growth curves of three different strains of *E. coli*. DH5α (non-pathogenic, K12); uropathogenic: UTI89 and EC958 (multi-drug resistant).

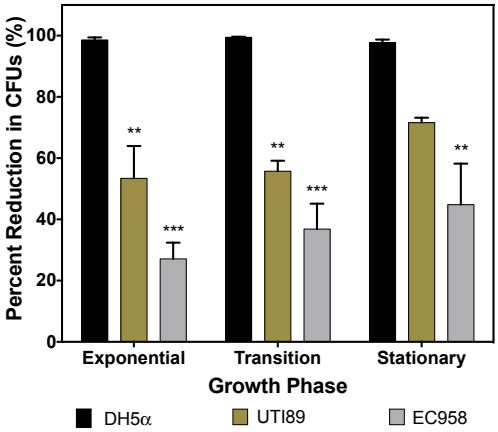

Figure 1.4. Percent reduction in CFUs for strains post-120 J/cm^2, 455 nm BLI. DH5α is an engineered, non-pathogenic strain, while UTI89 and EC958 (multi-drug resistant) are uropathogenic. Percent reductions were calculated using Equation 2.2. Statistical analyses were performed via One-way Anova. **, $P < 0.01$; ***, $P < 0.001$.

There is heterogeneity even within the same bacterial species.

Much of the work done evaluating the efficacy of BLI in growth reduction, especially with *E. coli*, has been performed on non-pathogenic and/or engineered strains for the corresponding species. While this provides an initial basis for comparison, understanding how pathogenic strains respond is essential. Many of the virulence (ability to cause infection/disease) factors are not present and/or expressed in non-pathogenic strains and subsequently the responses of non-pathogenic strains to BLI may not provide an accurate picture of how pathogens would respond to BLI. Simply comparing an engineered, laboratory strain of *E. coli*, DH5α, to two

uropathogenic strains isolated from bladder infections, UTI89 and ST131 EC958 (multi-drug resistant isolate), in **Figure 1.3**, there were observed differences in growth rates even in the absence of exposure. DH5α entered exponential phase of growth later, compared to the pathogens, but stayed in exponential phase for a longer time, consistent with its prominent use as a strain used for cloning purposes. This difference in how the bacteria grow, alone, could significantly impact its response to BLI or any perceived stress.

In initial studies examining the effects of BLI on different strains of *E. coli*, it was observed that resistance to BLI was significantly higher in pathogenic strains compared to a lab strain of *E. coli*, DH5α, during all growth phases where irradiated. In **Figure 1.4** growth reduction is less in uropathogenic *E. coli* (UPEC) strains UTI89 and ST131 EC958 than in the engineered *E. coli* lab strain, DH5α, in exponential, transition, and stationary growth phases. Likewise, comparing exponential (t = 3 hours), transition (t = 5 hours), and stationary (t = 8 hours) growth phases for the pathogenic strains, statistically significant differences were not seen. DH5α was reduced close to 100% during all growth phases.

Additional studies evaluating the effects of BLI on several mutant strains of (UPEC), strain UTI89, revealed that two mutants with reduced proton motive force, UTI89Δ*ubiI* and UTI89Δ*qseC* exhibited significantly greater resistance to BLI in the stationary growth phase (**Figure 1.5**). **Figure 1.5** shows the significant resistance of these mutants as compared to the wild-type (WT) strain UTI89.

Therefore, it was hypothesized that the growth phase of a given bacteria will influence its susceptibility to BLI.

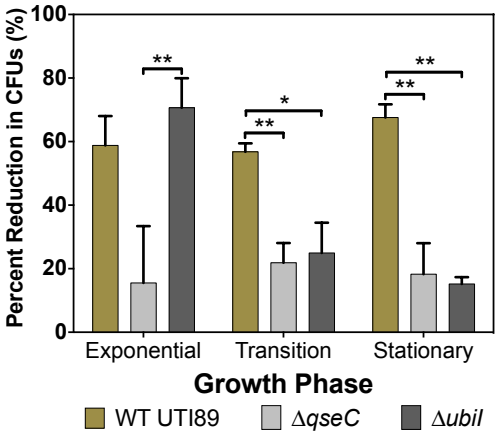

Figure 1.5. Percent reduction in CFUs for UTI89 and energy-deficient isogenic mutants, UTI89Δ*qseC*, and UTI89Δ*ubiI*. Percent reductions were calculated using Equation 2.2. Statistical analyses were performed via One-way Anova. *, $P < 0.05$; **, $P < 0.01$.

RESEARCH PLAN

Aim 1: Defined the longitudinal response of E. coli to BLI_{455}.

Introduction.

The overall objective of this aim was to understand why there are growth phase-dependent differences in the bacterial responses to BLI. **Based on initial studies, it was hypothesized that porphyrins associated with the *E. coli* electron transport chain are a target of BLI and that growth phase-dependent variability is a function of differential expression of genes encoding for porphyrin and porphyrin-containing enzymes.**

Research Design. To test this hypothesis the following studies were performed utilizing three strains: Wild-type (WT) UTI89, UTI89Δ*ubiI* and UTI89Δ*qseC*.

Study 1.1: Determined whether electron transport chain components and other porphyrin-containing factors in *E. coli* have growth-phase dependent changes in expression that may contribute to the altered susceptibility of *E. coli* to BLI.

Initial studies showed that two UPEC mutants, UTI89Δ*ubiI* and UTI89Δ*qseC* are more resistant to the effects of BLI occurring during the stationary growth phase, as compared to WT. UbiI is involved in ubiquinone synthesis, which is an active participant in the electron transport chain and is necessary to establish infection ([72] and [73]). QseC is a membrane sensor kinase that recognizes environmental signals and regulates virulence [74]. UTI89Δ*qseC* does not generate wild-type energy levels [74]. Lower proton motive force in UTI89Δ*ubiI* and UTI89Δ*qseC* has also been seen in ([73] and unpublished work).

While a linkage of energy usage/production of energy to light exposure has been extensively studied in the context of photosynthetic bacteria, there has been no connection drawn to the energy factor in the blue light response of pathogenic bacteria. In addition, no study has evaluated the basis of differential bacterial responses to blue light over the life cycle of bacteria.

Möbius *et al.* reported that heme biosynthesis is coupled to electron transport chains for energy generation. They suggested that HemG sits in the inner membrane and converts protoporphyrinogen IX to protoporphyrin IX This conversion occurs by transferring electrons to FMN (flavin mononucleotide), which is subsequently transferred to quinones. [67]

This information led to the hypothesis that in proton motive force-deficient mutants, because the electron transfer is lessened, decreased amounts of porphyrins are being produced and thus less light energy is being absorbed.

qPCR was used to understand the role of porphyrins in the phototoxic cascade.

To understand the role porphyrins play in the BLI phototoxic cascade, real-time quantitative polymerase chain reaction (qPCR or qRT-PCR) analysis of genes encoding porphyrin-containing factors in the WT UTI89, UTI89Δ*ubiI* and UTI89Δ*qseC* was used. As seen in **Figure 1.1**, different Hem enzymes lead to production of porphyrins or porphyrin intermediates. This work focused on two intermediates: HemC and HemY. HemC is further upstream in the porphyrin production pathway and HemY is the last enzyme before final porphyrin production. The expression of the genes that encode these intermediates: *hemC* (UTI89_C4364), and *hemY* (UTI89_C4361), were evaluated during bacterial growth over time in the absence and presence of BLI in WT UTI89 and the UTI89Δ*ubiI* and UTI89Δ*qseC* mutants. The unexposed samples elucidated the natural progression of expression over time in the WT strain and elucidated differences that result as a function of the loss of the *ubiI* and *qseC* genes. The exposed samples revealed transcriptional changes in response to BLI.

This method was approached knowing there was a possibility of several different outcomes. It was possible that evaluating transcript levels may uncover which, if any, Hem enzymes play an essential role in the porphyrin response, but the possibility remained that transcript levels may not provide this information because of the possibility of post-transcriptional responses to BLI.

If porphyrin absorption of light is responsible for cytotoxicity, there may be significant gene expression differences in genes encoding for the biosynthetic enzymes that produce porphyrins upon light exposure. It is possible that in response to protein damage there is induction in gene expression of affected proteins. In that case, higher levels of gene expression in the exposed samples are expected. However, if there were feedback regulation in response to

blue light, it is expected that a repression of gene expression in the exposed samples would occur. The gene expression results, combined with the expression levels in the proton motive force-defective mutants, could help elucidate which mechanism is occurring. To evaluate if there was a differential gene expression, *hemC* and *hemY* were targeted because they encode enzymes HemC and HemY, which directly lead to upstream formation of uroporphyrinogen III and protoporphyrin IX, respectively).

The possibility remained that no change in transcript levels would be observed by qPCR. An alternative approach would be to delete the *hem* genes to quantify the response difference by change in colony growth. The tradeoff to this approach is that it can be laborious making the independent mutations and possible multi-mutant knockouts. Therefore, the knockout approach was not used.

ATP release assay helped determine if BLI is bactericidal or bacteriostatic.

While these studies and others indicated that BLI significantly reduced colony-forming units (CFUs), it was still unknown whether the observed reduction in bacterial counts is due to cell lysis (bactericidal) or cessation of growth (bacteriostatic). To distinguish whether the BLI used in these studies was bactericidal or bacteriostatic an ATP release assay was performed to answer if the observed reduction effect killed bacteria or simply prevented further replication.

To measure ATP levels, CellTiter-Glo assay from Promega was used. This reagent induces cell lysis and provides a luminescent signal proportional to the amount of ATP present. With correct controls and standards, the amount of ATP from cells with and without BLI was quantified. This allowed for the determination of the "killing" ability of BLI.

An alternative to CellTiter-Glo® assay is Life Technologies™ LIVE/DEAD® Bacterial Viability Kit; however, it is not as specific for Gram (-) bacteria because it depends on cell

membrane permeability. This could pose a pitfall for use in *E. coli* because it is Gram (-) and as such, harbors both an inner and outer membrane.

The availability of a single LED setup vs. an LED array, limited the experimental setup and how accurately the relative differences for ATP and ROS measurements using the microplate reader could be captured. If samples could be exposed simultaneously, the relative differences in real-time could be compared. Because of this shortcoming, unexposed samples that were prepared under the same conditions served as controls.

Combined, these experiments informed on whether or not porphyrin absorption is critical in the BLI response and whether this absorption leads to production of singlet oxygen. In addition, it was also determined whether the reduction of growth was due to cell death or damage, which impedes replication. Together these studies assisted in the mechanistic determination of the BLI response of *E. coli*.

Study 1.2: Determined the contribution of the BLUF domain-containing sensor, UTI89_C1346, in response to BLI.

Many *E. coli* strains, including the UPEC strain used in these studies, UTI89, harbor only one BLUF-containing protein [19, 27], BluF (YcgF), encoded by gene *bluF* (*ycgF;* UTI89_C1346). Tschowri, *et al.* have previously shown (using a non-pathogenic *E. coli* strain) that in response to BLI, YcgF (BluF) directly binds to and releases the transcriptional regulator YcgE (BluR), encoded by gene *ycgE* (*bluR*; UTI89_C1344), from its operator DNA, thereby controlling gene expression [27].

In the 2009 Tschowri study [27], it was shown that BluF represses BluR, which is a direct repressor of virulence factors and a proposed regulatory model was given. From the model, an

up-regulation of virulence factors, i.e. the *ycgZ* gene, encoding for colanic acid, a component in biofilm formation is attenuated with repression of BluR [27]. Because of this response regulation and the fact there is only one BLUF domain in *E. coli*, it has been suggested to rename the *ycgF* and *ycgE* genes to *bluF* and *bluR*, respectively [28].

Therefore, it was hypothesized that BluF is part of a signaling transduction network that facilitates the response of UPEC strain UTI89 to BLI.

Given that BluF is the only BLUF domain protein in *E. coli*, this provided a unique opportunity to delineate the role of BluF in blue light sensing and response. The rationale was that if the mechanism by which BluF functions in a blue light tolerant strain could be understood, then this knowledge could be leveraged to identify differences in BluF function and regulation in more susceptible strains of *E. coli*.

bluR and bluF were deleted from the UTI89 genome

The resulting mutants: UTI89Δ*bluR* and UTI89Δ*bluF* were evaluated for their susceptibility to BLI, compared to the wild-type parent strain, UTI89. Understanding how these mutants behave over the course of growth provided more insight into the mechanism of BLI response. Results from these mutants also allowed for further understanding of how the pathogenic response of UTI89 differs from the K-12 response, as seen in the Tschowri [27, 28] studies. It was expected that virulence factors would decrease when knocking out the *bluF* gene because BluR will no longer be suppressed; it was not clear certain on the likely impact of knocking out the *bluR* gene, but hypothesized that it would have a negligible effect.

It was suspected that if the BLUF sensor were responsible for cytotoxicity, then knocking out the *bluR and bluF* genes would result in an insignificant decrease in CFUs as compared to an unexposed control sample. If knockout of the *bluR and bluF* genes caused a reduction in bacteria, but significantly less than WT it could be assumed that while the BLUF sensor plays a role in cytotoxic effects, it is not solely responsible.

As a proxy to identifying the BLUF sensor as a culprit of photo-toxicity, swimming assays on *bluR and bluF* knockouts were performed to see if motility was affected in any way after BLI. The ability of the UTI89Δ*bluR* and UTI89Δ*bluF* to form biofilms, an important virulence factor, was also assessed.

Suppressor screens were performed to detect additional players in the pathway leading to *E. coli* resistance to BLI

Suppressor screens/experimental evolution studies were also performed to identify and/or verify factors involved in the *E. coli* response to BLI. If bacteria are constantly exposed to a stressor, point mutations arise stochastically that inactivate bacterial proteins that are targeted by the stressor or are up-regulated and have a damaging effect in response to a stressor [75, 76]. A light-resistant colony was isolated after growth and it was used for the inoculum to start an overnight culture; this was sub-cultured, plated, subjected to BLI, and allowed to grow overnight. This procedure was continued for numerous passes. DNA of samples from each pass was extracted and will be sequenced for comparison.

A potential analogous study would include performing global transcriptional profiling to identify the target genes whose expression is altered by BluF. While minor transcript differences can be recognized, drawbacks include the cost and accuracy of analyzing transcript models [77]. Together with the proposed experiments, the response of BLI effects was identified. Further

insight was gained into whether porphyrin, the BLUF domain-containing sensor, or both are active in the response to BLI and to what extent. Future sequencing of samples from suppressor screens will help further understand the mechanism.

All together, Aim 1 elucidated the roles of porphyrins and the BluF/BluR network. The proposed experiments were designed to understand mechanistically what downstream effects BLI has on *E. coli*. While much work has been done in this field to identify potential participants in sensing and responding to blue light, a full mechanistic understanding has not been achieved.

Aim 2: Quantified the effects of exposure properties on E. coli growth.

Introduction.

Prior studies have shown that the effects of BLI on bacterial growth vary and depend on bacterial type and strain, as well as exposure properties [2, 37, 43, 51, 56, 63]. Higher dose exposures lead to greater reduction in bacterial growth [2, 43]. Exposures using shorter wavelengths are more effective in killing bacteria, for example UV sterilization.

The overall objective of this aim was to understand how exposure properties, such as wavelength, dose, and flux delivered to *E. coli* during different growth phases affect the post-BLI growth and how the ability to transport energy in *E. coli* influences the bacteria's response to exposure properties. Most work on the effects of blue light exposure on bacteria has been performed with Gram (+) bacteria [35, 38, 40, 42-44, 66, 78, 79]. I leveraged the expertise and resources in the Hadjifrangiskou lab to extend these studies to a Gram (-) bacterial species, *E. coli*.

As mentioned in the photosensitizer absorption mechanism (**Figure 1.1**) production of ROS, mainly singlet oxygen, is responsible for cytotoxicity. However, the preceding reactions require protons, H^+, via the Type 1 reaction. In the exponential growth phase, there is an abundance of protons and molecular oxygen, because the electron transport chain (ETC) is extremely active leading to exponential growth of cells. However, in the stationary phase not as much energy is needed because of a slower growth, leading to a down-regulation of ETC processes and less available protons and oxygen. The hypothesis was that in the exponential phase, there is an abundance of protons and oxygen to react with excited photosensitizers and other ROS, leading to a greater cytotoxic effect. Also, there is a possibility that bacteria may be more vulnerable to attack during the exponential phase because many of its resources are dedicated to producing essential components for cell replication. This rationale supports the greater reduction observed in the exponential growth phase, as compared to the transition and stationary growth phases.

To add to this rationale, it was shown that *E. coli* strains with deficiencies in their electron transport pathway are more resistant to BLI than their WT strain in the transition and stationary growth phases (**Figure 1.5**). Because of the proton motive force deficiencies in the mutants, UTI89Δ*ubiI* and UTI89Δ*qseC* (as mentioned in Aim 1), it was proposed that the increased resistance to BLI effects in the transition and stationary phase is due to an energy bottleneck in the cell. Since the proton pumps are deficient in the electron transport chain and down-regulated in later growth phases proton production is limited and therefore cytotoxic singlet oxygen production is limited.

Taken together, it was hypothesized:

1. **Under similar exposure conditions, the relative reduction in post-BLI growth of *E. coli* irradiated during the exponential growth phase will be greater than that of *E. coli* irradiated during the stationary growth phase.**
2. **As compared to WT, mutants will be less susceptible to the effects of the BLI parameters, until energy thresholds are overcome.**

Using a range of exposure properties, irradiations of uropathogenic *E. coli*, UTI89, and isogenic mutants UTI89Δ*ubiI,* UTI89Δ*qseC,* UTI89Δ*bluF* and UTI89Δ*bluR* were performed during their exponential, transition and stationary growth phases. The effects of wavelength, total dose, and energy flux (energy/area/time) were determined.

Research Design.

Study 2.1: Determined photo-toxicity of BLI on *E. coli* as a function of exposure wavelength.

Since porphyrins and the BLUF domain protein (discussed in Significance and Aim 1 studies) absorb light at different wavelengths, ~400 and ~450 nm, respectively, it was expected to that there would be significant differences in the growth response post-BLI. Due to the narrow range of wavelengths used in the study, the differences should be attributed to absorption of energy and not the energy per photon. To confirm this thought, the effects of photon energy were investigated in a later study.

	Wavelength	Dose	Flux	Time
Study 2.1				
420 nm	+	-	-	-
455 nm	+	-	-	-
470 nm	+	-	-	-
Study 2.2				
Dose 1	-	+	-	+
Dose 2	-	+	-	+
Dose 3	-	+	-	+
Study 2.3				
Flux 1	-	-	+	+
Flux 2	-	-	+	+
Flux 3	-	-	+	+

(+): changed (-): constant

Table 1.1. Aim 2 variable parameters by study.

It was proposed that there may be some competition or coordination between porphyrins and BLUF and the wavelength effects may give us some indication that the two are linked.

LED lamps at 420, 455, and 470 nm (Thorlabs Mounted High-Power LEDs: M420L3, M455L3, and M470L3) were used. These wavelengths have been designated as "safe" by ANSI (American National Standards Institute) standards [80]. Each exposure was performed using the same total dose, energy flux, and time (**Table 1.1**).

Study 2.2: Determine photo-toxicity as a function of total dose delivered.

E. coli samples in exponential, transition and stationary growth phases were irradiated using a range of total energy doses. The dose ranges chosen were 60, 120, and 180 J/cm^2 based on the initial studies of energy doses at 120 J/cm^2. The irradiation was performed at a constant energy flux and a variation of fluxes (leading to similar irradiation areas). The exposure time was varied to give the desired dose (**Table 1.1**). The purpose of this study was to determine how the total energy delivered during the irradiation affects bacterial growth. These studies were initiated using BLI_{455}, but were later extended to BLI at 420 nm (BLI_{420}) and 470 nm (BLI_{470}) to understand the combined effects of dose and wavelength and with hopes of maximizing the reductions in CFUs.

From a growth phase response, higher energy doses should lead to more susceptibility in the exponential phase, versus the stationary phase. Again, the rationale is that less protons and oxygen are available for production of singlet oxygen and other ROS during the stationary growth phase.

Study 2.3: Determined photo-toxicity as a function of energy flux.

Studies investigating both the wavelength and dose effects of BLI of bacteria have been reported [38, 40, 66, 79]. There is no known study investigating the effect of the energy flux of BLI on bacteria. The flux determines the irradiation time needed to deliver a given dose. If the irradiation time is on the order of a critical cycle in the bacteria (the replication cycle, for example) it may have a larger effect compared to a shorter irradiation delivering the same dose. The expectation from this study was for lower fluxes (greater irradiation times with the same total energy delivered slower) to be more effective in reducing *E. coli* growth. Increasing time will allow for greater energy transport in the electron transport chain, by decreasing the rate of delivery if there is a bottleneck in absorbing the light energy.

E. coli in exponential, transition and stationary phases was irradiated to a constant total dose using a range of energy fluxes (**Table 1.1**). These studies were investigated at BLI_{420}, BLI_{455}, and BLI_{470}.

The results from Aim 2 were used to determine if reduction of *E. coli* growth after BLI is more dependent on total energy delivered or the rate of energy delivery and what wavelength is most effective. This understanding provided insight into absorption and energy barriers. Both are critical in understanding the phototoxic mechanism.

CHAPTER 2

MATERIALS AND METHODS

Bacterial strains and culture conditions

The following *E. coli* strains were used: DH5α (laboratory-adapted strain [81]), MG1655 (K-12 [82]), UTI89 (UPEC cystitis isolate [83]), EC958 (UPEC multi-drug resistant isolate, ST131 lineage [84]), O157:H7 str. Sakai (EHEC isolate [85]), E343 and E402 (non-pathogenic B1 strains [86]), and E9034A (ETEC isolate [87]). Bacterial cultures were seeded in lysogeny broth (LB) and incubated at 37°C while shaking overnight. Aliquots of overnight cultures were sub-cultured into 15 mL or 25 mL (depending on the experiment) fresh LB the following morning, and normalized to a starting optical density (OD) at 600 nm of 0.05. Sub-cultures were incubated at 37°C under shaking conditions for all analyses described.

Growth curves

Bacteria were inoculated as described in the section above. A 120-µL aliquot was removed from each culture hourly. Of each aliquot, 100 µL were diluted in 900 µL fresh LB and the OD at 600 nm (OD_{600}) was recorded using a Thermo Scientific NanoDrop 2000 spectrophotometer. The remaining 20 µL were then serially diluted in 180 µL of LB for plating and counting of colony forming units (CFUs). A multichannel pipette was used to spot 8 different dilutions with 5 technical replicates per dilution. Incubation occurred overnight at room temperature. Growth curve experiments were repeated at least 3 times.

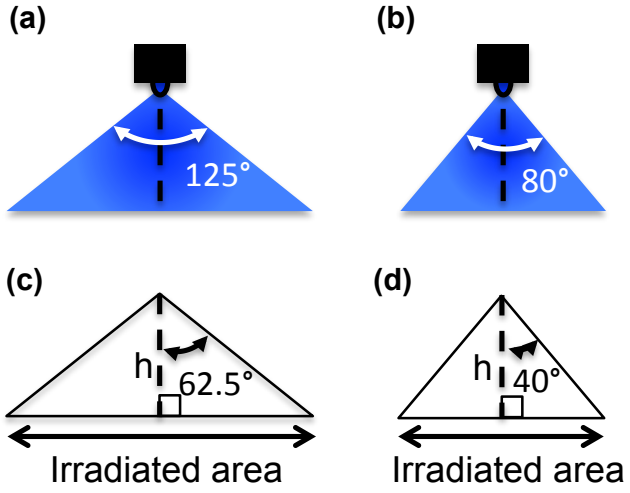

Figure 2.1. Viewing angles for LED lamps. The viewing angles of the LED lamps were used to calculate the irradiated area as a function of distance between the sample and LED, "h". a) Viewing angle for the 420 nm LED lamp. b) Viewing angle for the 455 nm and 470 nm LED lamps. The tangent of half of the viewing angle and the height was used to calculate half of the irradiated area. c) Calculation setup for the 420 nm LED lamp. d) Calculation setup for the 455 nm and 470 nm LED lamp.

In vitro* light delivery to *E. coli

Cultures were set up as described above. Aliquots were obtained for irradiation and plating during exponential (T = 3 h), transition (T = 5 or 6 h, depending on the strain) and stationary (T = 8 h) growth phases. Twenty microliter aliquots were serially diluted in 180 µL of LB for plating and counting of colony forming units (CFUs). Ten microliters from one serial dilution (10^1 to 10^2 cells) were spotted on solid LB agar and exposed to BLI as described below. BLI was carried out with Thorlabs Mounted High-Power LED lamps at 420 nm, 455 nm, or 470 nm and controlled by a high-powered LED driver (Thorlabs DC2100). The light source was placed 3 mm ± 1 mm at 420 nm, 10 mm ± 1 mm above the 10-µL spot for BLI at 455 nm (BLI_{455}), and 5 mm ± 1 mm to achieve a power flux output of ~280 mW/cm^2, ~520 mW/cm^2, ~615 mW/cm^2, respectively for BLI at 420 nm (BLI_{420}), BLI_{455}, and BLI at 470 nm (BLI_{470}). The fluxes were adjusted to keep the irradiated area fairly constant. The irradiated area was determined using the configuration in **Figure 2.1.** A total energy dose of 60, 120, 180 or 240 J/cm^2 was delivered to each sample. To increase the dose at a particular flux and wavelength, the irradiation time was increased. Petri dishes of irradiated and non-irradiated samples were then incubated overnight at ambient temperature. CFUs were counted the following day. Experiments

were performed with at least 3 biological replicates of 3 technical replicates. The overall work flow is depicted in **Figure 2.2**.

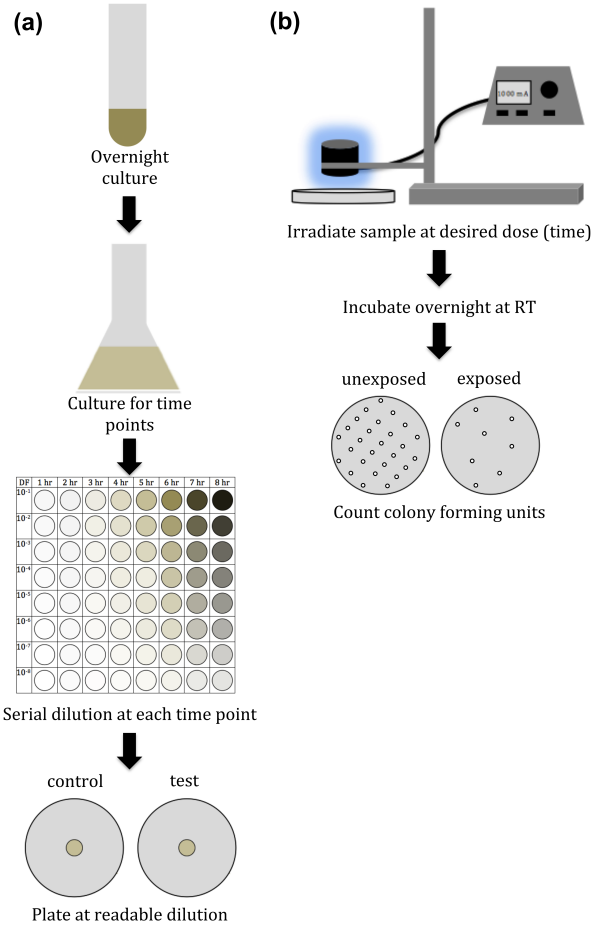

Figure 2.2. Experimental flow for blue light irradiation (BLI) experiments. a) Preparation procedure for BLI. b) BLI and quantitation of efficacy by comparing colony forming units of exposed vs. unexposed.

Calculations for varying wavelength, energy dose, and energy flux

The wavelengths used are deemed as safe by the American National Standards Institute (ANSI) as an allowable blue light in the 400-500 nm range. Each lamp is operated at different wavelengths: 420 nm, 455 nm, or 470 nm. The doses tested were within published ranges and were varied at intervals of 60 J/cm^2 from 60 to 240 J/cm^2. The original fluxes were chosen to keep the irradiated area within a similar range; however, fluxes were modulated for the flux

study to increased and decreased levels from the original fluxes. The irradiated area was calculated as a function of the distance from the sample using the manufacturer's light parameters found in **Figure 2.3**.

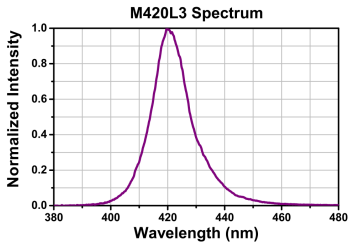

Specification	Value
Color	Violet
Nominal Wavelength	420 nm
Power LED Output[a] (Min)	750 mW
Power LED Output[a] (Typical)	820 mW
Test Current for Typical LED Power	1000 mA
Maximum Current (CW)	1000 mA
Forward Voltage	3.5 V
Bandwidth (FWHM)	15 nm
Viewing Angle (FWHM)	125°
Typical Lifetime	>10,000 h

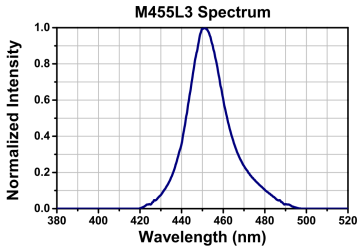

Specification	Value
Color	Royal Blue
Nominal Wavelength	455 nm
Power LED Output (Min)	900 mW
Power LED Output (Typical)	1020 mW
Test Current for Typical LED Power	1000 mA
Maximum Current (CW)	1000 mA
Forward Voltage	3.2 V
Bandwidth (FWHM)	18 nm
Viewing Angle	80°
Typical Lifetime	100,000 h

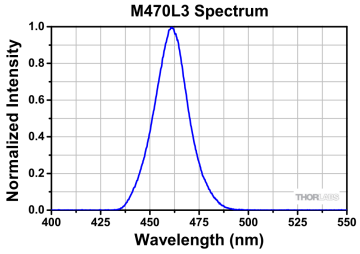

Specification	Value
Dominant Wavelength	470 nm
Power LED Output (Min)	650 mW
Power LED Output (Typical)	710 mW
Test Current for Typical LED Power	1000 mA
Maximum Current (CW)	1000 mA
Forward Voltage	3.2 V
Bandwidth (FWHM)	25 nm
Viewing Angle	80°
Typical Lifetime	100,000 h

Figure 2.3. **Manufacturer's light parameters** [88]. Peak wavelengths are seen at 420 nm, 455 nm, and 470 nm, respectively, while there is diminished intensity at wavelengths ≥20 nm ± the peak wavelength.

To determine the irradiation time for varied energy doses, the following calculation was used:

$$Irradiation\ time\ (s) = \frac{energy\ dose\ (J/cm^2)}{energy\ flux\ (mW/cm^2)} \frac{1\ W}{1\ J/s} \frac{10^3\ mW}{1\ W} \qquad \textbf{Equation 2.1}$$

From **Equation 2.1**, an increase in energy flux leads to a shorter irradiation time. Energy flux was determined as a function of the distance between the LED lamp and the irradiated sample (**Table 2.1**). The energy flux decreased as a power function with increasing distance between the light source and the sample. The measured power and energy flux were determined by using a power meter at varying vertical distances between the light source and sample at each wavelength. To determine the energy flux at a particular distance that was not measured, **Figure 2.4** was used. The energy flux decreased as a power function with distance between the light source and the sample. The flux that was used when energy flux was being modulated was determined assuming a straight line for the two nearest distances.

Reduction determination

To determine the percent change in exposed versus unexposed CFUs, the CFUs post-irradiation were enumerated and compared to the CFUs of corresponding, non-irradiated spots. The reductions were calculated using **Equation 2.2**. Reductions were also calculated as a percent change as calculated in **Equation 2.3**.

$$\text{Percent reduction in CFUs (\%)} = \left[1 - \frac{\text{exposed CFUs}}{\text{unexposed CFUs}}\right] \text{ x } 100\% \qquad \textbf{Equation 2.2.}$$

$$\text{Percent change in CFUs (\%)} = \left[\frac{\text{exposed CFUs}}{\text{unexposed CFUs}} - 1\right] \text{ x } 100\% \qquad \textbf{Equation 2.3.}$$

Wavelength (nm)	Current (mA)	Distance (mm)	Distance (mm)	Power (mW)	Flux (mW/ cm^2)	Effective Power (mW)	Delivery Rate (J/s)	Delivery Rate (J/cm^2•s)	Energy/ photon (J/photon)	Delivery Rate (photons/s)	Delivery Rate (photons/ cm^2•s)
470	1000	0	5.1	695.8	615.5	309.4	0.3094	0.6155	4.229E-19	7.316E+17	1.455E+18
470	1000	4.66	9.76	383.5	339.3	170.6	0.1706	0.3393	4.229E-19	4.033E+17	8.023E+17
470	1000	9.87	14.97	213.3	188.6	94.8	0.0948	0.1886	4.229E-19	2.242E+17	4.460E+17
470	1000	20.41	25.51	76.31	67.7	34.0	0.0340	0.0677	4.229E-19	8.044E+16	1.600E+17
470	1000	29.44	34.54	42.35	37.3	18.8	0.0188	0.0373	4.229E-19	4.435E+16	8.822E+16
470	1000	39.91	45.01	22.85	20.3	10.2	0.0102	0.0203	4.229E-19	2.415E+16	4.805E+16
470	1000	50.99	56.09	13.24	11.8	5.9	0.0059	0.0118	4.229E-19	1.403E+16	2.790E+16
455	1000	0	5.1	1019	902.0	453.4	0.4534	0.9020	4.369E-19	1.038E+18	2.065E+18
455	1000	4.85	9.95	592	523.0	262.9	0.2629	0.5230	4.369E-19	6.017E+17	1.197E+18
455	1000	10.41	15.51	278.5	246.0	123.7	0.1237	0.2460	4.369E-19	2.830E+17	5.631E+17
455	1000	20.42	25.52	113.5	100.4	50.5	0.0505	0.1004	4.369E-19	1.155E+17	2.298E+17
455	1000	30.72	35.82	58.5	51.6	25.9	0.0259	0.0516	4.369E-19	5.937E+16	1.181E+17
455	1000	41.08	46.18	34.6	30.6	15.4	0.0154	0.0306	4.369E-19	3.521E+16	7.004E+16
455	1000	49.73	54.83	24.8	21.9	11.0	0.0110	0.0219	4.369E-19	2.520E+16	5.013E+16
420	500	0	5.57	320.6	233.6	117.4	0.1174	0.2336	4.733E-19	2.481E+17	4.936E+17
420	500	5.7	11.27	145.6	128.6	64.6	0.0646	0.1286	4.733E-19	1.366E+17	2.717E+17
420	500	9.88	15.45	80.3	70.8	35.6	0.0356	0.0708	4.733E-19	7.519E+16	1.496E+17
420	500	20.24	25.81	28.7	25.4	12.8	0.0128	0.0254	4.733E-19	2.698E+16	5.367E+16
420	500	30.51	36.08	13.2	12.4	6.2	0.0062	0.0124	4.733E-19	1.317E+16	2.620E+16
420	500	40.7	46.27	8.9	8.0	4.0	0.0040	0.0080	4.733E-19	8.496E+15	1.690E+16
420	500	50.77	56.34	5.2	4.6	2.3	0.0023	0.0046	4.733E-19	4.885E+15	9.719E+15

Table 2.1. **Light source calibration.** Blue light irradiation (BLI) was used with three different LED lamps at three different wavelengths: 420 nm, 455 nm, and 470 nm. The current, measured in mA, was controlled by the power controller and kept constant. The maximum current allowed by the 420 nm light source was 500 mA as a safety feature because the wavelength is close to UV (<400 nm). The power and flux was measured as a function of the distance between the light source and the sample. The last five columns are calculations based on Equation 5.4 to determine the amount of energy per photon. Total photon count can be calculated from the energy per photon and the total energy delivered to a sample.

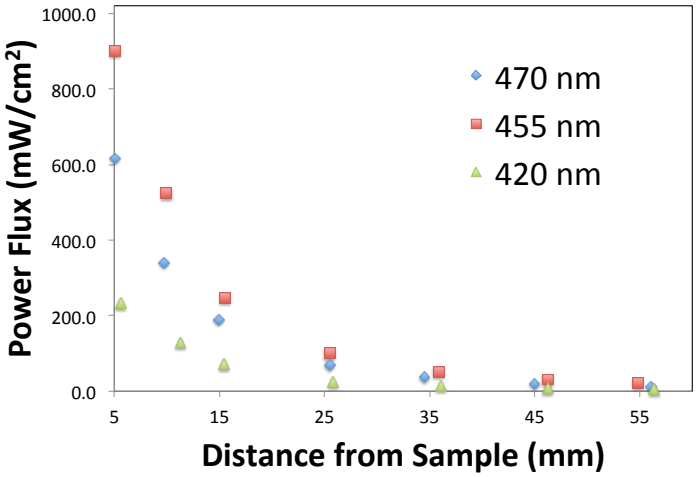

Figure 2.4. Light source calibration curve. The graph depicts the change in energy flux for the 470 nm, 455 nm, and 420 nm lamps as a function of the light distance from the sample. The flux decreases with increasing distance between the light source and the sample.

Viability Assay

Cell viability was determined using the CellTiter-Glo Luminescent Cell Viability Assay kit (Promega). Two assays were performed: one to determine the overall differences in ATP of unexposed and exposed samples (**Figure 2.5a**) and the second to determine if differences in ATP amounts of unexposed and exposed samples were due to cell death (cell lysis) or inhibition of replication (**Figure 2.5b**). For both assays, 50 µL of liquid culture were placed on a glass cover slip directly under the light source. The height between the light source and the sample was adjusted to deliver 120 J/cm^2 for the increased irradiated area because of the increased volume and spread on the glass slide, compared to the spread on agar plates. After BLI_{455}, the sample was transferred to a 96-well plate and allowed to incubate for 30 minutes, allowing for at least one replication cycle to occur. After incubation in the first assay, triplicate samples of unexposed and exposed aliquots were diluted ten-fold in LB and transferred to a black, 96-well plate (Costar). In the second assay, 200 µL of unexposed and exposed samples were collected in separate 1.5 mL plastic tubes for each strain. The plastic tubes were placed in a centrifuge for 2 min at 16,100 *x g* to pellet cells. After centrifugation, the supernatant was transferred to a new

1.5 mL plastic tube. The pellets were then re-suspended in 200 µL of LB. Triplicate samples (50 µL each) of supernatant or re-suspended pellet were added to individual wells in a black well, 96-well plate (Costar) and quantified as follows: For both assays, an equal volume of CellTiter-Glo substrate/buffer mix was added to each well and mixed thoroughly. After addition of the CellTiter-Glo, the plates were allowed to shake orbitally for 2 min to stabilize the signal and then luminescence values of ATP were measured using a SpectraMax i3 (Molecular Devices). Luminescence was also determined for wells filled only with LB to subtract background luminescence due to the media. The following equation was used to calculate the percent of non-viable cells:

$$\text{Percent of cells killed (\%)} = \left[1 - \frac{\text{luminescence of exposed}}{\text{luminescence of unexposed}}\right] \text{x } 100\% \qquad \textbf{Equation 2.4}$$

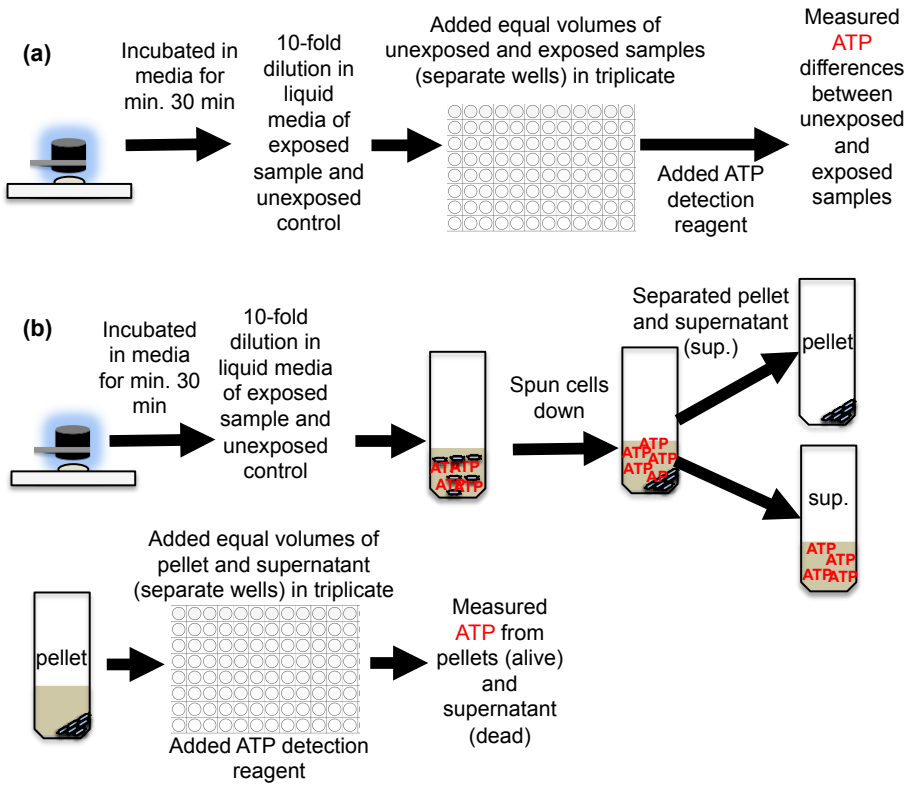

Figure 2.5. Work flow for ATP assay. (a) Relative ATP differences between unexposed and exposed samples were measured. (b) Relative ATP differences between unexposed and exposed supernatant and pellet samples were measured to determine whether total ATP differences were due to cell death or an inhibition in replication.

Persister assays

Persister assays were performed using ofloxacin, as described in Allison *et al* [89]. Stationary-phase cultures of WT UTI89 and UTI89Δ*ubiI* (grown in LB for 16 h, 37°C) were subjected to 5 mg/mL ofloxacin for 4 h, followed by a 1 h exposure to 20 mg/mL ofloxacin. Samples were withdrawn for CFU enumeration, prior to each ofloxacin exposure. Susceptibility assays were repeated 3 times. The average percent survival from the 3 independent experiments is reported.

Biofilm assay

Biofilm formation and quantification was performed as previously described [90].

Seeding biofilm plates

Cultures were grown exponentially in 5 mL LB and normalized to an OD at 600 nm (OD_{600}) of 1 before dilution in 200-fold in 1.2X yeast extract-Casamino Acids (YESCA) medium and seeded into 96-well PVC biofilm plates as described in [91]. With a multichannel pipette, 100 µL of 1:500 diluted bacterial samples were added to the 96 well plates. Plates were stored in a plastic container with wet paper towels to mimic a humid environment.

Quantifying biofilm formation

Biofilms were quantitatively measured 24 h and 48 h post-seeding, using crystal violet [86]. To stop biofilm formation, the excess liquid culture was shaken into a bin with water and 10% bleach. The plates were rinsed with ultra-pure water to remove any non-adherent bacteria from the wells. Plates were air-dried face-down for at least 15 min. One percent (1%) crystal violet (125 µL) was added to each well to stain biofilms for 15 min. Biofilm plates were rinsed three times with ultra-pure water, until the water in contact with the plates was clear. The washed plates were air-dried for at least 10 min. After drying, 150 µL of 35% acetic acid solution was

added and mixed into each well using a multichannel pipette, to dissolve the stained biofilms. One hundred microliters of the dissolved and mixed biofilms were transferred into a new 96-well flat-bottom plate. The luminescence of the dissolved biofilm was measured using a SpectraMax i3 (Molecular Devices) at 590 nm. All values were normalized to non-BLI-treated UTI89 (which was artificially set at 100% biofilm formation) samples. In all experiments, UTI89Δ*fimA-H*, which is deficient in its ability to form biofilms was used as a negative control. The average of at least three independent experiments is presented.

Motility Assay

Motility assays were performed as previously described [92]. A 10 % agar gel was made with 2.5 g of agar and 25 g of LB per 1 L of distilled water. The liquid was autoclaved for a minimum of 20 min. After the media was cool, 133 μL of 15% tetrazolium chloride was added to each liter. Twelve milliliters of media was added to each well of 6-well plates and allowed to gel overnight. From overnight shaking cultures, strains were stabbed in the soft LB agar and incubated at 37°C for 7 h in the presence of atmospheric oxygen. Motility was recorded as the diameter (in mm) containing bacteria migrating away from the inoculation point.

RNA extraction and qPCR

RNA extraction, DNAse treatment, reverse transcription, and real-time quantitative (q) PCR were performed as previously described [93].

Exposures for RNA Extraction

One hundred microliter samples were spotted on plastic coverslips and irradiated at 455 nm and 120 J/cm^2. Five technical replicates were pooled together in a 10 mL conical for a total

of 500 µL. After each addition of 100 µL of sample, the conical was flash-frozen using ethanol and dry ice. Samples were stored at -80°C until the RNA extraction was ready to be performed.

RNA Extraction

Samples stored at -80°C were removed and stored in an ice bucket to thaw. The work area, pipettes, and pipette tips were treated with RNaseZap to destroy any RNases that could degrade RNA. The RNEasy kit by Qiagen (#74106) was used to extract RNA. Because liquid volumes, instead of pellets, were used, all volumes before purifying the RNA were multiplied by 2.5 times, using the RNEasy kit protocol.

DNase Treatment

To remove any DNases that would degrade DNA, samples were DNase treated using the Ambion TURBO DNA-free™ kit by Life Technologies. Two micrograms of RNA were added to DNase- and RNase-free water to reach a total volume of 50 µL in 1.5 mL tubes. Two microliters of Turbo DNase enzyme was added to each sample, along with 6 µL of 10X Turbo DNase buffer. Samples were incubated for 30 min at 37°C in a heat block. After 30 minutes, an additional 2 µL of Turbo DNase enzyme was added to each sample and incubated for an additional 30 min. After the full hour reaction, 6 µL (~1/10 volume) of DNase inactivation reagent was added and mixed by pipetting at least 3 times at room temperature. The total solution was centrifuged for 1.5 min ≥ 8,000 x g. The supernatant was removed and transferred to a new 1.5 mL tube.

Checking for the effectiveness of the DNase treatment

To ensure the DNase treatment was effective, a polymerase chain reaction (PCR) was run to amplify the samples. If DNA were present it would be amplified to a level where it could be detected. Three microliters of sample and the following components were added to PCR tubes

and run in a thermocycler. One microliter of genomic DNA and 3 µL of RNase-free water were added as a positive and negative control, respectively, to separate PCR reaction tubes. All components were added to PCR tubes, individually.

Master Mix (volumes per sample)

- 1 µL dNTPs
- 2.5 µL 10x buffer
- 1 µL 16S F primer (10 µM)
- 1 µL 16S R primer (10 µM)
- 0.5 µL Taq polymerase
- 16 µL dH_2O

25 µL total (with RNA, DNA, or water)

The protocol for the PCR run is below.

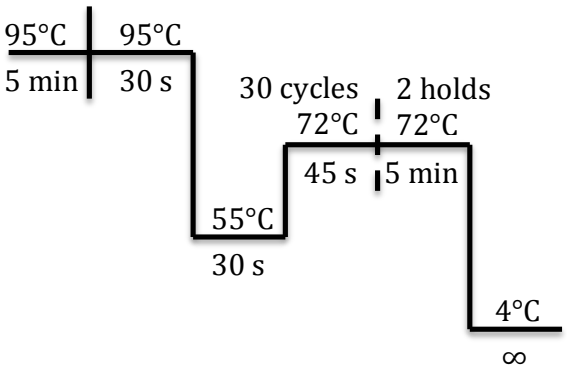

After the PCR run, a 1% agarose gel was made to run the samples on. The gel consisted of 1 g of molecular grade agarose and 100 mL of TAE (a mixture of Tris buffer, acetic acid, and EDTA- Ethylenediaminetetraacetic acid) buffer (used for separation of nucleic acids), which was mixed and microwaved for 90 s to dissolve the agarose in the buffer. Ten microliters of ethidium bromide, an intercalating agent, was added after microwaving as a fluorescent tag for nucleic acid staining. The gel was poured in a gel box with a 8-15 well comb for individual loading lanes (depending on the amount of samples) and was allowed to sit for at least 30 min to solidify.

Five microliters of the 1 Kb Plus DNA ladder (Invitrogen), which is used to determine the molecular weight of DNA fragments, was added into Lane 1. Two microliters of loading dye was added to each sample tube and 15 µL of the sample was added to each well. After loading the gel, it was run at 165 V for 30 min using the large gel holder or at 90 V for 30 min. The gel was imaged using a UV tray to visualize the presence of any DNA in sample lanes. A DNA-free gel consisted of an empty 16S band.

Reverse transcription of RNA

Once the samples were confirmed to be free of DNA, the concentrations were measured using the NanoDrop to move forward with the two-step reverse transcription PCR (RT-PCR) protocol to transcribe single-stranded DNA from the purified RNA. Using the NanoDrop concentrations, 1 µg of RNA was added to DNase- and RNase-free water to achieve a total volume of 50 µL in PCR reaction tubes. One microliter of random hexamers or random primers was added to the 50-µL reaction tubes. The contents of the reaction tube were mixed by pipetting and then spun briefly using the microcentrifuge. The samples were placed in a thermocycler and heated for 5 minutes at 65°C. After the 5 min cycle, samples were transferred to ice immediately, then spun briefly. The following components were added to each PCR tube to initiate the second step of the RT-PCR: 16 µL of 5X RT buffer, 1 µL RNase Out, 1 µL of reverse transcriptase, 1 µL of dNTPs (a nucleotide mix of nucleotides A, C, G, and T), 2 µL 0.1 M dTT (dithiothreitol-breaks down disulfide bonds) and 9 µL of nuclease-free water. The samples were mixed by pipetting and briefly spun using the microcentrifuge. All samples were placed in a thermocycler at 42°C for one hour. After the one hour incubation, the temperature was increased to 70°C for 15 min to inactivate the reverse transcriptase. The DNA concentrations were measured using the

NanoDrop and either stored at -20°C or samples were diluted for concentrations of 100, 50, 25, 12.5, 6.25, 3.125, 1.5625, and 0.78125 ng/µL.

Real-time quantitative PCR (qPCR)

qPCR analysis was performed with five concentrations of cDNA (100 ng, 50 ng, 25 ng, 12.5 ng, 6.25 ng; all per µL) each in triplicate for each sample, and internal DNA gyrase (*gyrB*) levels were used as the housekeeping (HK) gene for normalization. Forward and reverse primers from Integrated DNA Technologies were used for amplification for the gene of interest [94] and the HK gene. TaqMan® MGB probes for the gene of interest (GOI) and HK gene from Applied Biosystems were used for quantitation. A 100X master mix of primers, probes, TaqMan® master mix, and water was made with the following components: 1000 µL TaqMan master mix, 200 µL of GOI Forward Primer, 200 µL of GOI Reverse primer, 200 µL of HK gene Forward Primer, 200 µL of HK gene Reverse primer, 5 µL GOI probe, 5 µL HK gene probe, and 90 µL of nuclease-free water. Aliquots of 18.9 µL were added to each well of the 96-well plate. One microliter of samples, in addition to 2 wells each of controls: (+) genomic DNA, (-) RNA, and (-) nuclease-free water were added to each well of the 96-well plate. The 96-well plate was sealed with optical tape and spun down for 1 min to ensure all of the contents were at the bottom of each well. qRT-PCR was executed using a StepOnePlus™ Real-Time PCR System (#4376600) by Life Technologies.

Singlet Oxygen Generation

Singlet Oxygen Sensor Green (SOSG; Molecular Probes^{TM}) was used to quantify the singlet oxygen released after BLI. Hypericin, a known singlet oxygen generator was used to create a standard curve for singlet oxygen generation of *E. coli* samples. Fifty microliters of

liquid culture was placed on a glass cover slip directly under the light source. The height between the light source and the sample was adjusted to deliver 120 J/cm^2 for the increased irradiated area because of the increased volume and spread on the glass cover slip. After BLI, 1 µL of SOSG was added to 50 µL triplicate samples of unexposed and exposed aliquots and 50 µL of each replicate was transferred to a black well plate. The fluorescence emission was measured using a SpectraMax i3 (Molecular Devices) after excitation at 488 nm. The difference in peak emission intensities was used to correlate the amount of singlet oxygen generated from the hypericin standard curve. The fluorescence emission intensity was also determined for wells filled only with LB to subtract background intensity due to the media.

There were several hurdles in measuring singlet oxygen formation. Hypericin is insoluble in water, so DMSO (25 mg/mL) was used as the solvent. However, DMSO interacted with the signal of SOSG, so accurate readings were not obtained. Methanol was used as the solvent for the SOSG, so Hypericin (previously diluted in DMSO) was further diluted in methanol for working solutions. The plan was to excite the samples with light at a desired wavelength and intensity using the SpectraMax i3 plate reader, but the intensity was too low and could not be controlled. Therefore, excitation was achieved with BLI using our LED lamps. Methanol has a fast evaporation rate, so samples diluted in methanol dried out by the end of the exposure. To date, a standard curve has not been developed for the quantification and detection of singlet oxygen as a function of BLI.

CHAPTER 3

BLUE LIGHT IRRADIATION INDUCES A VIABLE, PERSISTER-CELL LIKE STATE IN *Escherichia coli*

ABSTRACT

Blue light irradiation (BLI) has been widely used to treat infections and other conditions, like aged skin. Although effective against a range of Gram-positive pathogens, BLI appears to be less effective at targeting Gram-negative bacteria and the basis of this phenomenon remains unknown. With resistance to antibiotics constantly rising, options like BLI are becoming more attractive, yet no studies have extensively evaluated how bacteria respond to BLI at different stages of growth. In this study the BLI responses by two *E. coli* pathotypes (enterohemorrhagic and uropathogenic), to those of non-pathogenic, K12 *E. coli* were compared. The growth retardation during different phases of bacterial growth was measured to capture growth-phase related responses. These studies revealed that growth retardation in response to BLI changed significantly as the bacterial culture senesced and this phenomenon varied in a strain-dependent manner. Subsequent ATP release assays indicated that BLI treatment does not kill *E. coli* at the wavelength tested, suggesting that BLI retards growth but is not bactericidal against *E. coli*. Conversely, a mutant with reduced proton motive force and higher levels of persister cell formation, UTI89Δ*ubiI*, was more tolerant to BLI, indicating that reduced metabolic activity is protective against BLI. Collectively, this work shows that the effectiveness of BLI varies in a bacterial growth phase- and strain-specific manner and that BLI may create a persister reservoir that could be competent for re-infection if BLI is used as a treatment option. These observations

have wide-ranging ramifications for the utility of BLI in the treatment of bacterial infections caused by Gram-negative pathogens.

INTRODUCTION

The steady increase in antibiotic resistance rates among bacteria has sparked a major research effort to identify new anti-bacterial and anti-virulence therapies [95-99]. Photodynamic therapy is among these alternative treatment approaches, and it has been used routinely to treat photo-aged facial skin, acne, and jaundice in neonates [1-10]. Photodynamic therapy employs visible blue light in the 400-700 nm wavelength range to activate either exogenous or endogenous photosensitizers [15, 41-44]. Endogenous bacterial photosensitizers, such as porphyrins and flavins, absorb light in the 400-500 nm wavelengths and have thus been suggested to respond to blue light irradiation (BLI) [2, 14, 16].

Porphyrin-containing cytochromes, along with flavin-containing enzymes, such as flavin adenine nucleotide (FAD), are integral components of the bacterial electron transport chain (ETC) and are involved in the generation of proton motive force (pmf) (**Figure 3.1a** and [100-102]). Pmf is produced when proton pumps actively transport protons (H^+) from the cytoplasm across the bacterial cell membrane, creating a proton gradient. The proton pumps are membrane-embedded and require energy from electrons to initiate the ETC. FAD is an electron acceptor, while cytochromes and another potential photosensitizer, ubiquinone, serve as both electron acceptors and mobile electron carriers in the ETC (**Figure 3.1a** and [100-104]). The presence of conjugated pi bonds in the aromatic rings in the molecular structure of these components allow for effective photon energy, making them ideal photosensitizers [105]. These photosensitizers

have varying absorption spectra: flavins have an absorption peak at 450 nm, porphyrins at 400 nm, and ubiquinones have various peaks in the 230-500 nm range [106-109].

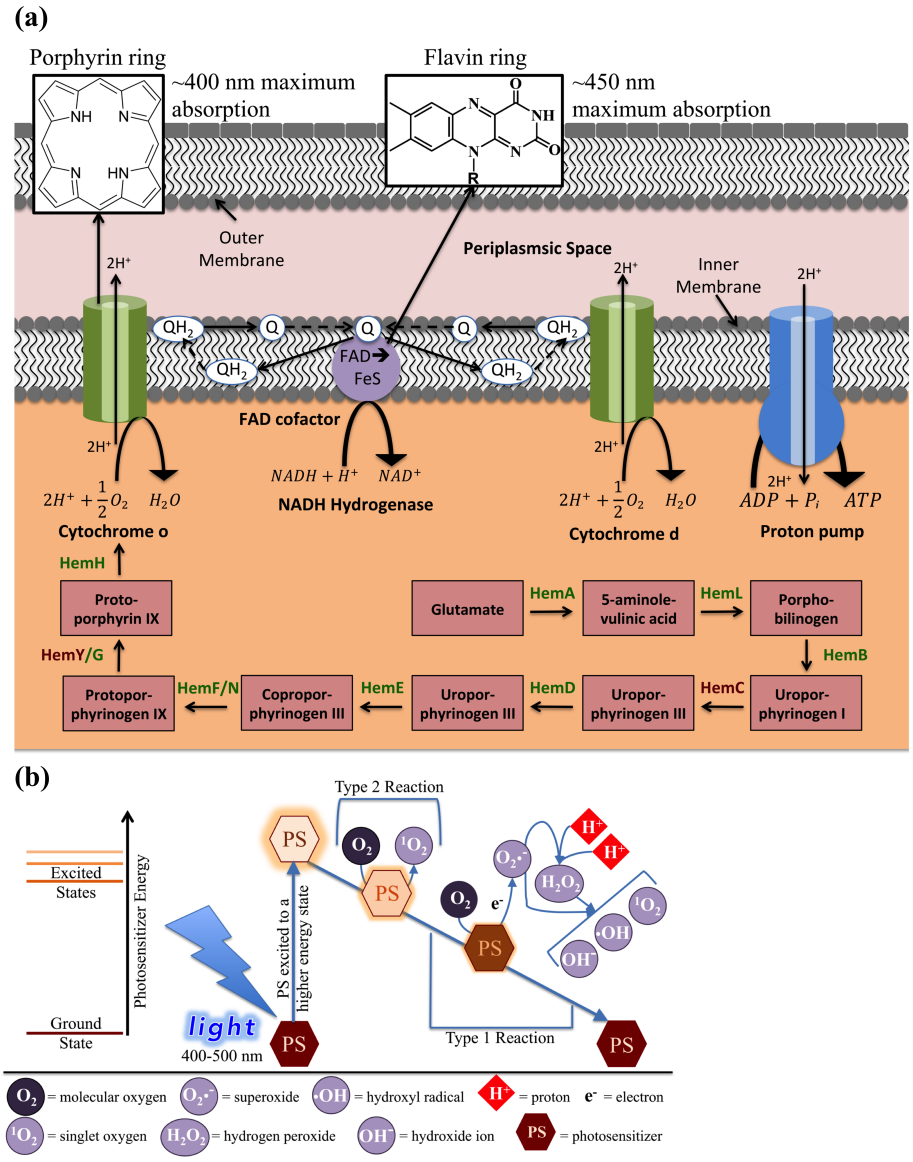

Figure 3.1. Photosensitizers play a major role in the response to visible light exposure. (a) Known endogenous photosensitizers (PS) are found in the electron transport chain (ETC) of bacteria. Porphyrins and flavins are two PS, which absorb in the blue light wavelength range (400-500 nm). Energy is transported by ubiquinones (Q/QH_2). Protons (H^+) cross the membrane by reduction reactions and are actively transported by proton pumps. This proton gradient is the proton motive force (pmf) that triggers the ETC. Flavin-containing FAD and porphyrin-containing cytochromes are an active part of generating pmf. Hem enzymes are necessary for porphyrin production. The boxes in pink represent the biosynthetic pathway for the production of porphyrins and subsequently cytochromes. The red-colored enzymes correspond to the genes evaluated by qPCR. (b) Proposed mechanism of blue light-mediated bacterial reduction. Photosensitizers are excited upon light absorption and energy and/or electrons are released to form reactive oxygen species (ROS). A Type 2 reaction proceeds at high energy levels, while a multi-step Type 1 reaction occurs at lower energy levels and requires the presence of both protons and oxygen. The production of singlet oxygen ($^1O_2$) is thought to be the major player in the phototoxic response.

Earlier studies have indicated that absorption of light promotes photosensitizers to an excited state, after which electrons are transferred to molecules such as molecular oxygen, forming reactive oxygen species (ROS) [14, 45, 54, 55, 110]. This proposed mechanism is

described pictorially in **Figure 3.1b**. There is a Type 2 reaction that proceeds at high energy levels, while a multi-step Type 1 reaction occurs at lower energy levels and requires the presence of protons and oxygen. Increased ROS levels can cause damage to cellular proteins, lipids, and DNA [11, 12, 50, 54, 58]. It is thought that photodynamic therapy is toxic to bacteria due to the generation of singlet oxygen ($^1O_2$) after electron donation from excited porphyrin-containing cytochromes (**Figure 3.1b** and [11, 13]).

In vitro and *in vivo* studies evaluating the efficacy of BLI on well-characterized human pathogens have demonstrated that BLI at various wavelengths and energy doses can inhibit the growth of Gram-positive bacteria like *Staphylococcus aureus*, *Enterococcus faecalis,* and *Streptococcus pyogenes* by as much as 90% with varying wavelengths and energy doses of light [2, 4, 12, 34, 41-43, 48, 111, 112]. However, studies have also demonstrated that the same wavelengths and energy doses shown to significantly reduce Gram-positive species, are not as effective at significantly inhibiting the growth of Gram-negative bacteria like *Porphyromonas gingivalis, Klebsiella pneumoniae,* and *Escherichia coli* [2, 4, 40, 43, 112].

To date, no studies have evaluated responses of planktonic bacteria to BLI during different phases of growth; BLI effects have mainly been evaluated for bacteria irradiated during the exponential phase of growth [11, 12, 16, 34, 37, 41, 44, 45, 64, 112, 113]. Given that stationary phase bacteria differ from their exponential phase counterparts in many respects [114-121] and combined with the fact that in the human host, bacteria are not always in the exponential phase of growth, it is imperative to thoroughly characterize how bacteria respond to BLI treatment at all phases of growth. Moreover, there is an increasing body of literature demonstrating extensive population heterogeneity in bacterial communities during infection; this heterogeneity has been shown to add to the recalcitrance of bacterial pathogens to antibiotic

treatment and the immune response [122-130]. In particular, subpopulations of "persister" cells exist in planktonic and biofilm cultures, which are metabolically inactive, yet amenable to resuscitation upon cessation of stress [131, 132]. The effects of BLI on the proportion of this subpopulation have not been elucidated. In this study, the effects of BLI at 455 nm wavelength (BLI_{455}) on the growth and viability of different non-pathogenic, pathogenic, and multi-drug resistant (extended spectrum beta-lactamase producers) *E. coli* strains during exponential, transition, and early stationary phases of growth were investigated. The 455 nm wavelength was chosen for investigation, given that it falls within the wavelength range of phototherapy devices approved for human use, including "bili-blankets" used to treat jaundiced neonates [5, 9]. It was determined that although BLI_{455} reduced the growth of *E. coli* in varying degrees in a strain- and growth-phase dependent manner, it did not significantly impact the viability of any strain. These findings suggest that BLI may be inducing a metabolically inactive/persister-like phenotype in *E. coli*. Subsequent analysis of the BLI responses of a mutant shown to contain higher numbers of persister cells in stationary phase, planktonic cultures, UTI89Δ*ubiI* demonstrated higher tolerance to BLI, suggesting that when found in a persister-like state, *E. coli* is not susceptible to BLI treatment.

MATERIALS AND METHODS

Bacterial strains and culture conditions

The following *E. coli* strains were used: DH5α (laboratory-adapted strain [81]), MG1655 (K-12 [82]), UTI89 (UPEC cystitis isolate [83]), EC958 (UPEC multi-drug resistant isolate, ST131 lineage [84]), O157:H7 str. Sakai (EHEC isolate [85]), E343 and E402 (non-pathogenic B1 strains [86]), and E9034A (ETEC isolate [87]). Bacterial cultures were seeded in lysogeny

broth (LB) and incubated at 37°C while shaking overnight. Aliquots of overnight cultures were sub-cultured in 25 mL fresh LB the following morning, and normalized to a starting optical density (OD) at 600 nm of 0.05. Sub-cultures were incubated at 37°C under shaking conditions for all analyses described.

Growth curves

Bacteria were inoculated as described in the section above. Refer to the "Growth Curves" section of Chapter 2 for more specific methods. A 120-µL aliquot was removed from each culture hourly. Of each aliquot, 100 µL were diluted in 900 µL fresh LB and the OD at 600 nm (OD_{600}) was recorded using a Thermo Scientific NanoDrop 2000 spectrophotometer. The remaining 20 µL were then serially diluted in 180 µL of LB for plating and counting of colony forming units (CFUs). A multichannel pipette was used to spot 8 different dilutions with 5 technical replicates per dilution. Incubation occurred overnight at room temperature. Growth curve experiments were repeated at least 3 times.

In vitro* light delivery to *E. coli

Cultures were set up as described above. Aliquots were obtained for irradiation and plating during exponential (T = 3 h), transition (T = 5 or 6 h depending on the strain) and stationary (T = 8 h) growth phases. Twenty microliter aliquots were serially diluted as described above and 10 µL from one serial dilution were spotted on solid LB agar and exposed to BLI as described below. BLI was carried out with a Thorlabs Mounted High-Power 455 nm LED lamp and controlled by a high-powered LED driver (Thorlabs DC2100). The light source was placed 10 mm ± 1 mm above the 10-µL spots, to achieve a power flux output of ~520 mW/cm^2. A total

energy dose of 120 J/cm^2 was delivered to each sample. Irradiated and non-irradiated controls were then incubated overnight at ambient temperature. CFUs were counted the following day. Experiments were performed with at least 3 biological replicates of 3 technical replicates. The lab-adapted strain, DH5α, was used as a control for comparison for analyses by growth phase.

Reduction determination

To determine the percent change in exposed versus unexposed CFUs, the CFUs post-irradiation were enumerated and compared to the CFUs of corresponding, non-irradiated spots. Changes in CFUs post-BLI are also presented as percent reductions in CFUs, following **Equation 2.2**.

Viability assay

Refer to the "Viability assay" section of Chapter 2 for more specific methods. CellTiter-Glo Luminescent Cell Viability Assay (Promega) was utilized to determine cell viability. Luminescence values of ATP were measured using a SpectraMax i3 (Molecular Devices). Luminescence was also determined for wells filled only with LB to subtract background luminescence due to the media. A standard curve was determined using ATP disodium salt hydrate (Sigma) to quantify the amount of ATP present pre- and post-exposure. Experiments were performed with at least 3 biological replicates of 3 technical replicates.

Persister assays

Persister assays were performed using ofloxacin, as described in Allison *et al* [89]. Stationary-phase cultures of WT UTI89 and UTI89Δ*ubiI* (grown in LB for 16 h, 37°C) were

subjected to 5 mg/mL ofloxacin for 4 h, followed by a 1 h exposure to 20 mg/mL ofloxacin. Samples were withdrawn for CFU enumeration, prior to each ofloxacin exposure. Susceptibility assays were repeated 3 times. The average percent survival from the 3 independent experiments is reported.

Biofilm assay

The effect of BLI on pre-formed colony biofilms was evaluated. Overnight cultures were normalized to a starting OD_{600} of 0.05. Agar plates were spotted with 10 μL of bacterial inoculum. Plates were left to grow in the dark at RT for 3 days. After 3 days of growth, half of the plates were irradiated with BLI_{455} at 120 J/cm^2. Plates were then placed in the dark at RT for 2 additional days. On day 5-post seeding, the diameters of unexposed and exposed biofilms were measured. Experiment was repeated with 3 biological replicates of each strain.

RNA extraction and qPCR

Refer to the "RNA extraction and qPCR" section of Chapter 2 for more specific methods. RNA extraction, DNAse treatment, reverse transcription, and real-time quantitative (q) PCR were performed as previously described [93]. qPCR analysis was performed with five concentrations of cDNA (100 ng, 50 ng, 25 ng, 12.5 ng, 6.25 ng) each in triplicate for each sample, and internal DNA gyrase (*gyrB*) levels were used for normalization. The following primers (Integrated DNA Technologies) were used for amplification: *hemC*_Fwd (5'—ATTTGTTCGGCATCTTGCGG—3'), *hemC*_Rev (5'—AATACCCGTCTCGAAGGCG—3'), *hemY*_Fwd (5'—GCCATTGATGGGATGATATCCA—3'), *hemY*_Rev (5'—TAATGAAAACCATGCAGCACG—3'), *gyrB*_L (5'—GATGCGCGTGAAGGCCTGAATG—

3'), *gyrB*_R (5'—CACGGGCACGGGCAGCATC—3'). The following probes (Applied Biosystems) were used for quantitation; *hemC* (5'—6FAM-CTCGGCGTAGCTACCAATTGG-MGBNFQ—3'); *hemY* (5'—6FAM-TAACTTCCAGCAGCTTATCCAC-MGBNFQ—3'); *gyrB* (5'—VIC-ACGAACTGCTGGCGGA-MGBNFQ—3'). Experiments were performed with at least 3 biological replicates of 3 technical replicates.

RESULTS

Strain- and Growth-phase specific responses to BLI_{455} for different *E. coli* strains

Much of the previous work evaluating the efficacy of BLI at 455 nm (BLI_{455}) in growth reduction of *E. coli* and other Gram-negative bacteria, investigated only one strain from each bacterial species [15, 27, 28, 51, 54, 56, 133]. While analyzing a single, model strain, provides an initial basis for comparison, understanding how different strains within a species respond to BLI is essential to develop successful therapeutic approaches against them, especially given the strain heterogeneity within species like *E. coli* [134].

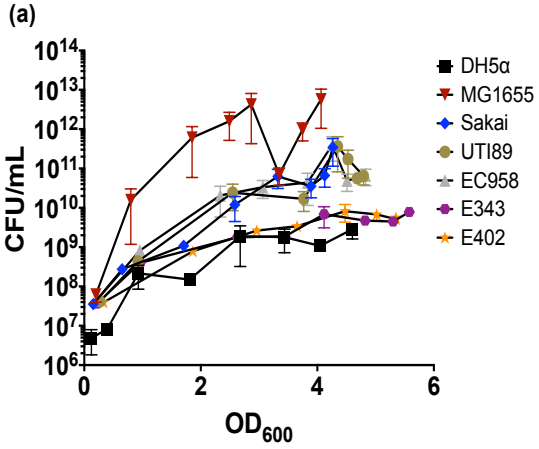

(b)

Strain	Generation time (min)
DH5α	9.92
MG1655	7.87
E343	11.69
E402	12.39
Sakai	9.64
UTI89	9.92
EC958	9.82

Figure 3.2. Growth rate heterogeneity exists between *E. coli* strains. Growth curves of *E. coli* strains ranging from non-pathogenic lab-engineered strain DH5α; commensal strains MG1655, E343, and E402; enterohemorrhagic strain Sakai; and uropathogenic *E. coli* (UPEC) strains UTI89 (cystitis isolate) and EC958 (multi-drug resistant isolate). Measuring the optical density alone can sometimes be misleading, depending on the surface factors of a particular strain, therefore the (a) growth curve is presented as colony forming unit per milliliter (CFU/mL) vs. OD600 for the seven strains. (b) To account for the varying growth rates, the generation time was measured between hours 2 and 4 for each strain. MG1655 has the fastest growth rate (lowest generation time); however, looking at OD600 alone, MG1655 appears to grow slower than every other strain tested. Growth curve experiments were repeated at least 3 times independently. Error bars represent the standard error mean.

E. coli strains belong to different phylogenetic groups, of which B2 and D harbor most pathogenic strains; while, B1 mostly comprises non-pathogenic strains. A range of strains from A, B1, B2, D, and E phylogenetic groups were selected for these analyses. The different strains were first evaluated for growth rate differences to pinpoint exponential, transition and stationary phase times for each one (**Figure 3.2a**). These analyses revealed differences in the growth rates of these strains, with the non-pathogenic strain MG1655, a K-12 derivative, exhibiting a generation time of ~8 min during exponential phase (**Figure 3.2b**). The uropathogenic *E. coli* (UPEC) isolates UTI89 and EC958, enterohemorrhagic *E. coli* (EHEC) strain Sakai, and the non-pathogenic lab-adapted DH5α, which is an MG1655 derivative, had nearly identical generation times (~9-10 min); while, the commensal E343 and E402 had a slower generation time of ~12 min (**Figure 3.2b**).

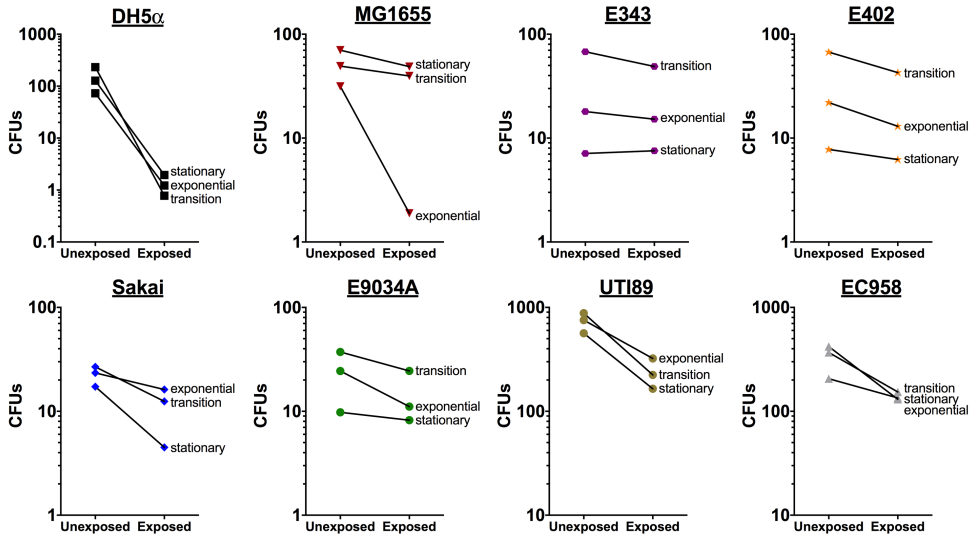

Figure 3.3. CFU reduction of different *E. coli* strains in response to BLI_{455} at different growth phases. Comparison of CFUs for unexposed and exposed samples during exponential, transition, and stationary growth phases. The following strains are represented: phylogenetic group A strains DH5α (laboratory-adapted) and MG1655 (K-12); group B1 strains E343 and E402 (non-pathogenic isolates); group B2 UPEC strains UTI89 and EC958 (multi-drug resistant); group D ETEC strain E9034A; and group E EHEC O157:H7 strain Sakai. Symbols represent the mean of independent experiments. Data represents the mean of 3 or more independent experiments.

Each strain was then tested for susceptibility to BLI_{455} at their corresponding exponential, transition and stationary growth phases, using the workflow depicted in **Figure 2.2**. Of all strains

tested, only DH5α displayed ~1.5-2.5 logs of decrease in CFUs following BLI_{455}, and this reduction was conserved during all phases of growth (**Figure 3.3**).

During stationary and transition phases, MG1655 exhibited a minimal trend in CFU reductions as a result of BLI_{455}; though, nearly a 1-log decrease in the amount of CFUs from the unexposed to the exposed samples was observed for this strain during exponential phase. The commensal E343 and E402 and multi-drug resistant UPEC strain EC958 exhibited modest susceptibility to the effects of BLI_{455} during all growth phases (**Figure 3.3**). The enterotoxigenic (ETEC) E9034A strain was more susceptible to BLI_{455} in exponential phase compared to transition and stationary phases where CFUs became minimally reduced (**Figure 3.3**). UTI89 and Sakai were most susceptible in stationary phase (**Figure 3.3**). These data indicate that there are strain-dependent responses to BLI_{455}. The ability to inhibit outgrowth of pre-formed colony biofilms was also assessed by treating biofilms with BLI_{455} after 3 days of growth and measuring the biofilm diameters 48 hrs after treatment. There were no differences in the size of the biofilms in unexposed and exposed samples of pre-formed biofilms with BLI_{455} with the same energy dose (120 J/cm^2) used for treatment of planktonic cells (**Figure 3.4**).

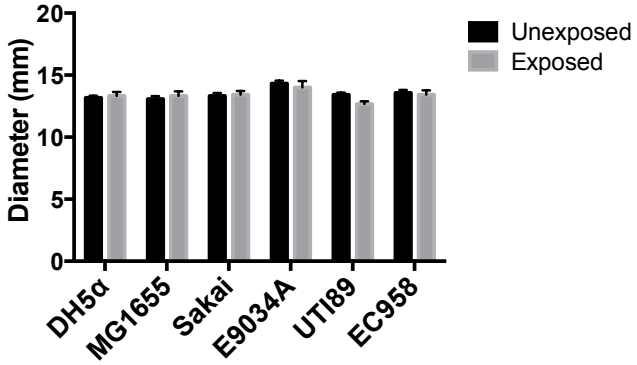

Figure 3.4. Effects of BLI on preventing pre-formed biofilms. BLI at 455 nm, 120 J/cm^2 was applied to colony biofilms after 3 days of growth. Biofilm diameters were measured 2 days after BLI (5 days after starting growth). There were no statistically significant differences in in biofilm diameter for the unexposed and exposed biofilms.

BLI_{455} and 120 J/cm^2 is not bactericidal against *E. coli*

A reduction in CFUs could be the result of bacterial cell lysis and/or altered bacterial growth. In the case of bacterial cell lysis, membranes become compromised, resulting in release of ATP to the extracellular milieu. On the other hand, altered

bacterial growth could result from a perturbation in proton flux across the inner membrane, which would lead to an overall reduction in ATP production via the ETC. An ATP quantitation assay was used to determine how BLI_{455} impacts total, intracellular and extracellular ATP levels (**Figure 2.5**). To enable accurate ATP measurements, the sample volume irradiated for the ATP assays was 50 µL, compared to 10 µL used to quantify the ability of BLI_{455} to reduce bacterial growth. The percent reduction in CFUs in response to BLI_{455} was determined for both volumes, using a representative set of strains (**Figure 3.5)**.

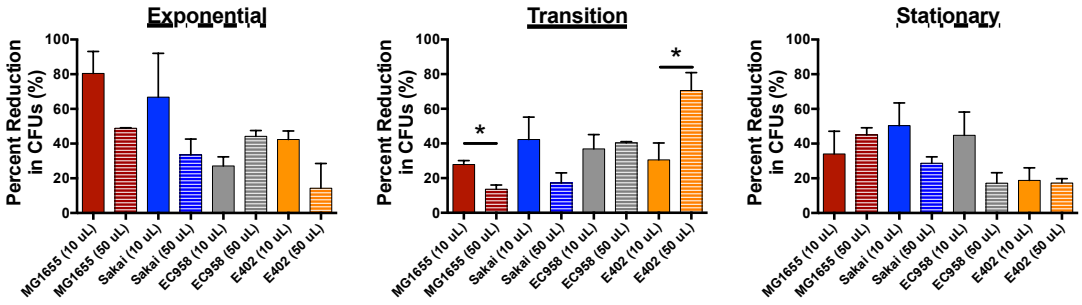

Figure 3.5. Percent reduction differences between CFUs on agar plate assay and glass slide assay. A few representative strains were chosen to show the minimal differences between BLI-induced reductions on 10 µL sample spots used in the agar plate assay and 50 µL glass slide assay. (a) Exponential, (b) Transition, and (c) Stationary growth phases. Percent reduction was calculated using Equation 2.2. All experiments were repeated 3 times and analyzed via an unpaired, two-tailed Student's *t*-test. *, $P < 0.05$.

First, the total ATP levels in bacterial samples were measured (**Figure 3.6a and Figure 2.5b**). DH5α, which had the greatest overall reduction in CFU in response to BLI_{455}, exhibited no changes in the overall ATP levels during exponential and transition phase, but had approximately a 25% reduction in ATP levels at the stationary growth phase (**Figure 3.6a**). For, MG1655 reduced ATP levels were observed in the exposed samples from exponential and stationary growth phases and corresponded to the reduction in CFUs (**Figure 3.3**). The Sakai strain, exhibited similar ATP levels between BLI and non-irradiated bacteria during exponential and transition phase and a modest reduction in ATP at stationary phase (**Figure 3.6a**). The ATP levels for strains UTI89 and EC958 were unchanged from BLI_{455} (**Figure 3.6a**). These results

suggested that BLI_{455} might induce altered ATP production or release in strains like DH5α, MG1655, and Sakai.

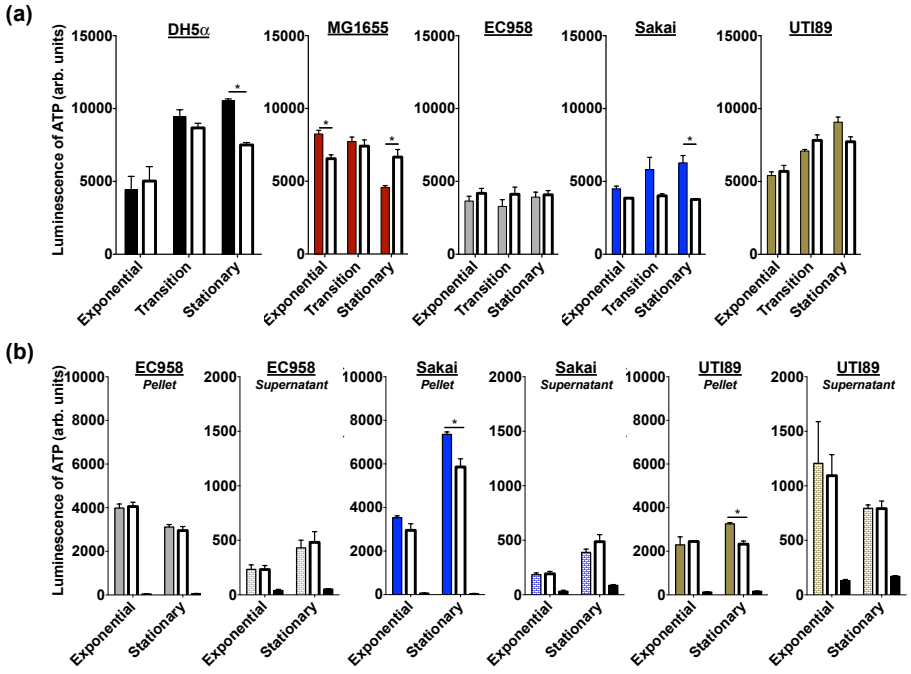

Figure 3.6. BLI_{455} is not completely bactericidal against *E. coli*. Viability assays, using an ATP release assay to measure ATP levels pre- and post-exposure to blue light. (a) The differences in relative ATP levels of unexposed (solid colored bars) and exposed (white bars) samples. (b) The differences in relative ATP in the supernatant (pre-lysed) and pellet (intact) of unexposed and exposed samples. Sakai, EC958, and UTI89 were chosen as three representative strains. Experiments were repeated 3 times. Error bars represent the standard error mean. Statistical analyses were performed via One-way Anova. *, $P < 0.05$.

ATP released into the supernatant fraction (indicative of cell lysis) was measured, as well as ATP levels in cellular pellets for three representative strains: EC958, Sakai, and UTI89 (Work flow is depicted in **Figure 2.5b**). The ATP in the supernatant and cellular fractions was measured for both unexposed and exposed samples. EC958 was the least susceptible to BLI_{455} (**Figure 3.3**). Consistent with this observation and the insignificant changes in total ATP levels in response to irradiation (**Figure 3.6a**), we saw no significant changes in extracellular and intracellular levels of ATP between exposed and unexposed samples (**Figure 3.6b**). These observations validated that, for this particular *E. coli* strain, BLI_{455} is not effective at eliminating growth. For Sakai and UTI89, there were no significant change in ATP levels during exponential phase between the unexposed and exposed supernatant fractions (**Figure 3.6b**), suggestive of no significant compromise to cellular membranes. Similarly, there were no significant changes in

the ATP levels between the cellular fractions from exposed and unexposed cells from the exponential growth phase. This was in agreement with the very modest reduction in CFUs observed during exposure in the exponential growth phase for strain Sakai (**Figure 3.3**). However, a significant reduction in intracellular ATP was observed for exposed fractions from the stationary growth phase, which was accompanied with a modest (but statistically insignificant) increase in the ATP levels in the corresponding supernatant fraction (**Figure 3.6b**). These data suggest that in the case of Sakai, BLI_{455} may exert some bactericidal effect (based on the modest increase in extracellular ATP), as well as bacteriostatic effects (based on the greater reduction in intracellular ATP that is not equivalent to the increase in extracellular ATP; note change in scale on the y-axes between pellet and extracellular measurements).

A mutant with a higher proportion of persister cells in its population is more tolerant to BLI

Persister cells are present in virtually all stationary phase cultures and have been shown to have tolerance to antibiotics, such as fluoroquinolones by exhibiting a reduced growth rate and by sustaining viable mutations that require DNA repair machinery upon post-treatment recovery [135]. In the case of persistence due to reduced growth and/or reduced expression of a stressor target (e.g. a photosensitizer), recent reports have demonstrated that reduced membrane potential in metabolically inactive persister cells is at least partly responsible for the antibiotic tolerance observed in persister cells [89]. Our lab recently discovered a UPEC mutant, UTI89Δ*ubiI (*formerly reported as Δ*visC)* that is deleted for an accessory aerobic ubiquinone synthase [72, 73, 90] UTI89Δ*ubiI* (*visC*) is defective in biofilm formation [90], exhibits reduced proton motive force [72, 73] and is intrinsically resistant/tolerant to antibiotics that require energy to be transported across the inner membrane [73]. It was thus reasoned that the *ubiI* mutant should

have higher levels of persister-like cells and if such, it should also be more tolerant to BLI. To test this hypothesis, the parent strain UTI89 and the isogenic UTI89Δ*ubiI* were grown to stationary phase and these bacterial cultures were treated with increasing concentrations of the fluoroquinolone ofloxacin. The CFUs recovered post treatment in the two strains were measured. UTI89Δ*ubiI* cultures had a higher population of persister/persister-like cells compared to the wild-type parent, UTI89 (**Figure 3.7a**). Our lab previously reported that UTI89Δ*ubiI (visC)* is defective in biofilm formation [90]. Thus, upon recovery of the populations in LB media, the ability of the recovered UTI89 and UTI89Δ*ubiI (visC)* cells to form biofilms was tested. Recovered UTI89Δ*ubiI (visC)* cells from the ofloxacin treatment remained defective in their ability to produce wild-type levels of biofilm (**Figure 3.7b**), indicating that no mutations accumulated in this population that altered a previously observed phenotype in UTI89Δ*ubiI (visC)*. Having established that UTI89Δ*ubiI (visC)* populations comprise higher levels of persister/persister-like cells, UTI89Δ*ubiI (visC)* were subjected to BLI during different phases of growth and reductions of CFUs were measured, as well as changes in ATP levels as a proxy to viability. The results indicated that significantly more UTI89Δ*ubiI* CFUs were recovered after BLI treatment during transition and stationary phases of growth compared to WT UTI89 (**3.7c**), suggesting that at these time-points the elevated numbers of persister/persister-like cells may be impervious to BLI. Subsequent measurement of live and dead cells using an ATP release assay indicated that in the *ubiI* mutant, the levels of dead cells were higher in the exponential phases of growth, compared to WT UTI89 (**Figures 3.7d and 3.6**). However, upon entry to stationary phase, the numbers of killed bacteria in UTI89Δ*ubiI* diminished (**Figure 3.7d**) indicative that persister cells have increased tolerance to BLI.

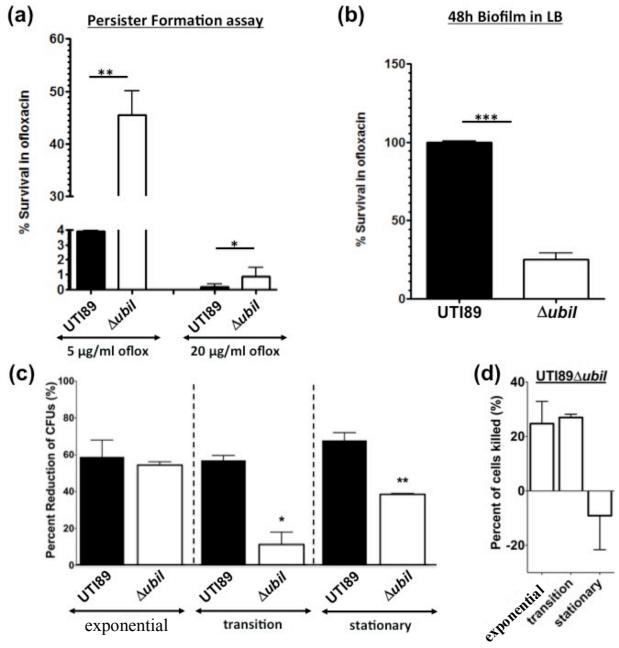

Figure 3.7. UTI89Δ*ubiI* contains more persister cells in stationary phase and exhibits higher tolerance to BLI (a) Graph depicts CFUs recovered for WT UTI89 (black) and UTI89Δ*ubiI* post exposure to 5 μg/ml and then 20 μg/ml ofloxacin. Percent survival is reported using the average of three independent experiments. (b) Graph depicts percent biofilm formation on PVC plates of WT UTI89 and UTI89Δ*ubiI* CFUs that were propagated from the CFUs recovered after ofloxacin treatment. Biofilm production for Δ*ubiI* was normalized to the WT UTI89 OD_{565} reading, which was arbitrarily set at 100% (c) CFU reduction percentage comparison by growth phase of WT UTI89 and UTI89Δ*ubiI* after BLI. Percent reduction was calculated using Equation 2.2. Statistical analyses were performed using a two-tailed unpaired *t*-test with Welch's correction, $P < 0.05$ (95% confidence interval) considered significant. *, $P < 0.05$; **, $P < 0.01$. (d) Determination of viability using an ATP release assay to measure ATP levels pre- and post-exposure to blue light. Negative values represent an increase in ATP levels post-exposure. Percent of cells killed was calculated using Equation 2.4. Statistical analyses were performed using One-way ANOVA with $P < 0.05$ (95% confidence interval) considered significant. All experiments were repeated a minimum of 3 times. Error bars represent the standard error mean.

The expression of genes encoding porpyhrin biosynthesis components is not significantly affected by BLI in uropathogenic *E. coli*

Studies have suggested that porphyrins (which are synthesized during heme production) or flavins may serve as endogenous photosensitizers in bacteria [2, 14, 16, 45, 54, 55, 60-65, 110]. Ubiquinones are another set of moieties that can absorb visible blue light [109]. Reduction in bacterial growth has been seen in a porphyrin content-dependent manner, i.e. the more porphyrin that is exposed to blue light, the more reduction in growth [11, 12, 64, 65]. In addition, porphyrin production differs among bacteria, thus contributing to species-specific responses to BLI [2, 16, 39, 44, 45, 61-67].

The ATP release assay for WT UTI89 and UTI89Δ*ubiI* indicated an inverse phenotype between the two isogenic strains with regard to viability during exponential phase of growth. Previous studies demonstrated that deletion of *ubiI* in *E. coli* diminishes the amounts of ubiquinone during aerobic growth, but is dispensable during anaerobiosis [72]. As in the case in K12 *E. coli*, deletion of *ubiI* in UPEC strain UTI89 leads to reduced production of pmf under

aerobic growth, indicating a similar defect in ubiquinone levels [73]. Recently it has been shown that loss of *ubiI* reduces the expression of *cydA*, which is a heme-binding protein that forms part of cytochrome bd-I in *E. coli* [73]. To determine if the basis of the inverse relationship between WT UTI89 and UTI89Δ*ubiI* viability during exponential growth was due to altered porphyrin/heme biosynthesis in the two strains, the transcript levels of two porphyrin-biosynthetic genes, *hemC* and *hemY* were measured (**Figure 3.8a**) in BLI-treated cells and compared them to the transcript levels obtained for BLI-treated and untreated WT UTI89. The *hemC* and *hemY* genes were chosen as they encode enzymes at different steps upstream (HemC is further upstream) of the final porphyrin production (**Figure 3.1**). The results indicated no differences between the two strains (**Figure 3.8a**), suggesting that there are no changes in the transcription of the porphyrin biosynthesis pathway in the absence of *ubiI*. These data suggest that BLI at the conditions tested may act through non-porphyrin photosensitizers such as ubiquinones or flavins, or that BLI affects the abundance, but not the transcription of porphyrins.

Baseline transcript levels were determined for the porphyrin biosynthetic genes between different strains of *E. coli*. qPCR analyses comparing UTI89 and the multi-drug resistant EC958 revealed no significant differences in *hemC* (**Figure 3.8b**) and *hemY* (**Figure 3.8c**) transcript

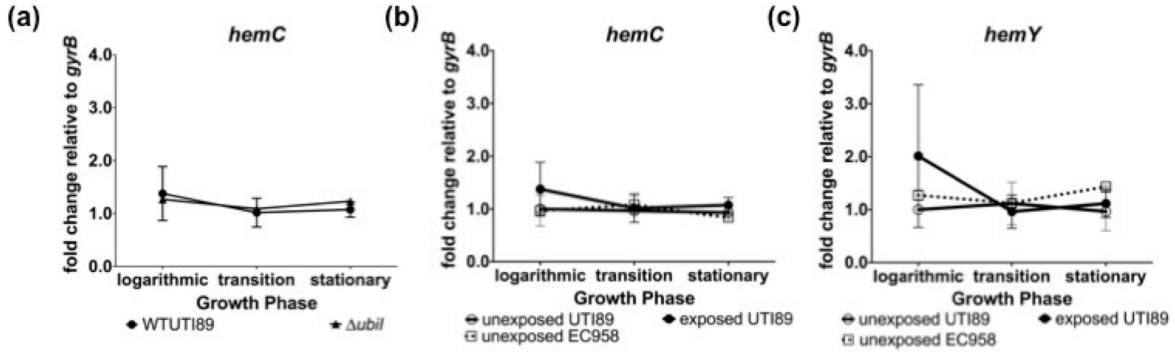

Figure 3.8. qPCR steady-state transcript levels of heme biosynthesis genes in UTI89, EC958 and UTI89Δ*ubiI*. Lines depict the transcript fold changes relative to the endogenous control, housekeeping gene, *gyrB*. Bars represent the corresponding percent log reduction in CFUs. The unexposed mid-exponential phase was arbitrarily set to 1. Unexposed samples were normalized to transcript levels in mid-exponential phase. Exposed samples were normalized to the corresponding unexposed growth phase. (a) *hemC*: exposed WT UTI89 vs. UTI89Δ*ubiI*. (b) *hemC*: unexposed EC958 (open square) vs. unexposed UTI89 (open circle) vs. exposed UTI89 (closed circle), (c) *hemY*: unexposed EC958 vs. unexposed UTI89 vs. exposed UTI89. Experiments were repeated 2 times. Error bars represent the standard error mean. Statistical analyses were performed using a Two-way ANOVA with $P < 0.05$ (95% confidence interval) considered significant.

abundance between the two strains and between growth phases, suggesting that at least on the transcriptional level, there are no significant differences in the expression of porphyrin-biosynthetic genes in two different uropathogenic *E. coli* strains. The changes in the percent reduction of UTI89 CFUs did not correlate with the invariable transcript levels of porphyrin encoding genese, *hemC* and *hemY* (**Figures 3.3 and 3.8**). These observations suggest that either porphyrins do not play a large role in the *E. coli* BLI_{455} response or that, while transcript levels do not change in response to treatment, porphyrin levels could change post-transcriptionally. Alternately, BLI_{455} may influence the expression or abundance of different *E. coli* photosensitizers, such as flavins, or ubiquinones.

DISCUSSION

In this study, BLI-induced growth reduction and bactericidal activity during different growth stages of non-pathogenic, pathogenic, and multi-drug resistant (extended spectrum beta-lactamase producers) *E. coli* strains were evaluated to determine intra-species variation. Growth phase influences blue light-mediated growth reduction in some of the tested strains of *E. coli* and the multi-drug isolate tested in this study displayed the highest BLI tolerance. Evaluation of a mutant deficient in ubiquinone synthesis and generation of pmf, indicated significantly higher tolerance of this mutant to the effects of BLI. This mutant, UTI89Δ*ubiI*, was shown to contain higher numbers of persister cells in planktonic cultures, compared to the wild-type parent. Evaluating the bactericidal efficacy of BLI on all strains tested in our studies demonstrated that BLI treatment at the wavelength and energy dose tested is bacteriostatic and not bactericidal. These findings suggest that BLI may be inducing a metabolically inactive/persister-like

phenotype in *E. coli* that leads to an apparent reduction in colony forming units, which does not correspond to cell death.

A comparison was made on the responses of several *E. coli* strains to BLI_{455}. While the 455 nm wavelength is used in numerous applications, including the treatment of jaundice in neonates, no studies have characterized the behavior of irradiated bacteria in a strain- and growth phase-dependent manner. Numerous studies have elegantly shown that there is extensive heterogeneity in bacterial populations, which changes as a function of external stimuli and as a function of the bacterial growth phase [114-121]. In addition, bacteria that are commonly associated with humans and other mammalian/vertebrate hosts are not typically growing exponentially, but are rather found in an extended stationary phase. Examining the bacterial responses in more physiologically relevant situations is essential. Here, we evaluated how BLI_{455} influences bacterial viability and growth in different strains of *E. coli*, as a function of the growth phase during irradiation.

These studies demonstrated that BLI_{455} treatment of *E. coli* leads to a strain- and growth phase-dependent reduction in growth, but not viability. This observation suggests that the use of BLI as an antimicrobial strategy may retard the growth of some strains, possibly including commensals, while conferring an advantage to pathogenic or opportunistic bacteria; or bacteria found at a different phase of growth; or strains with higher numbers of persister cells in their populations. The finding that BLI_{455} and 120 J/cm^2 is not bactericidal has wide-ranging ramifications in the way PDT may be used to treat or prevent infections. Viability assays indicated that although differences were observed in the countable CFUs of the different *E. coli* strains in response to BLI, the majority of irradiated cells were still viable, based on their ATP signature (**Figures 3.3 and 3.6**). This phenomenon was true for pathogenic and non-pathogenic

strains, suggesting that the mechanism of tolerance to BLI is conserved across the species and what may vary are the extent and/or severity of the response.

The accepted model describing the BLI mechanism of cytotoxicity is damage from the generation of reactive oxygen species (ROS), as has been observed and documented, especially for near-UV wavelengths [11, 12, 14, 45, 50, 54, 55, 58, 110]. Studies have also indicated that low-level stimulation of ROS can enhance proliferation of bacterial growth, with the resulting daughter cells sometimes exhibiting altered replication rates [2, 11-15]. This role of ROS could be one of the reasons of the reduced growth observed in response to BLI. Furthermore, lowering of the pH has been shown to protonate the cell membrane and "revive" bacteriostatic cells, indicating that in a biological application and in the optimal environment BLI-treated bacteria may revert to a viable, replicating state [127-130]. Therefore, it is possible that at wavelengths near 455 nm, irradiation of *E. coli* (and possibly other Gram-negative species) could lead to a persister-like state that can revive under appropriate conditions. This possibility raises questions with regards to long-term consequences in cases when BLI is used on areas that teem with bacterial communities, such as the human skin. For example, phototherapy at 455 nm is routinely used to treat jaundiced neonates. What are the consequences of these treatments on the emerging skin microbiota? This question would be very interesting to pursue in a longitudinal fashion, especially in the context of pre-maturely born neonates.

The mechanism by which pathogenic and commensal *E. coli* are able to tolerate BLI is not yet known. Why Gram-positive bacteria are more sensitive to the effects of visible light-induced growth reduction as compared to Gram-negative bacteria is also unknown. After screening a library of mutants, there was no significant change in growth reduction for surface factor mutants that vary between Gram-positive and –negative bacteria (data not shown). The

lack of a direct relationship in porphyrin transcript levels and reduction of CFUs suggest that another photosensitizer is playing a role in the phototoxic response. However, it is possible that actual porphyrin levels change, versus transcript levels, in response to BLI.

Notably, while the nominal wavelength of the light used was at 455 nm, LED light sources like the device we used, encompass a wavelength emission range of 420-495 nm. The emission intensity decreases as the wavelength gets farther from 455 nm, with a 70% intensity decrease at 455 ± 15 nm and a near 100% decrease at 455 ± 35 nm. The reduction response may therefore be attributed to another photosensitizer absorbing sub-optimally in the 420-490 nm wavelength range. Another photosensitizer of interest is flavin, which has an absorption peak around 450 nm. Flavins are incorporated in a number of ubiquinone synthases such as UbiI [72, 136], the deletion of which further protected *E. coli* from BLI.

In summary, these studies demonstrated a non-bactericidal effect of BLI on *E. coli* growth and demonstrated significant differences in intra-species responses to BLI. In addition, these studies suggest a persister-like response to BLI by *E. coli* that may facilitate survival in the presence of BLI stress. It is thus imperative to further study this phenomenon, given the important implications of the persister-state in recalcitrant and biofilm-related infections [131, 132].

CHAPTER 4

THE BLUE LIGHT SENSOR USING FLAVIN ADENINE DINUCLEOTIDE IS NEEDED TO REDUCE THE GROWTH OF UROPATHOGENIC *Escherichia coli* AT 455 nm

ABSTRACT

The BLUF (blue light sensor using flavin adenine nucleotide) family is one of six photoreceptor families representing bacteria and lower eukaryotes. In various organisms, the BLUF domain has been shown to be necessary for the sensing of blue light. In addition, published studies have shown that defects in the BLUF domain lead to defects in motility, biofilm formation, and other virulence factors. It has been reported that an effector domain interacts with the BLUF domain in the signaling pathway to result in downstream changes. In Chapter 3 it was shown that blue light irradiation (BLI), without the use of an exogenous photosensitizer, the amount of *E. coli* colony-forming units (CFUs) can be reduced *in vitro*. To understand the role of the BLUF domain in BLI-induced CFU reductions, both the *bluF* and *bluR* genes were mutated. *bluR* encodes for a transcriptional regulator and reported repressor to BluF, in a K12 strain of *E. coli*. In this study, it is reported that deletions in the *bluF* and *bluR* gene do not negatively impact growth, biofilm formation or motility in an uropathogenic strain of *E. coli*. In fact, an increased tolerance to BLI is observed when either *bluF* or *bluR* are deleted, specifically at 455 nm; this observation does not hold true at 420 nm and 470 nm wavelengths. Based on this data, it can be deduced that in response to BLI at 455 nm (BLI_{455}), both BluF and BluR are needed. The data also suggests that an additional BLI response pathway that seems to have a broad wavelength effect, at least in the blue range tested, may be playing a role in low levels of reduction.

INTRODUCTION

Light is an essential part of survival. Organisms from every kingdom have unique ways to sense and respond to the presence or absence of light through some type of photoreceptor [137]. In general, photoreceptors control a diversity of biochemical processes, including kinase activity, phosphodiesterase activity, DNA binding, and protein degradation [19, 25, 32]. Photoreceptors cannot only sense the presence of light, but also the quality and quantity of the light [32]. Responses to light vary from behavioral changes to phototaxis and photosynthesis to biofilm formation and virulence regulation [27, 64, 65, 138-141]. There are six photoreceptor families that respond to light: BLUF (blue light sensor using flavin adenine dinucleotide-FAD) domains; cryptochromes; LOV (light, oxygen, voltage) systems; photoactive yellow protein (PYP); phytochromes; and rhodopsins; the first three which respond specifically to blue light through flavin chromophores [31, 137].

The BLUF domain has been reported in various bacteria and lower eukaryotes including *Rhodobacter sphaeroides* [17], *Acinetobacter baumannii* [140], *Escherichia coli* [18, 25], *Euglena gracilis* [142] and cyanobacterium *Synechocystis* sp. PCC6803 [33]. In BLUF photoreceptors, the flavin portion is the photosensitizer and absorbs the light, leading to a signaling state change and resulting in a 10 nm red-shift in absorption [20, 30, 33]. A sequence of about 100 amino acids makes up the BLUF domain, in which a FAD chromophore is non-covalently bound [17, 19, 23]. The BLUF domain was discovered in the AppA protein in *Rhodobacter sphaeroides*. It was found that AppA not only responded to blue light, but also to reduction-oxidation signals, allowing for an interaction between the two signals [60, 138]. In many organisms, the BLUF domain modulates a corresponding effector domain, which in some cases is directly fused to the photoreceptor [23]. This blue light sensor has been shown to

regulate factors such as biofilm production, motility, and lead to attenuation of virulence factors, resulting in a higher susceptibility to reduction by blue light [2, 27].

In 2002, it was reported that in *E. coli* the BLUF protein, YcgF (also named BluF by [28]; also named BlrP-blue light regulated phosphodiesterase by [25]), an N-terminal BLUF domain, is linked to a C-terminal EAL domain that exhibits cyclic-di-GMP-specific phosphodiesterase activity [19]. Like the histidine kinase in two component systems, EAL domains are usually linked to sensory input domains [70, 143, 144]. However, in 2009 Tschowri et al. reported that in *E. coli*, the BLUF protein, BluF, acts by direct protein-to-protein interaction with YcgE (also named BluR [28]), a MerR-like repressor, to undock BluR from its DNA. They concluded that while other BLUF proteins have cyclic-di-GMP phosphodiesterase activity, the BLUF protein in *E. coli*, BluF, does not have PDE activity and instead directly interacts with BluR [27]. In a later manuscript on the possible evolution of the BluF/BluR system, Tschowri et al. hypothesized that BluR evolved from a phosphodiesterase, but now acts directly as an antagonist for BluF [28].

In *R. sphaeroides*, the BLUF protein, AppA, also interacts with a repressor, PpsR [33, 145]. In the presence of blue light, AppA cannot interact with PpsR and allows the repressor to bind to various promoters and inhibits the transcription of these genes [33]. Nakasone et al. reported that BluF also has the potential to serve as a temperature sensor, due to the temperature-dependent conformational changes when exposed to blue light irradiation [146]. It has also been suggested that BLUF domains play a role in responding to oxidative stress [63, 113].

Much work has been done to model the structure of the BLUF domain and find the basis of the red-shift of the flavin moiety upon blue light exposure, but not much work has been done to understand what role the BLUF domain plays in reducing bacterial growth. In many studies it

has been suggested that the blue light response is triggered by redox reactions and/or structural rearrangements of the flavin chromophore, leading to an induction of an excited signaling state of the photoreceptor [53]. Upon photo-excitation, the BLUF domain is believed to dimerize [21, 24-26].

Commonly accepted ideas hold that glutamine and tyrosine are essential for the activation of the BLUF domain to occur; when these two amino acids are missing, photoactivation of the BLUF domain does not occur [22, 29, 53]. It is also an accepted thought that proton-coupled electron transfer occurs shortly after photon absorption of the dark state [53]. In 2008, Domratcheva et al. published that absorption of a photon by the flavin resulted in a change in an amino acid residue and not the chromophore itself [17].

In a non-pathogenic strain of *E. coli*, MC4100 (K-12 strain), the BluF protein was found to directly bind to and release the MerR-like repressor, BluR, from its operator DNA, regulate biofilm formation and down-regulate curli production [27]. In some pathogenic *E. coli*, the ability to form biofilms is a crucial step in the virulence pathway. To date, no studies have been conducted on the BluF/BluR system in a pathogenic *E. coli* model to understand the possible role of the BluF blue light sensor in pathogenesis. The goal of this work was to investigate the role of BluF and BluR in reducing bacterial growth, the signaling pathway, and its potential impact in virulence.

In this study, the role of both BluF and BluR in the response to blue light irradiation (BLI) in the 420-470 nm wavelength range were investigated, in addition to their importance in factors that lead to elaboration of virulence strategies.

MATERIALS AND METHODS

Strains and constructs

The following *E. coli* strains were used: UTI89 (UPEC cystitis isolate (Mulvey et al., 1998)), UTI89Δ*bluF*, and UTI89Δ*bluR*. Non-polar deletion of the *bluF* and *bluR* genes in strain UTI89 was performed using λ Red Recombinase-mediated recombination as previously described [147]. The primers *ycgF* (*bluF*)_KO_Fwd: AATCTCCGTCGCCTCTACACGACCCAATAATACTTTGTACAATATATGCTAAAATTG GTGTAGGCTGGAGCTGCTTC / *ycgF* (*bluF*)_KO_Rev: ATTGCATCATTTAAATGACAACCTATACAGGTTTTTTCGCCAAACCGTCTTCAACCAT ATGAATATCCTCCTTA*G* were used for the *bluF* knockout and *ycgE* (*bluR*)_KO_Fwd: TGAATTCTCCCGGTGGGCATTTTGCAACGGACCAGCTCCGCTACAAACGTGTAGGCT GGAGCTGCTTC / *ycgE* (*bluR*)_KO_Rev: GTATTATTGGGTCGTGTAGAGGCGACGGAGATTTATGATCGCAAGGAGGCATATGA ATATCCTCCTTAG primers were used for the *bluR* knockout. Verification of the *bluF* deletion was performed using primers flanking the *bluF* sequence: *ycgF* (*bluF*)_Test_Fwd: GATCATAAATCTCCGTCGCCT / *ycgF* (*bluF*)_Test_Rev: CAATGCATTACGATAAAACATATTGC. Verification of the *bluR* deletion was performed using primers flanking the *bluR* sequence: *ycgE* (*bluR*)_Test_Fwd: TGAAAGGGGGATTACC TGAATTCTC / *ycgE* (*bluR*)_Test_Rev: AGCATATATTGTACAAAGTATTATTGGGTCG.

Culture conditions

Refer to the "Bacterial strains and culture conditions" section in Chapter 2 for more detailed methods. Bacterial cultures were seeded in lysogeny broth (LB) and incubated at 37°C

while shaking overnight. Aliquots of overnight cultures were sub-cultured in 15 mL fresh LB the following morning, and normalized to a starting optical density (OD) at 600 nm of 0.05. Sub-cultures were incubated at 37°C under shaking conditions for all analyses described.

Growth curves

Bacteria were inoculated as described in the section above. A 120-µL aliquot was removed from each time point. Of each aliquot, 100 µL were diluted in 900 µL fresh LB and the OD at 600 nm (OD_{600}) was recorded using a Thermo Scientific NanoDrop 2000 spectrophotometer. The remaining 20 µL were then serially diluted in 180 µL of LB for plating and counting of colony forming units (CFUs). A multichannel pipette was used to spot 8 different dilutions with 5 technical replicates per dilution. Incubation occurred overnight at room temperature. Growth curve experiments were repeated at least 3 times.

Motility assays

Refer to the "Motility assay" section in Chapter 2 for more detailed methods. Motility assays were performed as previously described [92]. Briefly, strains were stabbed in soft LB agar and incubated at 37°C for 7 h in the presence of atmospheric oxygen. Motility was recorded as the diameter (in mm) containing bacteria migrating away from the inoculation point.

Biofilm assays

Refer to the "Biofilm assay" section in Chapter 2 for more detailed methods. Strains were grown exponentially in 3 mL Lysogeny Broth (LB) and normalized to an OD_{600}=1. Cultures were then diluted 200-fold in fresh LB and used to seed biofilm plates. Biofilm assays in LB at

room temperature were performed in 96-well PVC plates as previously described [91] and quantitatively measured 48 h post-seeding, using crystal violet [148].

In vitro light delivery to *E. coli*

Refer to the "*In vitro* delivery to *E. coli*" section in Chapter 2 for more detailed methods. Cultures were set up as described above. Aliquots were obtained for irradiation and plating during exponential (T = 3 h), transition (T = 5 h) and stationary (T = 8 h) growth phases. BLI was carried out with a Thorlabs Mounted High-Power LED lamp at 420 nm, 455 nm, or 470 nm and controlled by a high-powered LED driver (Thorlabs DC2100). A total energy dose of 120 J/cm^2 was delivered to each sample. Irradiated and non-irradiated controls were then incubated overnight at ambient temperature. CFUs were counted the following day. Experiments were performed with at least 3 biological replicates of 3 technical replicates. WT UTI89 was used as a control for comparison for analyses by growth phase.

Reduction determination

To determine the percent change in exposed versus unexposed CFUs, the CFUs post-irradiation were enumerated and compared to the CFUs of corresponding, non-irradiated spots. The reductions in CFUs post-BLI were calculated using **Equation 2.2**.

Viability assay

Refer to the "Viability assay" section of Chapter 2 for more specific methods. CellTiter-Glo Luminescent Cell Viability Assay (Promega) was utilized to determine cell viability. Luminescence values of ATP were measured using a SpectraMax i3 (Molecular Devices). Luminescence was also determined for wells filled only with LB to subtract background luminescence due to the media. **Equation 2.4** was used to calculate the percent of non-viable cells. A standard curve was determined using ATP disodium salt hydrate (Sigma) to quantify the amount of ATP present pre- and post-exposure. Experiments were performed with at least 3 biological replicates of 3 technical replicates.

RESULTS

UTI89 Δ*bluF* and Δ*bluR* are more tolerant to the effects of BLI_{455} in transition and stationary growth phases

After exposing WT UTI89, Δ*bluF*, and Δ*bluR*, to BLI at 455 nm (BLI_{455}) at 120 J/cm^2, a tolerance to BLI with the Δ*bluF* and Δ*bluR* strains in both the transition and stationary growth phases was observed (**Figure 4.1a**). The reduction in CFUs was significantly less than the WT strain. BLUF systems have been reported to be photoprotective [25], but interestingly enough the strains survive better when the BLUF system is removed. The observed results suggest there is interconnectivity between *bluF* and *bluR*. Regardless of which component of this BluF/R system is missing, an increased tolerance to BLI_{455} is observed. The acquisition of blue light is diminished when the FAD component is not present to absorb the light. Interestingly, even when the *bluF* gene is present (in the Δ*bluR* strain), WT levels of reduction in transition and stationary

phases were not achieved; this observation points to the fact that downstream effects leading to reduction are dependent on the signaling pathway/interaction between BluF and BluR.

It was important to ensure the observed increased tolerance when either the *bluF* or *bluR* genes were missing was not due to a defect in growth, an energy deficiency, or a repression in virulence factors. As shown in **Figure 4.1b** there were no defects in growth of the two mutant strains. In fact, the mutant strains appear to be growing slightly better than the WT isogenic parent.

Hadjifrangiskou et al. have published significantly on the importance of biofilm formation in the virulence strategy of uropathogenic *E. coli* [74, 90, 149, 150]. In **Figure 4.1c**, after 24 hours, there was no significant difference between the Δ*bluF*, Δ*bluR*, and WT UTI89 strains in their abilities to form biofilms. The Δ*fimA-H* strain serves as a negative control because it is missing the genes required for type 1 pili formation, which have been shown to be a necessity in biofilm formation [151].

To ensure that a deletion in the BLUF domain did not have an effect on its energy transport, a highly energetic reporter assay was used. This was necessary because FAD is heavily involved in energy transport and a key component in the electron transport chain. In *E. coli*, motility is powered by a flagellum. During the assembly process of flagella and during movement, a large amount of energy is consumed [152]. If there are energy defects, motility will likely be impacted. Therefore, motility was used as the output to assess potential energy defects that arose from the deletion of *bluF* or *bluR*. In the deletion strains, motility was not negatively or positively impacted (**Figure 4.1d**).

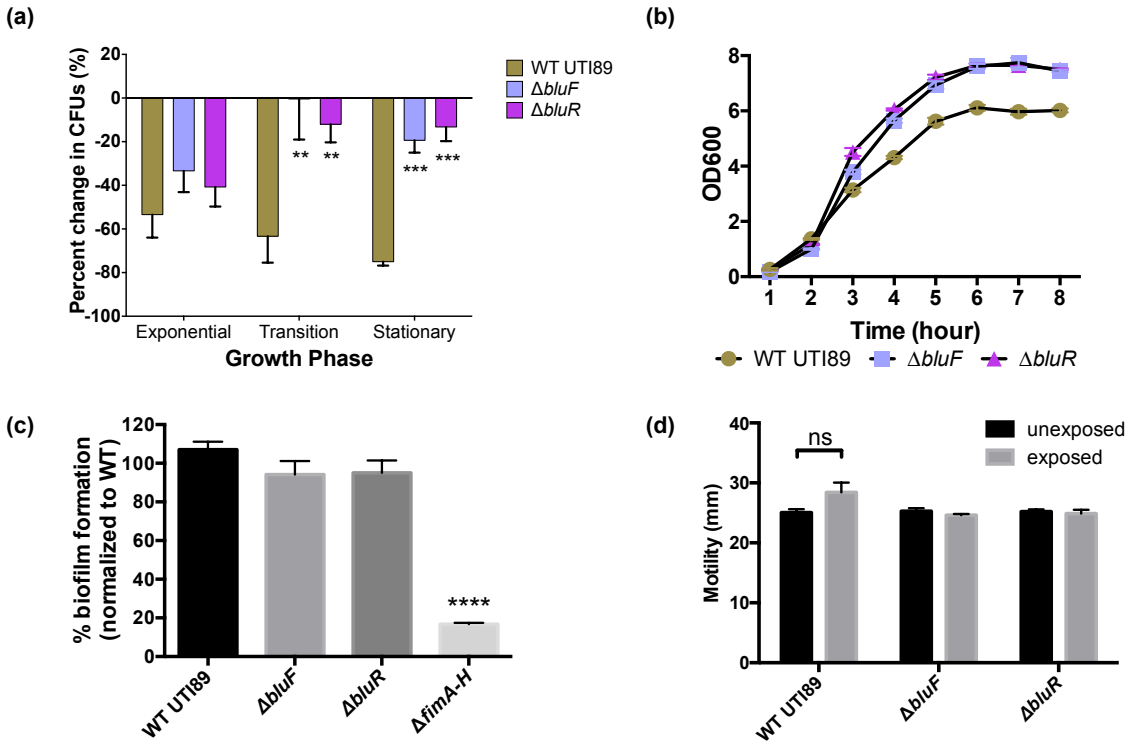

Figure 4.1. Tolerance to BLI by mutants lacking blue light sensor is not due to defects caused by mutation. . A) Comparison of percent change in CFUs post-BLI compared to CFUs pre-BLI of WT UTI89 and BLUF mutants, Δ*bluF* and Δ*bluR*. Percent change in CFUs were calculated using Equation 2.3. B) Growth curve of all strains by measuring the optical density at 600 nm. C) Biofilm formation normalized to WT biofilm formation. Δ*fimA-H* serves as a negative control because it lacks the type 1 pili necessary for biofilm formation. D) Swimming assay to assess the motility of the mutants with and without BLI. The exposed samples were irradiated at 455 nm, 120 J/cm^2 before being seeded in agar motility plates. The motility was measured in the amount of swimming that occurred from the inoculation point. Average heights of 3 technical replicates were obtained. All experiments were repeated 3 times and analyzed via One-way Anova. **, $P < 0.01$; ***, $P < 0.001$; ****, $P < 0.0001$.

To see if the presence of BLI would affect the energy-dependent motility, liquid cultures were exposed to BLI_{455} at 120 J/cm^2 before seeding motility plates. There was no observed statistical difference in motility between the unexposed and exposed strains (**Figure 4.1d**). However, in the presence of light *E. coli* has been shown to "tumble" or "phototax" away from the light source [64, 65]. There may be an effect on motility with constant BLI with bacteria attempting to "escape" the light; however, this was not investigated.

The BLUF response is specific for BLI_{455}

Based on the tolerance observed in stationary and transition growth phases with the *bluF* and *bluR* knockouts with BLI_{455}, the reduction assays were extended to additional wavelengths to investigate if this observation was replicated. A 420 nm and 470 nm lamp for BLI_{420} and BLI_{470}, respectively, was used to study the effect of different wavelengths on tolerance.

At BLI_{420}, (**Figure 4.2a**) there was a significantly higher reduction for all three strains in the exponential growth phase. Overall, BLI_{420} was more effective in reducing the CFUs. However, there was not a significant difference between the reductions in WT and the Δ*bluF* and Δ*bluR* strains at any growth phase. From this information it can be deduced that the observed reductions at BLI_{420} does not follow the same pathway as BLI_{455}. The BLUF system is likely not involved in light absorption at 420 nm since the reductions observed are independent of the BLUF system being present or absent. To fulfill the highly accepted hypothesis of ROS-mediated cytotoxicity by BLI, the photosensitizer at 420 nm would have to be different than at 455 nm. Another possibility is that BLI_{420} is causing significant DNA damage that is preventing replication. While the 420 nm wavelength is deemed as safe by the American National Standards Institute (ANSI) standards, the light source used has minimal amounts (<3%) of UV light (10-400 nm).

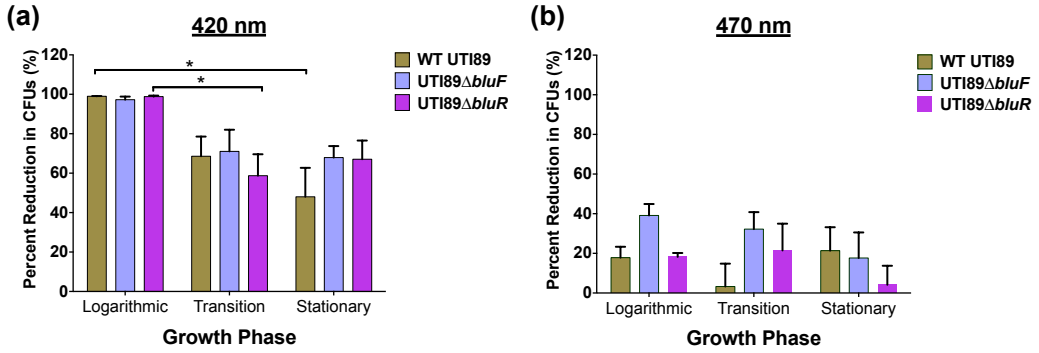

Figure 4.2. Percent reduction in CFUs of BLI_{420} and BLI_{470}. Percent reductions in CFUs of WT UTI89, Δ*bluF* and Δ*bluR* in exponential, transition, and stationary growth phases. A) BLI at 420 nm. B) BLI at 470 nm. Both experiments were repeated at least 3 independent times and analyzed via Two-way Anova. *, $P < 0.05$; **, $P < 0.01$; ***, $P < 0.001$; ****, $P < 0.0001$.

In **Figure 4.2b**, BLI_{470} is less effective in reducing the colony growth of all strains, independent of growth phase and the BLUF system. The observed reductions are 40% or less. Although the difference is not statistically significant, the Δ*bluF* knockout trends higher in reductions than WT and Δ*bluR* in the exponential and transition phase. Interestingly, when comparing the BLI_{455}-induced reductions of the Δ*bluF* and Δ*bluR* strains (**Figure 4.1a**) to the reductions at BLI_{470} (**Figure 4.2b**), the decreases in CFUs at each growth phase are within the same statistical range at the respective growth phases for each strain. The minimal reductions observed may be due to the same photosensitizer absorbing light at both wavelengths or be independent of the hypothesized reduction mechanism. When comparing the WT strain to reductions induced by BLI_{455} versus BLI_{470}, there was a significantly higher reduction with BLI_{455} than with BLI_{470} in each growth phase. This difference is indicative that the reductions observed above 20% (the WT reductions at BLI_{470}) at BLI_{455} are due to the signal transduction between BluF and BluR.

The BLI-induced reductions do not correlate with cell death

While reductions at all wavelengths tested and in each growth phase are observed, these reductions do not correlate to cell death. The total ATP difference of unexposed and exposed samples were measured to determine if BLI is bactericidal or bacteriostatic, especially at 420 nm where reductions in CFUs are the highest. Of the nearly 100% CFU reduction in the exponential growth phase at BLI_{420} of all three strains, the percent of cells killed only average between 30-40% (**Figure 4.3a**). In transition phase, the reduction in CFUs is ~60% or greater, yet there was an increase in the amount of ATP by greater than 70% post-BLI. At 470 nm, there was an increase in ATP post-BLI for all strains during all growth phases (**Figure 4.3b**). The differences in percent increases of ATP were independent of the presence or absence of the BLUF

components and growth phase, with the exception of a significantly increased amount of ATP in the WT strain in stationary phase as compared to the Δ*bluF* strain.

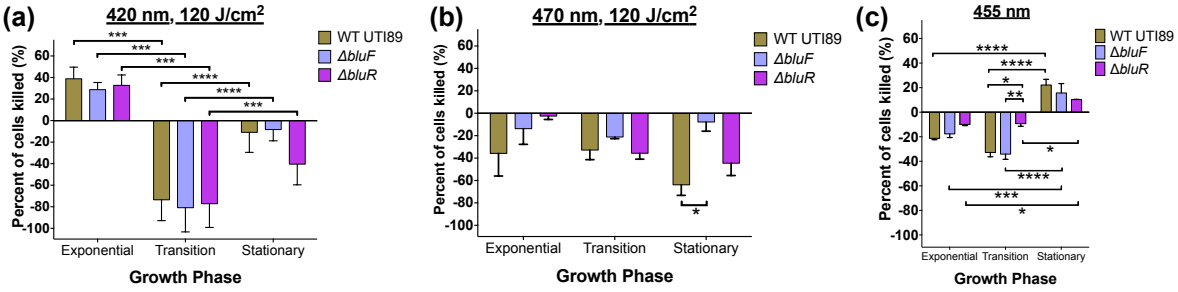

Figure 4.3. Viability of cells post-BLI. Viability was assessed by comparing the ATP levels of unexposed and exposed samples at the respective growth phases and wavelengths. Negative values of percent of cells killed correlates to an increase in ATP post BLI. Percent of cells killed was calculated using Equation 2.4. A) BLI_{420}. B) BLI_{470}. C) BLI_{455}. All experiments were repeated at least 3 independent times and analyzed via Two-way Anova. *, $P < 0.05$; **, $P < 0.01$; ***, $P < 0.001$; ****, $P < 0.0001$.

Conversely with BLI_{455}, there was an increase in ATP post-BLI in exponential and transition growth phases, but not in the stationary growth phases; this is independent of strain (**Figure 4.3c**). This was surprising, especially since the differences between the Δ*bluF* and Δ*bluR* strains are statistically significant than the WT strain in the transition and stationary phases. Within growth phases, there was only a difference in the amount of ATP with the Δ*bluR* strain in the transition phase. The increase in ATP is significantly less than both the WT and Δ*bluF* strain.

This phenomenon was also observed with various pathotypes and phylogenetic groups of *E. coli* at 455 nm (**Figure 3.5** and Mitchell et al., Microbiology, under revision). It was postulated that the increases in ATP, even when the reductions in CFUs are significant, could be due to an increase in persister-like cells. These cells are non-culturable, but viable, so would therefore have an ATP signature. It is possible that at sub-inhibitory levels, BLI serves to stimulate cell growth; this level of inhibition may be different at different growth phases and wavelengths. In low concentrations, non-singlet oxygen ROS have been shown to promote bacterial growth [11, 13, 15, 153].

DISCUSSION

Flavins have an absorption maximum around 450 nm. It is a widely accepted thought that the phototoxic effects of blue light occur by singlet oxygen generation after excitation of a photosensitizer in the presence of molecular oxygen. If flavin components are truly the photosensitizer that absorbs light at 455 nm, then it makes sense that we see less than one-third of the reduction in CFUs of Δ*bluF* and Δ*bluR* strains as compared to WT in transition and stationary growth phases.

If the BLUF system is supposed to serve a photoprotective function, it is expected that there would be greater reduction when the BluF protein is missing and not the opposite. It is speculated that resulting cytotoxicity after BLI could result from the lack of a photochemical channel for the excited photosensitizer [137]. Because of this lack, energy from an excited photosensitizer can be converted to free radicals in the presence of free molecules or ions.

What's happening in transition and stationary phases that would make *E. coli* more tolerant than WT? The significant tolerance by Δ*bluF* and Δ*bluR* strains to BLI_{455} in transition and stationary phase is indicative that the BLUF/R signaling pathway needs to be engaged to enhance phototoxic effects. However, it is not understood why there is not a significant tolerance in the exponential phase. Could there be an abundance of other FAD moieties in the exponential phase? Because the electron transport chain is highly active during the exponential growth, could the FAD redox cofactor also play the role of absorbing light in the exponential growth phase? These questions remained unanswered, but are important in understanding the tolerance to BLI by strains lacking the BLUF system.

There is also a necessary connectivity between BluF and BluR in the signaling pathway and resulting reduction in CFUs. The tolerance to BLI was insignificantly different for the Δ*bluF*

and Δ*bluR* strains. Higher emission intensity occurs when *bluR* was deleted, indicating a greater absorbance upon excitation for the same wavelength and excitation intensity (data not shown). From the absorption data with BLI_{455} and BLI_{470}, it seems BluR may be interacting with BluF and decreasing its ability to absorb blue light. When BluF is not present the emission intensity after excitation with 455 nm light is lower than when BluF is present without BluR or when both are present.

There were significant differences between the CFU reductions for the *bluF* and *bluR* mutants with BLI_{420} and BLI_{470} compared to BLI_{455}. The effects of BLI_{420} and BLI_{470} do not seem to have a BLUF-driven affect on reduction in CFUs. There are likely other photosensitizers activated at 420 nm and 470 nm. Discovering the photosensitizers at these two wavelengths would be beneficial to understanding the basis of these reductions. The possibility that the mechanism of action is not photosensitizer driven has not been ruled out, especially at 420 nm. It would be valuable information to investigate the possible mutagenic effects of BLI_{420}.

The BLUF system is clearly needed in the phototoxic reduction of *E. coli* at 455 nm. While the FAD of the BLUF domain is likely the culprit for photoabsorption at 455 nm, the interaction between BluF and BluR is more complicated than just absorption of light leading to singlet oxygen formation and reduction in CFUs. There is coordination between the two components that requires both to be present for a cytotoxic event to occur.

The low levels of reduction observed for the Δ*bluF* and Δ*bluR* strains with BLI_{455} are comparable to the reductions seen for the same strains with BLI_{470}. While the reductions BLI_{470} seem to be independent of the BLUF system, the mechanism of low-level reductions could be the same with BLI_{455} and BLI_{470}. If there was not an underlying mechanism of reduction occurring, it would be expected to see flat-lined reductions in CFUs of Δ*bluF* and Δ*bluR* strains with

BLI_{455}, specifically in the transition and stationary phases. While the reductions are significantly lower in Δ*bluF* and Δ*bluR* compared to WT, reductions around 20% still occur.

Biofilm formation is essential in the virulence strategy for uropathogenic WT UTI89. Deleting the *bluF* and *bluR* genes did not have an effect on the ability to form biofilm. However, the ability to form biofilm may be different in the presence of continuous BLI. Future studies will look at the impact of pre-exposing strains to BLI to see if the ability to form biofilms is diminished. This is essential in not only further understanding the mechanism of action for the BLUF system, but in also developing methods to combat virulence strategies against pathogenic bacteria.

CHAPTER 5

DETERMINING THE ENERGY THRESHOLD FOR EFFECTIVE BLUE LIGHT IRRADIATION-INDUCED CYTOXICITY OF UROPATHOGENIC *Escherichia coli*

ABSTRACT

Visible light therapy, i.e. photodynamic therapy, phototherapy, etc. has been used experimentally and clinically for treatment in acne, cancer, wounds, and other ailments. Much work has been done to understand how to optimize cell reductions with the use of exogenous photosensitizers in the dosimetry field. While research is now being done into the use of light therapy without exogenously added photosensitizers, there is a lack of understanding in how to optimally target endogenous photosensitizers. The goal of this work was to 1) understand how changing parameters such as wavelength, energy dose, and the energy flux affect reduction in CFUs and 2) optimize the parameters to enhance reduction in CFUs. This Chapter shows that reduction in CFUs can be achieved by either reducing the wavelength or by increasing the energy dose. There was no established pattern with modulating the rate of energy delivery. These trends only held completely true for the exponential growth phase. There was a clear resistance in the stationary phase, which is believed to be due to an increase in antioxidant molecules created in this later growth phase. While reductions in the stationary phase were statistically lower than reductions in the exponential growth phase, a greater than 90% reduction was achieved in the exponential, transition, and stationary growth phases with a wavelength of 420 nm and energy dose of 240 J/cm^2. Based on the trends observed, it is likely that the reductions in all three phases can be further increased above 90% by increasing the energy dose above 240 J/cm^2 at the 420 nm wavelength.

INTRODUCTION

High levels of reactive oxygen species (ROS) have been shown to damage living cells, most notably singlet oxygen [50]. ROS can be created by absorption of light by endogenous photosensitizers, or by exogenously added photosensitizers in the presence of oxygen [14, 45, 54, 55, 110]. The absorption of light energy by photosensitizers, leading to the formation of ROS, is widely accepted to be the mechanism of action in light-induced cytotoxicity, i.e. photodynamic therapy (PDT-with exogenously added photosensitizers) or phototherapy (with endogenous photosensitizers). The effect of PDT or phototherapy has been shown to be modulated by the available oxygen; in an anaerobic environment light-induced bacterial reduction has been shown to be ineffective [45, 121]. It has also been shown that Gram-negative bacteria are less susceptible to light-induced reduction compared to Gram-positive, suspected to be due to the presence of an additional cell membrane in Gram-negative bacteria [43, 110, 154, 155]

The wavelength of light chosen for light-induced cytotoxicity depends on the type of photosensitizers to be targeted and the application of the light treatment [7, 156-160]. As the wavelength increases, the light is able to penetrate the treatment area deeper. While different wavelengths target different photosensitizers, a greater cytotoxic effect has been seen for shorter wavelengths.

The effects of energy dose can be described by the Arndt-Schulz curve, where a weak stimulus can induce cell growth and a strong stimulus can inhibit cell growth [13]. This energy dose is the total energy delivered to a selected irradiated area, usually measured in J/cm^2. Many studies have described an increase in light-induced bacterial reduction with increasing energy dose [12, 16, 36, 43, 56, 78]. Following the accepted mechanism of singlet-oxygen mediated cell

reduction, a higher energy dose leads to an increased production of singlet oxygen, and thus a greater cytotoxic effect. In fact, direct singlet oxygen production by a Type II reaction has a higher energy demand, versus the multi-step Type I reaction that has a lower energy requirement to proceed. While studies have investigated the effects of modulating energy doses, no known studies have investigated the effects of modulating the rate of energy delivery (energy flux- mW/cm^2 or mJ/cm^2 s). Based on these studies, at higher energy doses an energy barrier may exist, inhibiting all of the light energy to be absorbed by photosensitizers. It was therefore hypothesized that by decreasing the rate of energy delivery at higher energy doses, the BLI reduction effects could be maximized further.

The goal of this work was to understand how light parameters such as the total energy dose, wavelength, and the energy flux (rate of energy delivery per area) affects the reducing ability of BLI-induced reduction of bacterial cells. Uropathogenic strain UTI89 was used as the model system in this chapter. To further investigate the effect of wavelength on the bacterial reducing ability of BLI, the 420 nm and 470 nm wavelengths were included, in addition to 455 nm. Energy doses ranged from 60 to 240 J/cm^2. Energy flux varied from 137 to 902 mJ cm^{-2} s^{-1}.

MATERIALS AND METHODS

Bacterial strains and culture conditions

Refer to the "Bacterial strains and culture conditions" section in Chapter 2 for more detailed methods. A uropathogenic *E. coli* (UPEC) strain was used, UTI89 (UPEC cystitis isolate [83]). Bacterial cultures were seeded in lysogeny broth (LB) and incubated at 37°C while shaking overnight. Aliquots of overnight cultures were sub-cultured in 15 mL fresh LB the

following morning, and normalized to a starting optical density (OD) at 600 nm of 0.05. Sub-cultures were incubated at 37°C under shaking conditions for all analyses described.

In vitro light delivery to *E. coli*

Refer to the "*In vitro* delivery to *E. coli*" section in Chapter 2 for more detailed methods. Cultures were set up as described above. Aliquots were obtained for irradiation and plating during exponential (T = 3 h), transition (T = 5 h) and stationary (T = 8 h) growth phases. BLI was carried out with a Thorlabs Mounted High-Power LED lamp at 420 nm, 455 nm, or 470 nm and controlled by a high-powered LED driver (Thorlabs DC2100). A total energy dose of 120 J/cm^2 was delivered to each sample. Irradiated and non-irradiated controls were then incubated overnight at ambient temperature. CFUs were counted the following day. Experiments were performed with at least 3 biological replicates of 3 technical replicates. WT UTI89 was used as a control for comparison for analyses by growth phase.

Calculations for varying wavelength, energy dose, and energy flux

Refer to the "Calculations for varying wavelength, energy dose, and energy flux" section in Chapter 2 for more detailed methods. The doses tested were within published ranges and were varied at intervals of 60 J/cm^2 from 60 to 240 J/cm^2. The original fluxes were chosen to keep the irradiated area within a similar range; however, fluxes were modulated for the flux study to increased and decreased levels from the original fluxes. The irradiated area was calculated as a function of the distance from the sample using the manufacturer's light parameters found in **Figure 2.3**. To determine the irradiation time for varied energy dose, **Equation 2.1** was used. From **Equation 2.1**, an increase in energy flux leads to a shorter irradiation time. Energy flux

was determined as a function of the distance between the LED lamp and the irradiated sample (**Table 2.1**). The energy flux decreased as a power function with increasing distance between the light source and the sample. To determine the energy flux at a particular distance that was not measured, **Figure 2.4** was used. The energy flux decreased as a power function with distance between the light source and the sample. The flux that was used when energy flux was being modulated was determined assuming a straight line for the two nearest distances.

Reduction determination

To determine the percent change in exposed versus unexposed CFUs, the CFUs post-irradiation were enumerated and compared to the CFUs of corresponding, non-irradiated spots. The reductions were calculated as percent reductions in CFUs, following **Equation 2.2**.

RESULTS

A wavelength-dependent reduction in CFUs holds true at the highest energy dose tested

To determine the effect of increasing wavelength at constant energy dose, three energy doses were tested: 60, 120, and 180 J/cm^2 with irradiations at three different wavelengths: 420 nm (BLI_{420}), 455 nm (BLI_{455}), and 470 nm (BLI_{470}). At the lowest tested energy dose, 60 J/cm^2, the greatest reduction was observed in exponential phase for BLI_{420} and BLI_{470}, 80 and 40%, respectively (**Figure 5.1a**). In transition growth phase with BLI_{470} this was the only instance where there was an increase in CFUs after BLI. With BLI_{455}, there was no growth-phase dependency and reductions were less than 20%. For all growth phases and wavelengths at 60 J/cm^2, reductions ranged from ~-40 to 80%.

For 120 J/cm^2, a wavelength dependency was only observed in exponential phase; as wavelength increased, the reduction in CFUs decreased (**Figure 5.1b**). In the transition and stationary phases, there was no statistically significant difference between reductions with BLI_{420} and BLI_{455}. BLI_{470} induced the lowest reduction in CFUs in all growth phases. Close-to-100% reduction was achieved in exponential phase with BLI_{420}; the next highest reduction was less than 70%. At each wavelength, the difference between reductions in transition and stationary phases were statistically insignificant. Overall, at 120 J/cm^2, reductions ranged from ~10 to ≥99%.

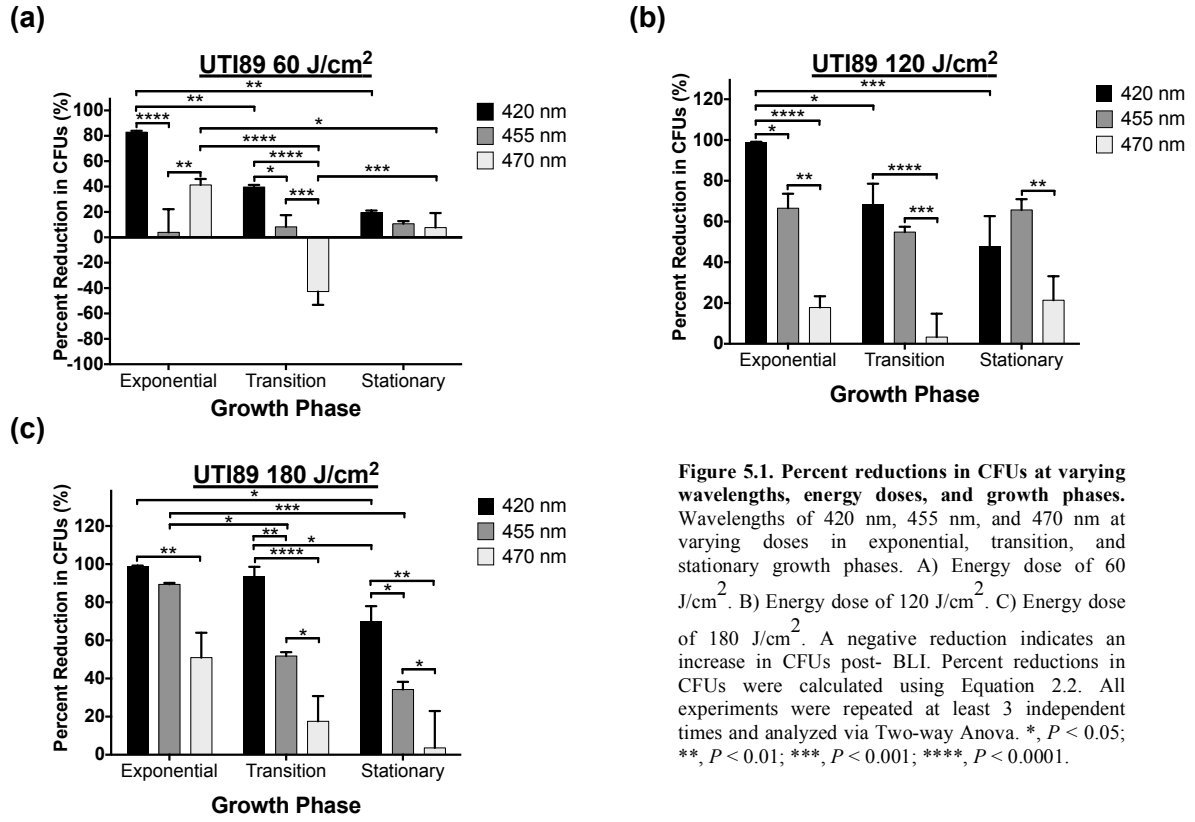

Figure 5.1. Percent reductions in CFUs at varying wavelengths, energy doses, and growth phases. Wavelengths of 420 nm, 455 nm, and 470 nm at varying doses in exponential, transition, and stationary growth phases. A) Energy dose of 60 J/cm^2. B) Energy dose of 120 J/cm^2. C) Energy dose of 180 J/cm^2. A negative reduction indicates an increase in CFUs post- BLI. Percent reductions in CFUs were calculated using Equation 2.2. All experiments were repeated at least 3 independent times and analyzed via Two-way Anova. *, $P < 0.05$; **, $P < 0.01$; ***, $P < 0.001$; ****, $P < 0.0001$.

At 180 J/cm^2, a wavelength-dependent reduction is observed in each growth phase; as wavelength was increased, the reduction in CFUs decreased (**Figure 5.1c**). In the exponential growth phase 50-100% reduction was achieved, 20-95% reduction in transition phase, and 5-

70% reduction in stationary phase. For $BLI_{420,}$ in each growth phase, 70% and greater reduction is achieved. A reduction of 40-90% was achieved in each growth phase with BLI_{455}. With BLI_{470} in each growth phase, 5-50% reduction is achieved. Reductions ranged from ~5 to ≥99% at 180 J/cm^2.

Out of the three energy doses tested, wavelength dependencies were only present at the 180 J/cm^2 energy dose for all three growth phases. For 180 J/cm^2, an increase in wavelength resulted in a decrease in reduction of CFUs (**Figure 5.1c**). A wavelength-dependent reduction was also observed at 60 J/cm^2 in the transition phase (**Figure 5.1a**) and at 120 J/cm^2 in the exponential phase (**Figure 5.1b**). The total energy delivered to the 10-uL *E. coli* sample was the same at each wavelength; however, the 470 nm wavelength resulted in less reduction when compared to 420 and 455 nm in each growth phase and at each total energy dose.

While the total energy delivered to the samples at each wavelength was the same, there were variations in the energy per photon (packet of light energy) delivered to the samples. The amount of energy per photon can be determined using the following equation:

$$E = \frac{hc}{\lambda} \qquad \textbf{Equation 5.4.}$$

where E is the energy per photon; *h* is Planck's constant, 6.626x10^{-34} J•s; c is the speed of light, 2.998x10^8 m/s; and λ is wavelength in nm. From these calculations, the energy per photon is 4.733x10^{-19}, 4.369x10^{-19}, and 4.229 x10^{-19} J/photon for 420 nm, 455 nm, and 470 nm, respectively. When delivering the same energy dose at each wavelength, the amount of photons increases with increasing wavelength.

To test if the observed effects were simply absorption differences, the effect of varying energy dose within each wavelength was investigated.

Lower wavelengths result in an increased reduction in CFUs and permit a dose-dependent reduction

When observing the data in **Figure 5.1** from the perspective of constant wavelength, there was only a dose-dependent reduction for all three growth phases BLI_{420}. For BLI_{420}, an increase in dose resulted in an increase in reduction of CFUs. A dose-dependent reduction was also observed with BLI_{455} in the exponential phase and with BLI_{470} in the transition phase.

With BLI_{420}, a dose-dependent reduction in CFUs occurred as energy dose was increased from 60 to 180 J/cm^2 for each growth phase. The most reduction was seen in the exponential growth phase—80% for 60 J/cm^2 and ≥ 99% reduction for 120 and 180 J/cm^2. The least amount of reduction was seen in the stationary phase—less than 20% reduction for 60 J/cm^2; max reduction was seen at 180 J/cm^2 at ~70%. Reduction in transition phase ranged between 40 and 95%. At 60 J/cm^2, a growth phase-dependent reduction where the reduction decreased with later growth phases was observed.

A dose-dependent reduction only held true in exponential phase—less than 20% to ~90% reduction in exponential phase with BLI_{455}. In transition and stationary phase, max reduction in CFUs occurred at 120 J/cm^2. At 60 and 120 J/cm^2 there was no statistically significant difference as a function of growth phase. At 180 J/cm^2 we saw a growth phase-dependent reduction where the reduction decreased with later growth phases.

With the BLI_{470} wavelength, there were no dose-dependent reductions in exponential or stationary phases. However, in transition phase, reductions in CFUs increased as dose increased. In this phase there was also an increase in CFUs observed at 60 J/cm^2; this could be a stimulating energy dose. Less reduction was seen in stationary phase for 60 and 180 J/cm^2 as compared to the reductions in exponential phase.

It was expected that as the total energy delivered to the samples is increased, the reduction in CFUs would increase. This hypothesis was founded on the thought that an increase in total energy would lead to an increased production of singlet oxygen and subsequently greater CFU reduction. However, from this data, it was observed that an increase in the total energy dose did not necessarily lead to a reduction in CFUs. This finding led to the belief that there was possibly a bottleneck in the bacteria's ability to absorb the light energy, causing some of the energy to not reach its target. To investigate whether this was occurring, the rate of energy delivery was varied.

Reductions are not strongly impacted by modulating energy flux

The middle energy dose at 120 J/cm^2 was selected to vary the energy flux, or rate of energy delivery. To vary the flux, the distance between the light source and the sample was increased. Increasing the distance between the light source and the sample decreases the energy flux because the area the light source covers (irradiated area) increases. Since the 10 uL sample area (effective area) remains constant and is less than a square-centimeter, the effective amount of energy that reached the sample was less than the irradiated area in the same period of time. Therefore, to achieve the same total energy dose, the effective area had to be irradiated longer. Conversely, decreasing the distance between the light source and the sample concentrates the light into a smaller irradiated area so less time is needed to deliver the same total energy dose to the effective area. The energy fluxes were chosen arbitrarily. However, the energy flux of 250 mJ cm^{-2} s^{-1} was chosen as the close-to-maximum flux that could be achieved and held constant with each light source (the 420 nm lamp can only achieve a maximum current of 500 mA) and 137 mJ cm^{-2} s^{-1} was chosen because this is the average solar flux that we feel from the sun on the Earth. There was no clear established pattern for flux dependencies.

At BLI_{420}, percent reduction in CFUs was independent of changes in energy flux in both exponential and stationary growth phases (**Figure 5.2a**). Close to 100% reduction in CFUs was achieved in the exponential phase and ~50% in the stationary phase. In the transition phase, there was an initial increase in reduction from 55-95% as the energy flux was increased more than 60 mJ cm^{-2} s^{-1}; however a 30 mJ cm^{-2} s^{-1} increase above 250 mJ cm^{-2} s^{-1} resulted in a decrease in reduction, only slightly higher than the reduction at solar flux.

With BLI_{455}, there was a lot of fluctuation in the reduction in CFUs as a function of flux, but no established pattern could be drawn (**Figure 5.2b**). In the exponential phase, greater than 90% reduction was achieved, except for the intermediate flux of 523 mJ cm^{-2} s^{-1}. The reduction in CFUs significantly decreased from exponential to transition phase. In transition phase, the reductions of 137 and 523 mJ cm^{-2} s^{-1} were identical; 250 and 902 mJ cm^{-2} s^{-1} decreased significantly to +/-5% reduction. In stationary phase, all fluxes are insignificantly different, ~20 to 40%, with the exception of the intermediate flux 523 mJ cm^{-2} s^{-1}, which had the highest reduction at ~60%. All fluxes and growth phases resulted in reductions in CFUs below 40% with BLI_{470}. There was no dependency on energy flux at any growth phase, nor a statistically significant difference as a function of growth phase or as a function of flux.

When observing the data at constant energy flux, in exponential phase at 137 mJ cm^{-2} s^{-1}, both 420 and 455 nm exposures led to ≥ 99% reduction, while the reduction of CFUs dropped to ~30% at 470 nm. In transition phase, both BLI_{420} and BLI_{455} led to ~55% reduction, while the reduction of CFUs remained constant from exponential phase at ~30% for 470 nm. During the stationary phase, the average reductions in CFUs decreased with increasing wavelength, although the reductions as a function of wavelength were statistically insignificant. At BLI_{420}, the reduction in CFUs was significantly reduced in transition and stationary phases; there was no

difference between transition and stationary phase and the average reduction was ~55%. The reduction in CFUs with BLI_{455} was significantly reduced in transition and stationary phases;

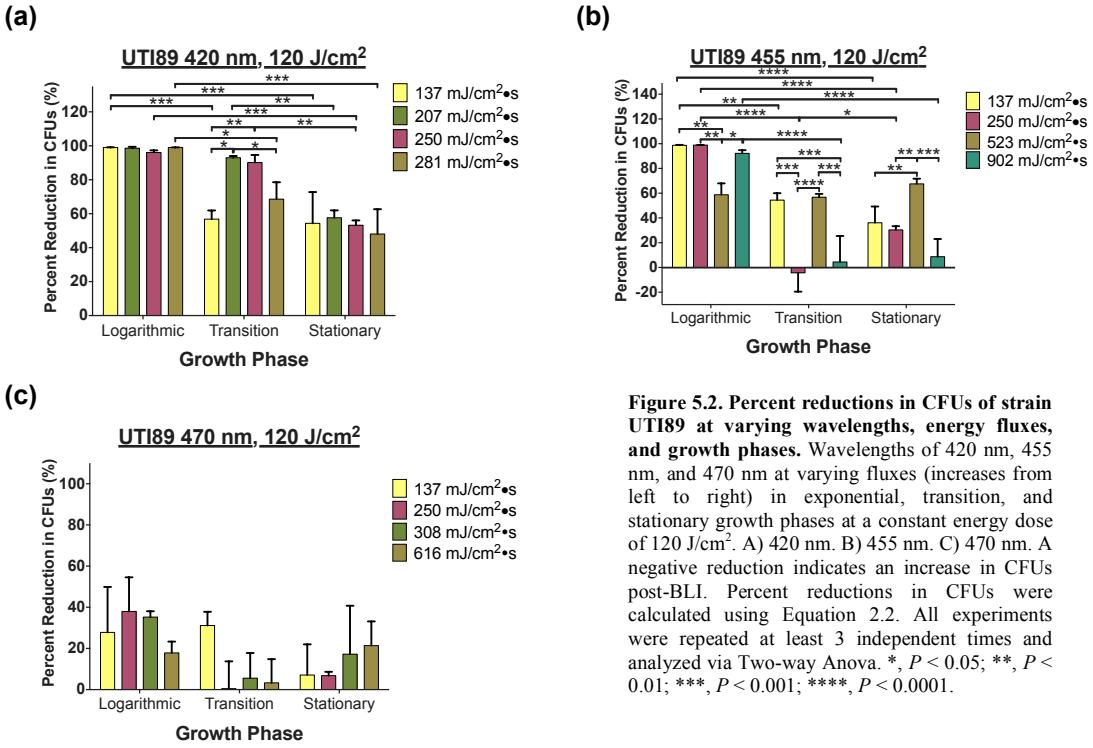

Figure 5.2. Percent reductions in CFUs of strain UTI89 at varying wavelengths, energy fluxes, and growth phases. Wavelengths of 420 nm, 455 nm, and 470 nm at varying fluxes (increases from left to right) in exponential, transition, and stationary growth phases at a constant energy dose of 120 J/cm^2. A) 420 nm. B) 455 nm. C) 470 nm. A negative reduction indicates an increase in CFUs post-BLI. Percent reductions in CFUs were calculated using Equation 2.2. All experiments were repeated at least 3 independent times and analyzed via Two-way Anova. *, $P < 0.05$; **, $P < 0.01$; ***, $P < 0.001$; ****, $P < 0.0001$.

moving from transition to stationary phase the average reduction in CFUs decreased from ~55% to 40%, but this change was statistically insignificant. For BLI_{470}, the reduction in CFUs was the lowest in stationary phase at ~10%, but this change was statistically insignificant from the ~30% reduction observed in exponential and transition phases.

At the largest constant flux between the wavelengths, 250 mJ cm^{-2} s^{-1}, a similar trend to the reductions observed at 137 mJ cm^{-2} s^{-1} was observed. In exponential phase, both BLI_{420} and BLI_{455} led to ≥ 99% reduction, while the reduction of CFUs dropped to ~40% at 470 nm. The close-to-100% reduction was held within transition phase for BLI_{420}. The reductions in CFUs significantly decreased in transition phase for BLI_{455} and BLI_{470}; there was ~-5% reduction in CFUs at BLI_{420} and BLI_{455}, but essentially no reduction at BLI_{470}. With BLI_{420} in stationary

phase, the reduction in CFUs decreased to ~50%. For the reductions in stationary phase, the reductions in CFUs for 455 and 470 nm were less than what was observed for exponential phase, but more than the reductions (or lack of) in transition phase. Overall, reductions in transition and stationary phases at 250 mJ cm^{-2} s^{-1} were more tolerant to the effects of BLI when compared to exponential phase responses at the same energy flux.

420 nm and higher doses are the most effective in reducing CFUs in all three growth phases

Based on the observed data, the most effective wavelength in reducing CFUs was 420 nm, while the most effective dose was 180 J/cm^2; energy flux had less of an effect. To further increase the reductions observed at 420 nm, specifically in the stationary growth phase, the reducing effects of 420 nm with a further increased dose of 240 J/cm^2 and flux of 281 mJ cm^{-2} s^{-1} was combined. **Figure 5.3** shows over 90% reduction in the stationary phase, in addition to ≥ 99% reduction in both the exponential and transition phases. This was the highest reduction observed with modulations in wavelength, energy dose, and energy flux.

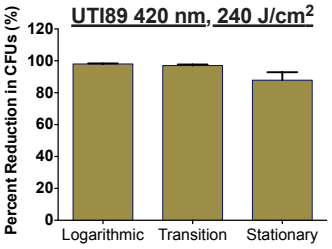

Figure 5.3. Percent reduction in CFUs of strain UTI89 at 420 nm, 240 J/cm^2. Reductions were calculated during exponential, transition, and stationary growth phases. The energy flux was 281 mJ cm^{-2} s^{-1}. Percent reductions in CFUs were calculated using Equation 2.2.

DISCUSSION

Uropathogenic *E. coli* strain, UTI89, was used to investigate the effects of wavelength, energy dose, and energy flux on BLI-induced bacterial reduction. Gram-negative *E. coli* was chosen as a model system because, in general, Gram-negative species are more tolerant to phototherapy than Gram-positive species [43, 110, 154, 155]. While the reason for this difference is unknown, it is possible that the differences may be due to an inhibition of light penetration in Gram-negative species [43, 110, 154, 155]. Gram-negative bacteria have an

additional membrane that is not found in Gram-positive species. Understanding the influences light parameters play in reducing the bacterial viability will help further increase the reduction during all three growth phases, but most importantly the stationary phase of growth. The stationary phase of growth is implicated in infections and where you find most bacteria, so it is important to optimize reductions during stationary phase. It is in this later growth phase where virulence characteristics are more highly expressed [121].

With the original parameters tested, more than 70% reduction was achieved in stationary phase, even when the energy conditions allowed for a >90% reduction in exponential and transition phases. Clearly, there is a resistance built in the stationary phase that allows the bacteria to be tolerant to the effects of BLI. The goal of this work was to 1) understand how changing parameters such as wavelength, energy dose, and the energy flux affect reduction in CFUs and 2) optimize the parameters to enhance reduction in CFUs. As mentioned in Chapter 3, the most reduction is generally seen in the exponential phase when bacteria are actively dividing. It is possible that the bacteria's defense mechanisms are attenuated in the exponential phase because machinery is dedicated to other processes. The possibility of the reduction differences simply being because of cell density was ruled out by exposing similar amounts of cells (10^1 to 10^2).

Increasing the total energy dose at each wavelength led to an increased or negligible change in reduction of CFUs, with the exception of the stationary phase at 455 nm. With BLI_{455}, there was a decrease in CFU-reduction from the 120 to 180 J/cm^2 energy dose. Conversely, increasing the wavelength at a particular dose, led to a decreased reduction, while there are minor changes as a function of the rate of energy delivery. The total energy delivered at each wavelength was kept constant. However, the amount of energy delivered per photon varied with

wavelength. The lowest wavelength, 420 nm, had the highest amount of energy per photon, so there were less photons needed to deliver a constant dose as compared to less energy per photon (and therefore the need for more photons) at 470 nm.

Because there was not a significant difference in varying energy flux, there is a strong possibility that the observed differences with varying wavelengths are not an effect of how fast the energy is delivered. However, it is possible that the excitation mechanism is a single-photon event, where one photosensitizer is excited by one photon. If this were the case, then photosensitizers would be excited to a higher energy level with BLI_{420} compared to BLI_{455} and BLI_{470}. Photosensitizers at higher energy can transfer this energy to ground-state oxygen and form singlet oxygen directly. The energy released from 455 nm and 470 nm may not be high enough to directly form singlet oxygen and would therefore take longer to form singlet oxygen through the Type I multi-step reaction. The possibility cannot be ruled out that there is a small portion of light released from the 420 nm wavelength lamp that is in the UV range and may reduce growth by another mechanism.

By increasing the total energy dose in the exponential and transition growth phase at 455 nm, reduction levels comparable to those at BLI_{420}. This result also supports the idea of a single photon event. At the same rate of delivery and energy per photon, higher reductions were achieved as the total energy delivered was increased. If the photons released with BLI_{455} are only going through the multi-step Type 1 reaction, it would be plausible that increasing the total energy delivered would allow for the formation of a greater amount of ROS and thus form more singlet oxygen, leading to reductions on par with those BLI_{420}. There was no increase in reductions with increasing dose during the stationary phase of growth; in fact, a decreased reduction from 120 to 180 J/cm^2 at BLI_{455} was observed. Overall at most wavelengths and doses,

the stationary phase was the most resistant to the BLI effects. Wang, et al. have reported that a σ^S-regulated stress-response, induced antioxidant defense protects the stationary phase [121]. This defense may be responsible for the increased resistance to BLI in the stationary phase and the decreased reductions seen with increasing energy dose in the stationary phase. Other antimicrobial agents have also been shown to be less effective in the stationary phase of growth [121, 125]. As more ROS are formed, a greater antioxidant effect is triggered; this is also supported by the Arndt-Schulz rule for photobiostimulation, where after a certain level of stimulation the effect on bacterial viability decreases. Unlike other ROS, singlet oxygen is unable to be broken down by enzymes, but can be quenched by antioxidants [2, 13]. Having lower antioxidant content allows bacteria to be more susceptible to the effects of BLI, and is likely the case for exponential and transition growth phases [12, 14].

For energy flux of BLI_{455}, the decrease and then increase in reduction as a function of flux in transition phase may be attributed to a bottleneck being reached at the 523 mJ cm^{-2} s^{-1} flux, where the antioxidant response supersedes the effect of the BLI.

While BLI_{420} and 240 J/cm^2 (highest energy per photon and highest total energy delivered) was the most effective wavelength and energy dose combination in reducing CFUs in all three growth phases, the wavelength may have safety concerns because it is close to UV. The 420 nm wavelength is deemed safe by ANSI standards, but it was not investigated into whether there was DNA damage, resulting from the light source we used.

Overall, increasing the total energy dose can be an effective way to increase bacterial reductions, until the antioxidant effect is greater than the accumulation of ROS. Moving forward, it would be helpful to understand the mechanism that drives the antioxidant production to determine the maximum reduction that can be achieved.

CHAPTER 6

KINETIC ANALYSIS OF PHOTOSENSITIZER EXCITATION AND SINGLET OXYGEN FORMATION

INTRODUCTION

Mechanism of BLI

The widely accepted mechanism of light-induced cytotoxicity is the generation of singlet oxygen by interaction of an excited photosensitizer with ground-state molecular oxygen. Singlet oxygen is known to damage cell membranes and to interact with cellular compounds, specifically amino acids possessing an aromatic or heterocyclic side chain (i.e. tryptophan, tyrosine, histidine, etc.), amino acids containing sulfur (i.e. cysteine, methionine, etc.), and pyrimidine and purine bases of DNA/RNA (i.e. guanosine) [161]. The use of exogenously added photosensitizers has been widely researched, specifically for photodynamic therapy (PDT) in cancer treatments [108, 157, 162, 163]. Exogenously added photosensitizers have advantages in the fact that the absorption maxima of the photosensitizer can be used as the dominant excitation wavelength. This allows for specificity in treatment. There are about a dozen clinically-approved exogenous photosensitizers for PDT [164].

Visible light treatment, without the addition of photosensitizers, has also been researched. This field of study involves the use of endogenous photosensitizers/chemical compounds that are found within the cell and able to absorb light in the visible spectrum [14, 16, 57, 155, 165]. Much of the work done with endogenous photosensitizers has focused on porphyrins as the target molecule [2, 45, 51, 61, 62, 64, 65, 166, 167]. However, in Chapter 3 (**Figure 3.8)**, the data did not show a transcriptional surge of genes encoding for porphyrin enzymes post-BLI. It was

concluded that either porphyrins are not involved in the BLI_{455} response for the Gram-negative *Escherichia coli* strain UTI89 or changes occur post-transcriptionally.

Potential endogenous photosensitizers

A strong photosensitizer usually possesses aromatic rings and highly-conjugated pi bonds [105]. Bacterial components that can serve as endogenous photosensitizers include cytochromes, porphyrins, flavins, and ubiquinones. Porphyrin- and flavin-containing moieties can be found throughout the cell, but all four of the components are also found in the membrane-bound electron transport chain (ETC). Porphyrin-centered cytochromes, flavin adenine dinucleotide (FAD), and ubiquinones are integral players in the generation of proton motive force, which initiates and maintains the balance of flow in the ETC [100-102]. This work has shown that the target endogenous photosensitizers are likely those found in or near the membrane-bound ETC. In fact, for effective exogenously added photosensitizers, a vast majority have been found to localize to the cytoplasmic membrane [161]. In Chapter 3 and Chapter 4, it was shown that defects in both the ubiquinone synthase gene, *ubiI*, and FAD-containing blue light sensor genes, *bluF* and *bluR*, led to increased tolerance to BLI by the uropathogenic *E. coli* strain UTI89. While the defect in ubiquinone synthase genes may be due to decreases in energy transfer in the ETC and not the lack of blue light absorption by ubiquinone, the data was supportive for BLI effects occurring in or near the ETC.

Only certain wavelengths of light can be absorbed by photosensitizers. These allowed wavelengths correspond to the energy difference between two different eigenstates of the photosensitizer. Porphyrins, flavins, and ubiquinones can all absorb in the blue light range of 400-500 nm, though the absorption maximums for these three components vary. In Chapter 4 (**Figure 4.1**), it was shown that flavins optimally absorb ~455 nm and defects in the flavin-based

BluF sensor led to a significant decrease in BLI-induced reduction in colony forming units. In **Figure 6.1**, there was a change in the emission spectrum after excitation of blue light at different wavelengths. This is indication that the photosensitizers activated with BLI_{420}, BLI_{455}, and BLI_{470} are all different. The flavin-containing BluF sensor has been identified as the photosensitizer at 455 nm, but the photosensitizers activated by BLI at 420 nm and 470 nm are still unknown.

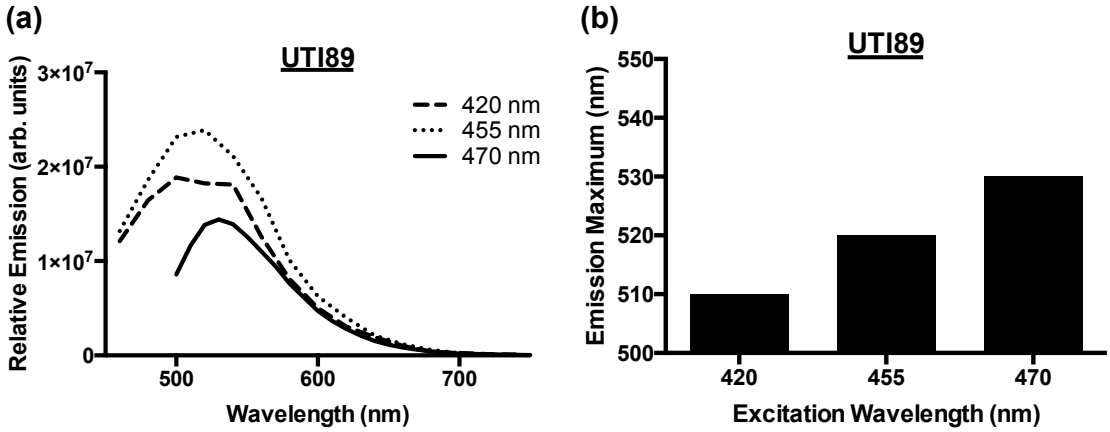

Figure 6.1. Red-shift of emission wavelength as a result of a red-shift in excitation wavelength. (a) Emission spectrum for UTI89 after excitation at 420 nm, 455 nm, and 470 nm. The intensities of the spectrum are not normalized, so no information can be deduced from the differences in emission intensities. (b) Changes in emission maximum observed with varying wavelengths. A 10 nm red-shift between 510 nm and 530 nm in emission is observed for excitations at 420 nm, 455 nm, and 470 nm, respectively.

Upon absorption of light by a photosensitizer, the photosensitizer is excited to a higher energy state. It is in this higher energy state, where it can interact with molecular oxygen to form cytotoxic singlet oxygen [11, 13].

Formation of Singlet Oxygen

Almost all molecules, including photosensitizers, exist in a singlet state as its ground state, with one exception being oxygen, which exists in a triplet state, $^3O_2$, in its ground state energy. Intracellular singlet oxygen can be formed by either a Type I or Type II reaction. In both the Type I and Type II reactions, a photosensitizer is excited (*) to either a singlet or triplet state after absorption of light. The triplet state, while a forbidden process, is the more common route

for singlet oxygen generation, because the lifetime of the excited photosensitizer is increased, increasing the probability of interaction with ground-state oxygen.

The Type I reaction, proceeds from a lower excited photosensitizer state, in which an electron (or proton) is transferred from the excited photosensitizer to ground-state molecular oxygen as seen in **Scheme 6.1**. Upon transfer of the electron (or proton) a radical ion is created. This radical can interact with other ions or compounds in a multi-step reaction, leading to the formation of other reactive oxygen species, including singlet oxygen.

Scheme 6.1.

$$1)\ {}^1PS + h\nu \rightarrow {}^3PS*$$
$$2)\ {}^3PS* \rightarrow {}^1PS + e^-$$
$$3)\ e^- + {}^3O_2 \rightarrow O_2^{-\cdot}$$
$$4)\ O_2^{-\cdot} + 2H^+ \rightarrow H_2O_2$$
$$5)\ H_2O_2 \rightarrow OH^- + \cdot OH + {}^1O_2$$

At a higher energy state, singlet oxygen can be formed directly after transfer of energy from the excited photosensitizer to ground-state molecular oxygen by the Type II reaction seen in **Scheme 6.2**.

Scheme 6.2.

$$1)\ {}^1PS + h\nu \rightarrow {}^3PS*$$
$$2)\ {}^3PS* \rightarrow {}^1PS + energy$$
$$3)\ energy + {}^3O_2 \rightarrow {}^1O_2*$$
$$4)\ {}^1O_2* \rightarrow {}^3O_2 + energy$$

Detection of Singlet Oxygen

Singlet oxygen can be detected in both direct and indirect methods. While direct measurement is the most reliable, sophisticated methods must be used because singlet oxygen is short-lived; its emission maximum is outside of the wavelength detection of most photodetectors, at 1270 nm (infrared); and it has a weak maximum emission [168]. These shortcomings make the direct detection of singlet oxygen difficult. Time-resolved direct detection can be employed for

direct measurement, but requires the use of sophisticated detectors which operate at low temperatures (~ -70°C) to minimize the signal to noise ratios [168]. To overcome the difficulties in directly measuring singlet oxygen formation, indirect measurement of singlet oxygen can be accomplished by monitoring the appearance and disappearance of a molecule known to interact directly with singlet oxygen. Optical techniques have also been employed to indirectly measure singlet oxygen. Luminescence and fluorescence-based reporter assays are also available for indirect measurement of reactive oxygen species (ROS), including singlet oxygen. Most reporter assays do not distinguish between ROS and singlet oxygen; one exception is the highly-specific Singlet Oxygen Sensor Green (Molecular Probes™).

Detection of Singlet Oxygen by Singlet Oxygen Sensor Green

Singlet Oxygen Sensor Green (SOSG; Molecular Probes™) was used to assist in the detection of singlet oxygen. This luminescence-based assay has an emission maximum at 531 nm, with a maximum excitation at 488 nm. To quantify the amount of singlet oxygen formed after BLI, the proper controls and standards are needed. Hypericin (**Fig. 6.2**), a known singlet oxygen producer, was used as a standard using stoichiometric ratios and the published quantum yield of hypericin of 0.72-0.73 (measured in both deuterium and ethanol) [169]. The reaction for hypericin to produce singlet oxygen is seen in **Scheme 6.3**, where hypericin can either be excited to its singlet state or its triplet state before being quenched by molecular oxygen. It is important to note that the energy needed to excite molecular oxygen from its ground-triplet state to its singlet state, ΔE_{TS}, is 94.3 kJ/mol (1.566×10^{-19} J/molecule). If the energy transferred from the excited photosensitizer is less than ΔE_{TS}, singlet oxygen will not be formed. Instead, an excited triplet state with higher energy than the ground state will be formed, $^3O_2$*.

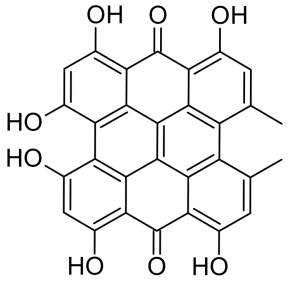

Figure 6.2. Chemical structure of hypericin.

Scheme 6.3.

$$1)\ {}^{1}hypericin \xrightarrow{hv} {}^{1}hypericin*$$
$$2)\ {}^{1}hypericin \xrightarrow{hv} {}^{3}hypericin*$$
$$3)\ {}^{1}hypericin* + {}^{3}O_2 \rightarrow {}^{1}hypericin + {}^{1}O_2$$
$$3)\ {}^{3}hypericin* + {}^{3}O_2 \rightarrow {}^{1}hypericin + {}^{1}O_2$$

There were several hurdles in measuring singlet oxygen formation. Hypericin is insoluble in water, so DMSO (25 mg/mL) was used as the solvent. However, DMSO interacted with the signal of SOSG, accurate readings were not achieved with DMSO alone. Methanol was used as the solvent for the SOSG, so to overcome the shortcoming of signal interactions, Hypericin was diluted in methanol for working solutions from the stock solution diluted in DMSO. The plan was to excite the samples with light at a desired wavelength and intensity using the SpectraMax i3 plate reader, but the intensity was too low and could not be controlled. Therefore, samples were excited with BLI using the LED lamps. Methanol has a fast evaporation rate, so samples diluted in methanol dried out by the end of the exposure. To date, a standard curve has not been developed for the quantification and detection of singlet oxygen as a function of BLI. The goal was to determine differences in singlet oxygen formation by varying BLI parameters.

MODEL

In this work, molecular biological approaches were taken to pinpoint the photosensitizer(s) involved in blue light irradiated (BLI)-induced cytotoxicity between 420-470

nm of *Escherichia coli*, to determine if the reductions in CFUs were growth-phase dependent, and to understand the effects of modulating wavelength, energy dose, and flux. The ultimate goal of this work was to understand the factors involved in bacterial reductions of *E. coli* induced by BLI to make recommendations for parameters used in other Gram-negative and other bacterial species.

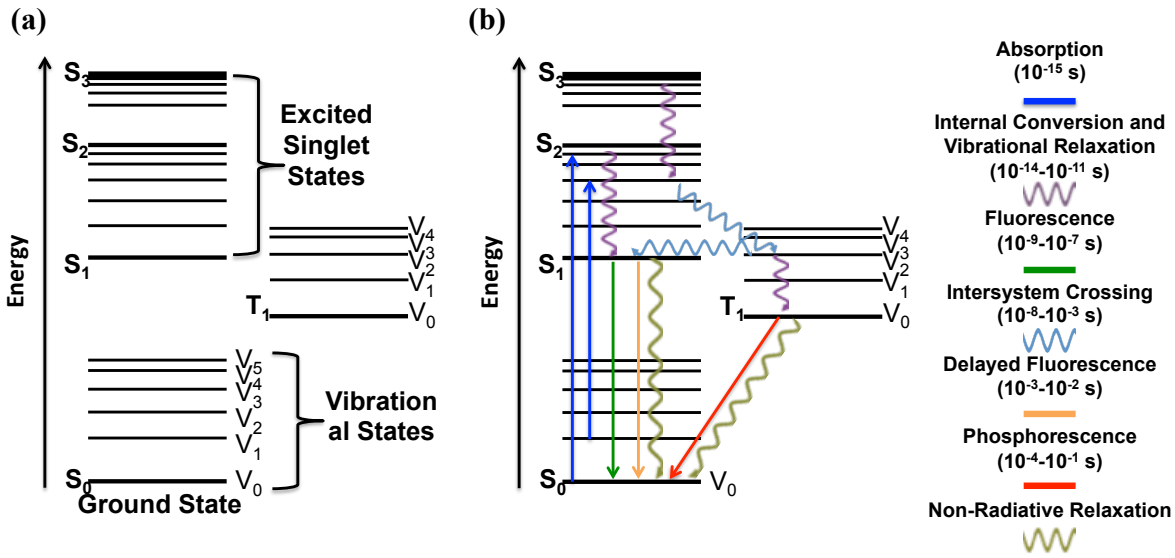

Figure 6.3. Jablonski diagram. (a) Simplified Jablonski diagram showing the electronic states, S_1, S_2, and $S_3 \ldots S_n$ and the vibrational states, V_1, V_2, and $V_3 \ldots V_n$. (b) Major photophysical processes involved in photon excitation of an electron and energetic decay back to ground state. The diagram can be used to predict or assume a pathway for excitation and decay. The time scales of these processes vary and faster processes outcompete slower processes.

Jablonski diagram

Jablonski diagrams (**Figure 6.3**) are used to explain the energetics of photon absorption by a molecule and subsequent emission of the light energy. These diagrams can be used to understand photosensitization and decay. Jablonski diagrams are usually broken up by columns representing the different spin multiplicities of the electronic state of a given molecule. Within the columns are horizontal lines representing energy states. Vertical lines cross the horizontal lines to explain the transition between eigenstates upon interaction with a photon of light and the molecule's electron. Curved lines also cross the horizontal lines, representing the transition of

electrons, independent of light. A Jablonski diagram is a good way to show potential pathways an electron can accept and transfer energy from a photon. S_0, S_1, and S_2 are electronic levels, with S_0 representing the ground-state energy level. Rotation and vibration levels are in between the electronic levels and are represented by thinner horizontal lines in the Jablonski diagram.

Upon ***absorption*** of a photon, electrons get excited to a higher energy state. The timescale of absorption is extremely fast on the order of 10^{-15} s. From this excited state electrons rotate and vibrate down to the closest electronic level; this is called ***vibrational relaxation***, which follows Kasha's rule, stating that an electron must relax to a semi-stable level after excitation [170]. It is also possible for electrons to transition from a vibrational level in one electronic state to a vibrational level in a lower electronic state if there is overlap in vibrational and electronic energy states, in a process called ***internal conversion***. Both vibrational relaxation and internal conversion occur on a timescale of 10^{-14}-10^{-11} s. Electrons are not released during internal conversion nor vibrational relaxation—both non-radiative processes. During the relaxation of an electron from an excited singlet state to its ground state, a photon can be emitted in the emission spectra. This radiative relaxation is known as ***fluorescence***. Fluorescence is most often observed between the first excited state and the ground state; vibrational relaxation and internal conversion dominate at higher electronic levels. If relaxation occurs and a photon is not emitted, it is a non-radiative relaxation. The timescale for fluorescence and the analogous non-radiative relaxation is 10^{-9} to 10^{-7} s. The energy loss via internal conversion and other non-radiative relaxations represents the difference in energy or stokes shift from the excitation and the emission spectra seen in the fluorescence spectrum. Transition from a singlet excited state to a triplet state is a forbidden transition in a process called ***intersystem crossing***. A depiction of the differences between the ground state, excited singlet state, and excited triplet state can be found

in **Figure 6.4**. The probability of intersystem crossing occurring is higher when the vibrational levels of the excited singlet and excited triplet states overlap. Overlap of vibrational levels occurs at higher energy levels. Because of the difference in time scales between intersystem crossing and internal conversion compared to the lifetime of singlet oxygen, intersystem crossing can compete with fluorescence when the transition between singlet and triplet vibrational levels are closest to the electronic level of the singlet state. However, internal conversion, a much faster process, will always outcompete intersystem crossing [171]. The energy difference between the transitions from vibrational levels in intersystem crossing is usually negligible. Relaxation from the triplet state to the ground state can occur in a non-radiative process or a radiative process called ***phosphorescence***. This relaxation is one of the slowest and is on the order of 10^{-4}-10^{-1} s. Once the electron has transitioned to the triplet state via intersystem crossing, it can alternatively undergo intersystem crossing again and go back to the excited singlet state; from there it can transition to the ground state in a process called ***delayed fluorescence*** or an analogous non-radiative process. Delayed fluorescence is order of magnitudes slower than fluorescence and occurs on the timescale of 10^{-3}-10^{-2} s. The competition between processes that dissipate energy back to the ground state from an excited state is rate-determined. Faster processes outcompete slower processes.

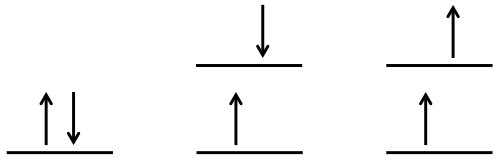

Figure 6.4. Representation of spin multiplicities for electrons in singlet and triplet states.

A photosensitizer in an excited singlet state is very short lived. Therefore, transfer of an electron or energy to ground state oxygen, likely occurs with an excited photosensitizer in its triplet state. The triplet state is forbidden, so decays to ground state in a much slower process. The probability of singlet oxygen being formed is limited by the quantum yield or likelihood that the excited photosensitizer will be excited to its triplet state. This quantum yield, $\boldsymbol{\phi_{TS}}$, can be estimated by **Equation 6.1**. k_f, k_{isc}, k_p and k_{ic} are the rate constants for the decay by fluorescence, intersystem crossing, phosphorescence, and internal conversion, respectively.

$$Quantum\ yield\ of\ triplet\ state, \phi_{TS} = \frac{k_{isc}}{k_{ic}+k_f+k_{isc}+k_p} \qquad \textbf{Equation 6.1}$$

From **Equation. 6.1** and the timescales for the photophysical processes found in **Figure 6.3**, the range of possible quantum yields can be estimated. The longer the time frame of intersystem crossing, the higher the quantum yield of the triplet state, leading to an increased probability of singlet oxygen formation.

In addition to the decay processes mentioned above, during the time in the excited state, an electron can interact via collisional quenching, fluorescence energy transfer (FRET), and rotational motion [170]. These processes are all non-radiative (no photon released), but allow for the transfer of energy so the electron can return to its ground-state energy. Excited photosensitizers can collide with other molecules, resulting in an energy transfer process. Quenching, a process that occurs when absorbing molecules are close to each other (usually within 2-10 nm) and have overlapping absorption and emission spectra, can also allow for the transfer of energy without emission. Non-radiative decay by a photosensitizer from its triplet state is more common than phosphorescence because the likelihood of interaction with molecular oxygen is enhanced because of the slow decay of the triplet photosensitizer [171].

The Type II reaction for singlet oxygen formation is an example of quenching. Energy is transferred directly from the excited photosensitizer to ground-state molecular oxygen, and singlet oxygen is formed directly. The Type I reaction is a radiative process, in which the transfer of an electron from the excited photosensitizer occurs.

Excited photosensitizers are likely absorbing multiple photons

Since flavins, specifically the flavin adenine dinucleotide (FAD) bound to the BluF sensor, was identified as the photosensitizer at the 455 nm BLI wavelength (refer to Chapter 4), an energetic model will be described using a Jablonski diagram at the 455 nm wavelength. Flavins have an optical absorption in the 400-500 nm range, have a high quantum yield of intersystem crossing, and have a high oxidation potential of the triplet state [172, 173]. Moore et al. determined the quantum yield of intersystem crossing for flavin to be between 0.6 and 0.7, depending on the solvent [173]. At 455 nm, the energy released per photon is 4.369×10^{-19} J, as determined by **Eq. 5.4**. This photon energy, which will be absorbed by the photosensitizer upon BLI, is above the minimum energy needed to excite ground-state molecular oxygen to its triplet state (1.566×10^{-19} J/molecule O_2). While $E_P > \Delta E_{TS}$, where E_P is the energy of the photosensitizer and ΔE_{TS} is the energy needed to excite oxygen from its triplet state to its singlet state, the energy loss due to internal conversion/vibrational relaxation has to be taken into consideration. The emission spectrum of the target photosensitizer in our UTI89 sample is seen in **Figure 6.1**. The emission maximum after excitation at 455 nm is 520 nm. Earlier, it was mentioned that the red-shift from excitation to emission is due to the loss of energy through non-radiative processes like internal conversion and vibrational relaxation. Using **Equation 5.4**, the energy difference was calculated for the red-shift from the excitation and emission maximum of 455 nm and 520 nm, respectively. The energy difference was determined to be 0.549×10^{-19} J, almost three-times less

than the energy required to excite one molecule of oxygen from its triplet state to its singlet state. It is possible for an electron to be excited by multiple photons. In order for this to occur, the timescale of photon delivery must be shorter than photon absorption (~10^{-15} s). In the experiments from Chapter 5, the rate of photon delivery (or flux) was varied, but the time scale for all fluxes ranged from ~10^{-19}-10^{-16} s (**Table 2.1**). The rate of photon delivery is much faster than the rate of absorption, making it a likely possibility that photosensitizers are excited by multiple photons to form singlet oxygen. Another possibility is that multiple excited photosensitizers interact with the same molecule of ground-state oxygen to form singlet oxygen to transfer the required energy for a state change. The latter is less likely because the probability of collision of multiple electrons in their forbidden triplet state with ground-state oxygen is low. There is also an increased chance of an excited photosensitizer transitioning from an excited singlet state to an excited triplet state, the higher the energy of the singlet state. At higher energy levels, the overlap of vibrational energy levels is inevitable and would therefore increase the chances of intersystem crossing. The high quantum yield of singlet to triplet hypericin supports the thought of multiple photons exciting one electron, leading to an abundance of singlet oxygen formation.

The minimum number of photons needed to interact with one electron, n_p, can be estimated using **Equation 6.2**. ΔE_{TS} is the energy required for singlet oxygen formation from the triplet ground-state oxygen, $\Delta E_{ex\text{-}em}$ is the difference between the excitation energy, E_{ex}, and emission energy, E_{em}, of one photon, and ϕ_{isc} is the intersystem crossing quantum yield.

$$n_p = \frac{\Delta E_{TS}}{(\Delta E_{ex-em})\cdot\phi_{isc}} \qquad \textbf{Equation 6.2}$$

ΔE_{TS} is 1.566x10^{-19} J. In the flavin photosensitizer system with BLI_{455}, the $\Delta E_{ex\text{-}em}$ between the excitation at 455 nm and emission of 520 nm was calculated as 0.549 x10^{-19} J. The ϕ_{isc} was

previously reported as 0.6-0.7 [173]. Based on the energy requirement of E_{abs}, the n_p must be ≥ 5. The total energy absorbed must be well above ΔE_{TS} to account for losses via internal conversion, intersystem crossing, and fluorescence.

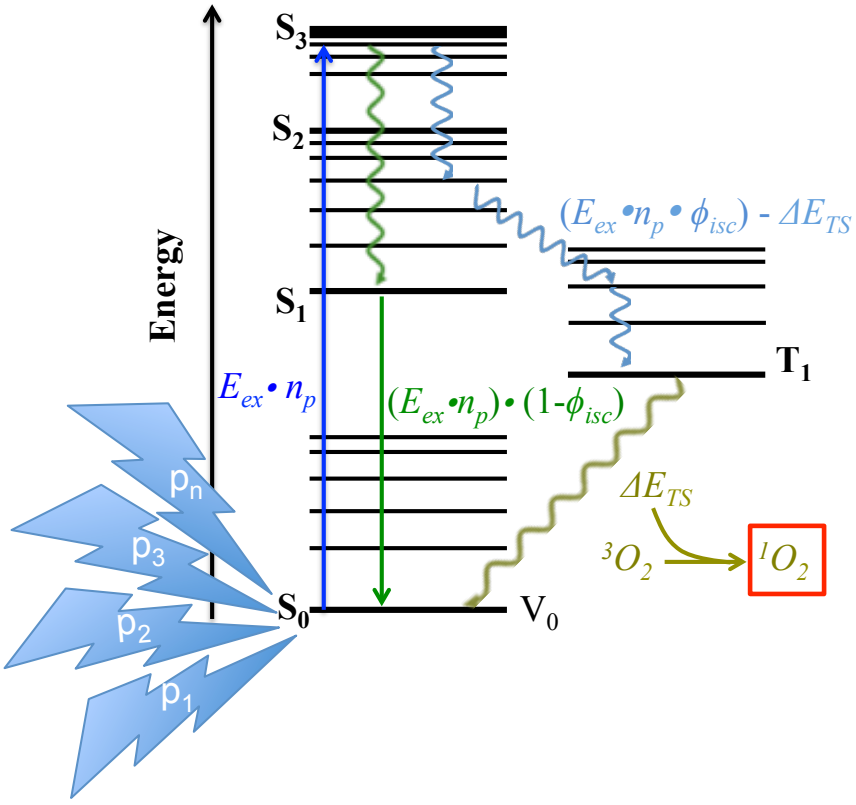

Figure 6.5. Jablonski diagram for the multi-photon interaction with a ground-state photosensitizer and subsequent singlet oxygen formation. Due to the time scale of the photon delivery, photosensitizers can absorb multiple photons (p_1 to p_n) and be excited to a higher electronic energy state. Once the excited singlet state is reached (represented by the dark blue line), the electron will relax down to the closest electronic state via Kasha's rule and then to the ground state energy via fluorescence (represented in green). At high energy levels, there will be competition between fluorescence and intersystem crossing (represented in light blue) because the vibrational levels of the singlet and triplet state will overlap. The probability of an electron transitioning to the forbidden triplet state is determined by its quantum yield ϕ_{isc}. Once in long-lived the triplet state, the excited photosensitizer can collide with ground-state triplet oxygen to form singlet oxygen. The transfer of energy from the triplet photosensitizer to triplet oxygen is represented in gold, where E_{TS} is the required transition energy from the triple to singlet state of molecular oxygen.

Based on this kinetic analysis, the Jablonski diagram in **Figure 6.5** was developed to describe the likely energy absorption and decay of electrons in the photon absorption of flavin photosensitizers in the UTI89 strain by BLI_{455}. The total energy absorbed, E_{abs}, can be found in **Equation 6.3**.

$$E_{abs} = E_{ex} \cdot n_p \qquad \textbf{Equation 6.3}$$

It was assumed the two dominating processes were fluorescence and intersystem crossing leading to a non-radiative decay through collisional energy transfer of the triplet photosensitizer and ground-state molecular oxygen. Because of the high quantum yield of intersystem crossing

to the triplet state, this assumption can be taken. For this reason, the delayed fluorescence process was not included. The internal conversion leading to fluorescence and the energy decay by fluorescence was coupled as one energy term, E_f, found in **Equation 6.4**.

$$E_f = (E_x \cdot n_p)(1 - \phi_{isc}) \qquad \textbf{Equation 6.4}$$

Similarly, the internal conversion leading to the intersystem crossing, the intersystem crossing, and the vibrational relaxation/internal conversion leading to the lowest triplet electronic state were grouped as one term, E_{isc}, and can be found in **Equation 6.5**. The energy difference from intersystem crossing is negligible because this process proceeds by overlapping vibrational levels, which have essentially the same energy.

$$E_{isc} = \left(E_x \cdot n_p \cdot \phi_{isc}\right) - \Delta E_{TS} \qquad \textbf{Equation 6.5}$$

CONCLUSION

The amount of BLI reductions can be determined using the model in **Figure 6.5**. Quantum yield values can be found in literature ([173] is a great resource for a list of measured quantum yields in various solvents) or measured experimentally for the desired photosensitizer. The excitation and emission spectrum can be measured using UV-Vis Spectroscopy to determine the excitation and emission maximums. Using **Equation 5.4**, the corresponding energies for the excitation and emission maximums can be calculated. From this model and the time scales listed in **Figure 6.3**, a relative comparison can be drawn for the amount of singlet oxygen that should theoretically be formed by varying light parameters. Once the Singlet Oxygen Sensor Green assay is optimized for the measurement of singlet oxygen for the BLI setup, quantum yields and rates of reactions can be determined for other wavelengths and photosensitizers.

CHAPTER 7

CONCLUSIONS

The previous six chapters presented results from investigations into the effects of blue light (specifically 420, 455, and 470 nm wavelengths) exposure on *E. coli.* These results support the conclusion that blue light irradiation (BLI) reduces the number of cells able to replicate, measured by the number of colony forming units (CFUs), in irradiated *E. coli* populations compared to that in non-irradiated *E. coli* populations.

The magnitude of the difference between CFUs in irradiated and non-irradiated populations depends on *E. coli* strain. The nonpathogenic, lab-adapted strain included in this work experienced the largest reduction in the number of CFUs due to BLI. BLI reduced the number of CFUs in populations of uropathogenic strains, those that infect the urinary tract, to a larger extent than that in commensal and pathogenic strains, those typically found in the gut. The extent of the difference in the number of CFUs in irradiated and non-irradiated populations of a multi-drug resistant uropathogenic strain was less than that in a drug-sensitive uropathogenic strain.

The magnitude of BLI-induced differences in the number of CFUs in irradiated and non-irradiated *E. coli* populations also depends on the growth phase the bacteria are in during the irradiation. This work is the first to report on these growth phase-specific responses to BLI. Most published studies have only investigated bacteria exposed while they are in the exponential phase of growth [11, 12, 16, 34, 37, 41, 44, 45, 64, 112, 113]. A few recent reports on investigations of BLI on biofilms have been published [114, 121, 174, 175]. The largest differences between the number of CFUs in irradiated and non-irradiated populations were achieved when the *E. coli* populations were irradiated during the exponential growth phase. BLI of most pathogenic strains

while in the stationary growth phase reduced the number of CFUs greater than BLI of these strains in other growth phases. This result is contrary to the fact that pathogenic bacteria in the stationary and extended stationary growth phases are generally more tolerant to treatment than bacteria in the earlier growth phases [114, 121]. Since bacteria in the environment and in infections are primarily found in the treatment-resistant stationary phase or in biofilms [114, 116, 119-121, 135], the ability of BLI to affect reproduction of *E. coli* in the stationary growth phase is a positive attribute. The differences between CFUs in irradiated and non-irradiated populations of the pathogenic strains were greater than those in the non-pathogenic, non-lab-adapted strains. The ability of BLI to reduce the number of CFUs in populations of pathogenic *E. coli* strains to a greater extent than that in populations of non-pathogenic strains, even in the more resistant later growth phases, is attractive. Traditional antibiotic treatments are indiscriminate of non-pathogenic and pathogenic bacteria. These results suggest that BLI has the potential to be optimized to preferentially affect the pathogenic bacteria over non-pathogenic bacteria, making it a promising antimicrobial treatment strategy.

The magnitude of the difference between the number of CFUs in irradiated and non-irradiated *E. coli* populations also depends on the wavelength and total energy dose of the irradiation. Irradiations at 420 nm (BLI_{420}) induced the largest differences between the number of CFUs in irradiated and non-irradiated populations. This result is consistent with the fact that ultraviolet light (UV) (< 400 nm) is widely used for sterilization due to its ability to damage nucleic acids [40, 156]. While wavelengths less than 420 nm may decrease the number of CFUs to a greater extent than longer wavelengths, irradiations at these shorter wavelengths may create a greater risk of mutations in not only the bacteria, but also in the host.

Results of investigations using *bluF* and *bluR* mutants led to the conclusion that flavins bound to BluF proteins are the photosensitizer moieties involved in *E. coli*'s response to BLI at 455 nm (BLI_{455}). BLI_{455} of *E. coli* with *bluF* (encodes for the BluF protein) or *bluR* (encodes for the BluR protein) gene deletions resulted in a smaller difference in the number of CFUs between unexposed and exposed populations compared to BLI_{455} of the non-mutated, wild-type parent strain. No difference was observed between wild-type and mutant strain responses when irradiated with BLI_{420} or BLI_{470}. These findings suggest that the presence of both the BluF sensor and the BluR transcriptional regulator are essential in achieving wild-type levels of BLI_{455}-induced reduction in CFUs. These results also suggest that irradiations with light at 420, 455, and 470 nm induce different mechanisms in *E. coli*. Different photosensitizer molecules are capable of absorbing light at different wavelengths. Therefore, irradiations using the different wavelengths will most likely activate different photosensitizers, which may initiate different mechanisms within the bacteria.

Findings from two luminescence-based ATP assays determined that BLI_{455} at a dose of 120 J/cm^2 is not bactericidal for the *E. coli* strains tested in this study. While BLI_{455} reduced the number of CFUs in irradiated populations of all tested strains of *E. coli* compared to non-irradiated controls, the bacteria were not killed. The levels of cell death measured were similar in all irradiated samples and their respective controls. Therefore, the observed cell death is not a result of BLI. This finding is important because many studies have implicated that irradiation with visible light induces cell death of various bacteria, including *E.* coli, because of an observed reduction in CFUs over time [4, 12, 14, 16, 34-37, 63, 79, 111, 156, 166, 176-178]. However, as observed in this work, a decrease in the number of CFUs between non-irradiated and irradiated samples does not signify cell death.

WORKING MODEL FOR BLI REDUCTIONS

Upon light absorption by FAD with BLI_{455}, the FAD photosensitizer is excited and initiates the signal pathway between BluF and BluR. When BluR is missing, the signal is not transduced. When BluF is missing, the photons are not absorbed. At BLI_{455}, there were reductions due to both photosensitizer-mediated absorption of light in addition to absorption of light by the FAD-containing BLUF sensor. When the *bluF* or *bluR* gene was deleted there was minimal reduction with BLI at 455 nm. This minimal reduction can be attributed to a non-BLUF photosensitizer-mediated response. Reductions with BLI_{420} and BLI_{470} were independent of the signaling pathway between BluF and BluR and followed the mechanism of an excited photosensitizer leading to a transfer of energy or an electron to produce ROS and cytotoxic singlet oxygen. Higher energy doses led to an increased reduction, which follows the model of increased ROS and singlet oxygen production, leading to an increased cytotoxicity. The working model is depicted in **Figure 7.1**.

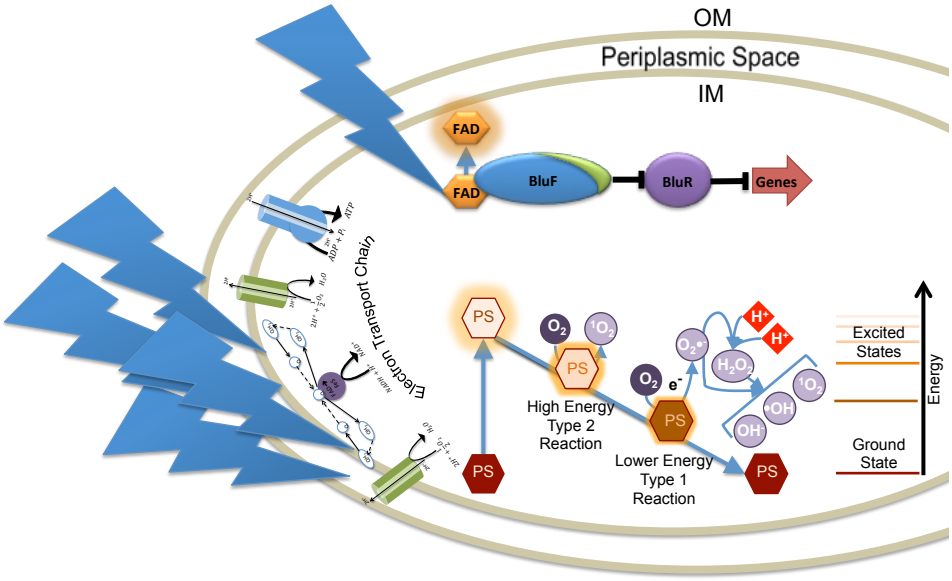

Figure 7.1. Working model for BLI-induced reductions in *E. coli*. All BLI-induced reductions follow the pathway of an excited photosensitizer leading to formation of ROS and/or singlet oxygen upon energy or electron transfer from the excited photosensitizer to ground state molecular oxygen. In addition to the singlet oxygen-mediated reductions, at BLI_{455} the FAD domain of the BLUF sensor also absorbs blue light. Upon absorption of light by FAD, the excited FAD activates the signaling pathway between BluF and BluR. This signaling pathway aids in the reduction of CFUs by BLI_{455}.

BROADER IMPLICATIONS

BLI's ability to reduce the number of *E. coli* that can replicate in a population could be leveraged to prevent the population from proliferating to an infectious level. Hospital acquired infections were dramatically decreased between 2011 and 2014 [179]. Catheter-associated urinary tract infections (CAUTIs) are the exception this decrease [179]. Between 2009 and 2014 CAUTIs increased by 6% [179]. Eighty-five percent of UTIs are caused by *E. coli* [180]. In the context of a CAUTI, these bacteria can proliferate and ascend the catheter to the bladder [180]. Results from this work suggest that BLI could inhibit the replication of *E. coli*, especially those that are introduced into the catheter during insertion. By inhibiting replication, BLI could prevent bacterial colonization on a catheter. To date, no study has evaluated the potential of using BLI as a deterrent to bacterial colonization on devices. More work is needed to investigate the potential of preventing CAUTIs with BLI. Some of the important questions that need to be investigated are discussed below.

Is the inhibition of replication permanent or can the inhibited *E. coli* "revive" from this dormant/damaged state? Lowering the pH of the nutrient environment revived dormant persister cells [127-130]. This suggests that replication-inhibited *E. coli* could be revived. Potential external stimuli such as temperature, pH, and enriched nutrient sources should be investigated. Also, populations should be monitored over extended periods to determine if they eventually regain their ability to replicate.

What are the effects of multiple irradiations on *E. coli* populations? Multiple irradiations might be necessary in an infection prevention strategy. Multiple irradiations could induce mutations in cells that could make them impervious to BLI. Future work should identify

mutations induced by multiple BLI exposures. Also, studies elucidating the cause of the replication inhibition are needed to optimize BLI for CAUTI prevention.

What are the mechanisms involved in BLI-induced replication inhibition? Studies detailing growth inhibition mechanisms using these lower wavelengths are needed. Results from these studies are needed to optimize the irradiation properties, such as wavelength, dose and frequency of treatment. Wavelengths less than 420 nm should be included. BLI within a catheter could be designed such that the light would not interact with human tissue, eliminating the potential of the irradiations causing mutations in the patient's cells. Viability assays are needed to determine at what wavelength, if any, BLI becomes bactericidal.

Can replication-inhibited *E. coli* express the fibers needed to adhere to the catheter's surface? If motile bacteria like *E. coli* cannot adhere to the catheter surface and replicate, contact with the urinary tract can be prevented. These non-adherent bacteria can then be voided by urine flow through the catheter.

What is the maximum concentration at which BLI is effective? Exposing different *E. coli* concentrations to BLI to determine where the relationship between exposure concentration and growth inhibition would identify this maximum concentration.

Does BLI induce replication inhibition in other bacterial species? Gram-negative *Klebsiella pneumoniae* and *Pseudomonas aeruginosa* along with Gram-positive *Streptococcus* species, *Enterococcus* species and *Staphylococcus epidermis* account for a majority of the remaining ~15% UTIs, not caused by *E. coli* [180, 181]. The effects of BLI on these uropathogenic species need to be investigated. Based on previous studies, BLI is more effective in inhibiting growth of Gram-positive species, suspected to be due to the presence of an additional cell membrane in Gram-negative bacteria [37, 42, 43].

How does BLI affect the properties of the catheter material? Does the refractive index and absorption spectra of common catheter materials, including, but not limited to, silicone, latex, and Teflon change as a function of BLI dose, wavelength or time? It is also imperative to test the structural integrity of catheters after constant exposure to BLI. Cross-linking, weakening of the polymer (leading to cracks or holes), or morphological changes could be induced by the light alone or by reactive oxygen species secreted from bacteria as a response to the irradiation.

All together this work and proposed future work shows promises for clinical applications of BLI. With the increasing need for alternative antimicrobial strategies, BLI may be able to play a role in decreasing the incidences of CAUTIs.

REFERENCES

1. Bitter, P.H., *Noninvasive rejuvenation of photodamaged skin using serial, full-face intense pulsed light treatments.* Dermatologic Surgery, 2000. **26**(9): p. 835-843.
2. Dai, T., A. Gupta, C.K. Murray, M.S. Vrahas, G.P. Tegos, and M.R. Hamblin, *Blue light for infectious diseases: Propionibacterium acnes, Helicobacter pylori, and beyond?* Drug Resistance Updates, 2012. **15**(4): p. 223-236.
3. Kale, Y., O. Aydemir, Ü. Celik, S. Kavurt, S. Isikoglu, A.Y. Bas, and N. Demirel, *Effects of phototherapy using different light sources on oxidant and antioxidant status of neonates with jaundice.* Early Human Development, 2013. **89**(12): p. 957-960.
4. Maisch, T., A. Eichner, A. Späth, A. Gollmer, B. König, J. Regensburger, and W. Bäumler, *Fast and effective photodynamic inactivation of multiresistant bacteria by cationic riboflavin derivatives.* PLoS ONE, 2014. **9**(12): p. e111792.
5. Morris, B.H., J.E. Tyson, D.K. Stevenson, W. Oh, D.L. Phelps, T.M. O'Shea, G.E. McDavid, K.P. Van Meurs, B.R. Vohr, C. Grisby, Q. Yao, S. Kandefer, D. Wallace, and R.D. Higgins, *Efficacy of phototherapy devices and outcomes among extremely low birth weight infants: multi-center observational study.* Journal of Perinatology: official journal of the California Perinatal Association, 2013. **33**(2): p. 126-133.
6. Opel, D.R., E. Hagstrom, A.K. Pace, K. Sisto, S.A. Hirano-Ali, S. Desai, and J. Swan, *Light-emitting Diodes: A Brief Review and Clinical Experience.* The Journal of Clinical and Aesthetic Dermatology, 2015. **8**(6): p. 36-44.
7. Pei, S., A.C. Inamadar, K.A. Adya, and M.M. Tsoukas, *Light-based therapies in acne treatment.* Indian Dermatology Online Journal, 2015. **6**(3): p. 145-157.

8. Piccolo, D., D. Di Marcantonio, G. Crisman, G. Cannarozzo, M. Sannino, A. Chiricozzi, and S. Chimenti, *Unconventional use of intense pulsed light.* BioMed Research International, 2014. **2014**: p. 618206.

9. Sherbiny, H.S., D.M. Youssef, A.S. Sherbini, R. El-Behedy, and L.M. Sherief, *High-intensity light-emitting diode vs fluorescent tubes for intensive phototherapy in neonates.* Paediatrics and International Child Health, 2015. **0**(0): p. 2046905515Y.0000000006.

10. Vandborg, P.K., B.M. Hansen, G. Greisen, and F. Ebbesen, *Dose-response relationship of phototherapy for hyperbilirubinemia.* Pediatrics, 2012. **130**(2): p. e352-e357.

11. Lipovsky, A., Y. Nitzan, H. Friedmann, and R. Lubart, *Sensitivity of Staphylococcus aureus strains to broadband visible light.* Photochemistry and Photobiology, 2009. **85**(1): p. 255-260.

12. Lipovsky, A., Y. Nitzan, A. Gedanken, and R. Lubart, *Visible light-induced killing of bacteria as a function of wavelength: Implication for wound healing.* Lasers in Surgery and Medicine, 2010. **42**(6): p. 467-472.

13. Lubart, R., R. Lavi, H. Friedmann, and S. Rochkind, *Photochemistry and photobiology of light absorption by living cells.* Photomedicine and Laser Surgery, 2006. **24**(2): p. 179-185.

14. Lubart, R., A. Lipovski, Y. Nitzan, and H. Friedmann, *A possible mechanism for the bactericidal effect of visible light.* Laser Therapy, 2011. **20**(1): p. 17-22.

15. Nussbaum, E.L., L. Lilge, and T. Mazzulli, *Effects of 630-, 660-, 810-, and 905-nm laser irradiation delivering radiant exposure of 1-50 J/cm2 on three species of bacteria in vitro.* 2002. **20**(6): p. 325-333.

16. Cieplik, F., A. Späth, C. Leibl, A. Gollmer, J. Regensburger, L. Tabenski, K.-A. Hiller, T. Maisch, and G. Schmalz, *Blue light kills Aggregatibacter actinomycetemcomitans due to its endogenous photosensitizers.* Clinical Oral Investigations, 2014. **18**(7): p. 1763-1769.

17. Domratcheva, T., B.L. Grigorenko, I. Schlichting, and A.V. Nemukhin, *Molecular models predict light-induced glutamine tautomerization in BLUF photoreceptors.* Biophysical Journal, 2008. **94**(10): p. 3872-3879.

18. Gomelsky, M. and S. Kaplan, *AppA, a redox regulator of photosystem formation in Rhodobacter sphaeroides 2.4.1, Is a flavoprotein: Identification of a novel FAD binding domain.* Journal of Biological Chemistry, 1998. **273**(52): p. 35319-35325.

19. Gomelsky, M. and G. Klug, *BLUF: a novel FAD-binding domain involved in sensory transduction in microorganisms.* Trends in Biochemical Sciences. **27**(10): p. 497-500.

20. Hasegawa, K., S. Masuda, and T.-a. Ono, *Structural intermediate in the photocycle of a BLUF (sensor of blue light using FAD) protein Slr1694 in a Cyanobacterium Synechocystis sp. PCC6803.* Biochemistry, 2004. **43**(47): p. 14979-14986.

21. Hasegawa, K., S. Masuda, and T.-a. Ono, *Light Induced Structural Changes of a Full-length Protein and Its BLUF Domain in YcgF(Blrp), a Blue-Light Sensing Protein That Uses FAD (BLUF).* Biochemistry, 2006. **45**(11): p. 3785-3793.

22. Kraft, B.J., S. Masuda, J. Kikuchi, V. Dragnea, G. Tollin, J.M. Zaleski, and C.E. Bauer, *Spectroscopic and mutational analysis of the blue-light photoreceptor AppA: a novel photocycle involving flavin stacking with an aromatic amino acid.* Biochemistry, 2003. **42**(22): p. 6726-6734.

23. Mathes, T., I.H.M. van Stokkum, M. Stierl, and J.T.M. Kennis, *Redox modulation of flavin and tyrosine determines photoinduced proton-coupled electron transfer and photoactivation of BLUF photoreceptors.* Journal of Biological Chemistry, 2012. **287**(38): p. 31725-31738.

24. Nakasone, Y., T.-a. Ono, A. Ishii, S. Masuda, and M. Terazima, *Transient dimerization and conformational change of a BLUF protein: YcgF.* Journal of the American Chemical Society, 2007. **129**(22): p. 7028-7035.

25. Rajagopal, S., J.M. Key, E.B. Purcell, D.J. Boerema, and K. Moffat, *Purification and initial characterization of a putative blue light-regulated phosphodiesterase from Escherichia coli.* Photochemistry and Photobiology, 2004. **80**(3): p. 542-547.

26. Schroeder, C., K. Werner, H. Otten, S. Krätzig, H. Schwalbe, and L.-O. Essen, *Influence of a joining helix on the BLUF domain of the YcgF photoreceptor from Escherichia coli.* ChemBioChem, 2008. **9**(15): p. 2463-2473.

27. Tschowri, N., S. Busse, and R. Hengge, *The BLUF-EAL protein YcgF acts as a direct anti-repressor in a blue-light response of Escherichia coli.* Genes & Development, 2009. **23**(4): p. 522-534.

28. Tschowri, N., S. Lindenberg, and R. Hengge, *Molecular function and potential evolution of the biofilm-modulating blue light-signalling pathway of Escherichia coli.* Molecular Microbiology, 2012. **85**(5): p. 893-906.

29. Unno, M., S. Masuda, T.-a. Ono, and S. Yamauchi, *Orientation of a key glutamine residue in the BLUF domain from AppA revealed by mutagenesis, spectroscopy, and quantum chemical calculations.* Journal of the American Chemical Society, 2006. **128**(17): p. 5638-5639.

30. Unno, M., R. Sano, S. Masuda, T.-a. Ono, and S. Yamauchi, *Light-induced structural changes in the active site of the BLUF domain in AppA by raman spectroscopy.* The Journal of Physical Chemistry B, 2005. **109**(25): p. 12620-12626.

31. van der Horst, M.A. and K.J. Hellingwerf, *Photoreceptor proteins, "star actors of modern times": A review of the functional dynamics in the structure of representative members of six different photoreceptor families.* Accounts of Chemical Research, 2004. **37**(1): p. 13-20.

32. Zoltowski, B.D. and K.H. Gardner, *Tripping the light fantastic: Blue-light photoreceptors as examples of environmentally modulated protein-protein interactions.* Biochemistry, 2010. **50**(1): p. 4-16.

33. Masuda, S., K. Hasegawa, A. Ishii, and T.-a. Ono, *Light-induced structural changes in a putative blue-light receptor with a novel FAD binding fold sensor of blue-light using FAD (BLUF); Slr1694 of Synechocystis sp. PCC6803.* Biochemistry, 2004. **43**(18): p. 5304-5313.

34. Guffey, J.S. and J. Wilborn, *In vitro bactericidal effects of 405-nm and 470-nm blue light.* Photomedicine and Laser Surgery, 2006. **24**(6): p. 684-688.

35. Gad, F., T. Zahra, K.P. Francis, T. Hasan, and M.R. Hamblin, *Targeted photodynamic therapy of established soft-tissue infections in mice.* Photochem Photobiol Sci, 2004. **3**(5): p. 451-8.

36. Bumah, V.V., D.S. Masson-Meyers, S.E. Cashin, and C.S. Enwemeka, *Wavelength and bacterial density influence the bactericidal effect of blue light on methicillin-resistant Staphylococcus aureus (MRSA).* Photomed Laser Surg, 2013. **31**(11): p. 547-553.

37. Guffey, J.S. and J. Wilborn, *Effects of combined 405-nm and 880-nm light on Staphylococcus aureus and Pseudomonas aeruginosa in vitro.* Photomedicine and Laser Surgery, 2006. **24**(6): p. 680-683.

38. Liu, G., C. Pan, K. Li, Y. Tan, and X. Wei, *Phototherapy for mild to moderate acne vulgaris with portable blue and red led.* Journal of Innovative Optical Health Sciences, 2011. **4**(1): p. 45-52.

39. Papageorgiou, P., A. Katsambas, and A. Chu, *Phototherapy with blue (415 nm) and red (660 nm) light in the treatment of acne vulgaris.* British Journal of Dermatology, 2000. **142**(5): p. 973-978.

40. Chui, C., K. Hiratsuka, A. Aoki, Y. Takeuchi, Y. Abiko, and Y. Izumi, *Blue LED inhibits the growth of Porphyromonas gingivalis by suppressing the expression of genes associated with DNA replication and cell division.* Lasers in Surgery and Medicine, 2012. **44**(10): p. 856-864.

41. Lambrechts, S.A., T.N. Demidova, M.C. Aalders, T. Hasan, and M.R. Hamblin, *Photodynamic therapy for Staphylococcus aureus infected burn wounds in mice.* Photochem Photobiol Sci, 2005. **4**(7): p. 503-9.

42. Maclean, M., S.J. MacGregor, J.G. Anderson, and G. Woolsey, *High-intensity narrow-spectrum light inactivation and wavelength sensitivity of Staphylococcus aureus.* FEMS Microbiol Lett, 2008. **285**(2): p. 227-32.

43. Maclean, M., S.J. MacGregor, J.G. Anderson, and G. Woolsey, *Inactivation of bacterial pathogens following exposure to light from a 405-nanometer light-emitting diode array.* Appl Environ Microbiol, 2009. **75**(7): p. 1932-7.

44. Orenstein, A., D. Klein, J. Kopolovic, E. Winkler, Z. Malik, N. Keller, and Y. Nitzan, *The use of porphyrins for eradication of Staphylococcus aureus in burn wound infections.* FEMS Immunol Med Microbiol, 1997. **19**(4): p. 307-14.

45. Feuerstein, O., I. Ginsburg, E. Dayan, D. Veler, and E.I. Weiss, *Mechanism of Visible Light Phototoxicity on Porphyromonas gingivalis and Fusobacterium nucleatum.* Photochemistry and Photobiology, 2005. **81**(5): p. 1186-1189.

46. Buonanno, M., G. Randers-Pehrson, A.W. Bigelow, S. Trivedi, F.D. Lowy, H.M. Spotnitz, S.M. Hammer, and D.J. Brenner, *207-nm UV Light - A promising tool for safe low-cost reduction of surgical site infections. In vitro studies.* PLoS ONE, 2013. **8**(10): p. e76968.

47. Donlan, R.M. and J.W. Costerton, *Biofilms: Survival mechanisms of clinically relevant microorganisms.* Clinical Microbiology Reviews, 2002. **15**(2): p. 167-193.

48. Enwemeka, C.S., D. Williams, S. Hollosi, D. Yens, and S.K. Enwemeka, *Visible 405 nm SLD light photo-destroys methicillin-resistant Staphylococcus aureus (MRSA) in vitro.* Lasers in Surgery and Medicine, 2008. **40**(10): p. 734-737.

49. Epstein, A.K., B. Pokroy, A. Seminara, and J. Aizenberg, *Bacterial biofilm shows persistent resistance to liquid wetting and gas penetration.* Proceedings of the National Academy of Sciences, 2011. **108**(3): p. 995-1000.

50. Farr, S.B. and T. Kogoma, *Oxidative stress responses in Escherichia coli and Salmonella typhimurium.* Microbiological Reviews, 1991. **55**(4): p. 561-585.

51. Hanakova, A., K. Bogdanova, K. Tomankova, K. Pizova, J. Malohlava, S. Binder, R. Bajgar, K. Langova, M. Kolar, J. Mosinger, and H. Kolarova, *The application of antimicrobial photodynamic therapy on S. aureus and E. coli using porphyrin*

photosensitizers bound to cyclodextrin. Microbiological Research, 2014. **169**(2-3): p. 163-170.

52. Hernroth, B., Å. Lothigius, and I. Bölin, *Factors influencing survival of enterotoxigenic Escherichia coli, Salmonella enterica (serovar Typhimurium) and Vibrio parahaemolyticus in marine environments.* FEMS Microbiology Ecology, 2010. **71**(2): p. 272-280.

53. Kennis, J.T.M. and T. Mathes, *Molecular eyes: proteins that transform light into biological information.* Interface Focus, 2013. **3**(5).

54. Liang, J.-Y., J.-M.P. Yuann, C.-W. Cheng, H.-L. Jian, C.-C. Lin, and L.-Y. Chen, *Blue light induced free radicals from riboflavin on E. coli DNA damage.* Journal of Photochemistry and Photobiology B: Biology, 2013. **119**(0): p. 60-64.

55. Marugán, J., R. van Grieken, C. Pablos, and C. Sordo, *Analogies and differences between photocatalytic oxidation of chemicals and photocatalytic inactivation of microorganisms.* Water Research, 2010. **44**(3): p. 789-796.

56. Popov, D.E., E.S. Tuchina, J.A. Chernova, D. Podshibyakin, D.V. Rudik, M. Samsonova, I. Gromov, and V.V. Tuchin. *The affect of low-coherent light on microbial colony forming ability and morphology of some gram-positive and gram-negative bacteria*. 2005.

57. Tegos, G., T. Dai, B.B. Fuchs, J.J. Coleman, R.A. Prates, C. Astrakas, T.G. St Denis, M.S. Ribeiro, E. Mylonakis, and M.R. Hamblin, *Concepts and principles of photodynamic therapy as an alternative antifungal discovery platform.* Frontiers in Microbiology, 2012. **3**.

58. Feuerstein, O., D. Moreinos, and D. Steinberg, *Synergic antibacterial effect between visible light and hydrogen peroxide on Streptococcus mutans.* Journal of Antimicrobial Chemotherapy, 2006. **57**(5): p. 872-876.

59. Meysick. *Oxidase Test*. Microbiology 2815 [cited 2015 2/12/2015]; Available from: https://http://www.studyblue.com/notes/note/n/oxidase-test-/deck/853298.

60. Braatsch, S. and G. Klug, *Blue Light Perception in Bacteria.* Photosynthesis Research, 2004. **79**(1): p. 45-57.

61. Kim, J.-S., H.K. Lim, M.H. Lee, J.-H. Park, E.C. Hwang, B.J. Moon, and S.-W. Lee, *Production of porphyrin intermediates in Escherichia coli carrying soil metagenomic genes.* FEMS Microbiology Letters, 2009. **295**(1): p. 42-49.

62. Kwon, S.J., A.L. de Boer, R. Petri, and C. Schmidt-Dannert, *High-level production of porphyrins in metabolically engineered Escherichia coli: Systematic extension of a pathway assembled from overexpressed genes involved in heme biosynthesis.* Applied and Environmental Microbiology, 2003. **69**(8): p. 4875-4883.

63. Nitzan, Y., Z. Malik, M. Kauffman, and B. Ehrenberg. *Induction of endogenic porphyrin production in bacteria and subsequent photoinactivation by various light sources*. in *Proceedings of SPIE Conference*. 1997.

64. Yang, H., H. Inokuchi, and J. Adler, *Phototaxis away from blue light by an Escherichia coli mutant accumulating protoporphyrin IX.* Proceedings of the National Academy of Sciences of the United States of America, 1995. **92**(16): p. 7332-7336.

65. Yang, H., A. Sasarman, H. Inokuchi, and J. Adler, *Non-iron porphyrins cause tumbling to blue light by an Escherichia coli mutant defective in hemG.* Proceedings of the National Academy of Sciences, 1996. **93**(6): p. 2459-2463.

66. Kawada, A., Y. Aragane, H. Kameyama, Y. Sangen, and T. Tezuka, *Acne phototherapy with a high-intensity, enhanced, narrow-band, blue light source: an open study and in vitro investigation.* Journal of Dermatological Science, 2002. **30**(2): p. 129-135.

67. Möbius, K., R. Arias-Cartin, D. Breckau, A.-L. Hännig, K. Riedmann, R. Biedendieck, S. Schröder, D. Becher, A. Magalon, J. Moser, M. Jahn, and D. Jahn, *Heme biosynthesis is coupled to electron transport chains for energy generation.* Proceedings of the National Academy of Sciences, 2010. **107**(23): p. 10436-10441.

68. Jung, A., T. Domratcheva, M. Tarutina, Q. Wu, W.-h. Ko, R.L. Shoeman, M. Gomelsky, K.H. Gardner, and I. Schlichting, *Structure of a bacterial BLUF photoreceptor: Insights into blue light-mediated signal transduction.* Proceedings of the National Academy of Sciences of the United States of America, 2005. **102**(35): p. 12350-12355.

69. Wu, Q. and K.H. Gardner, *Structure and insight into blue light-induced changes in the BlrP1 BLUF domain.* Biochemistry, 2009. **48**(12): p. 2620-2629.

70. Hengge, R., *Principles of c-di-GMP signalling in bacteria.* Nature Reviews Microbiology, 2009. **7**(4): p. 263-273.

71. Carroll, J.D. *A 3D dose model for low level laser / led therapy biostimulation and bioinhibition*. in *SPIE 6846*. 2008.

72. Hajj Chehade, M., L. Loiseau, M. Lombard, L. Pecqueur, A. Ismail, M. Smadja, B. Golinelli-Pimpaneau, C. Mellot-Draznieks, O. Hamelin, L. Aussel, S. Kieffer-Jaquinod, N. Labessan, F. Barras, M. Fontecave, and F. Pierrel, *ubiI, a new gene in Escherichia coli coenzyme Q biosynthesis, is involved in aerobic C5-hydroxylation.* Journal of Biological Chemistry, 2013. **288**(27): p. 20085-20092.

73. Floyd, K.A., C.A. Mitchell, A.R. Eberly, S. Colling, E.W. Zhang, W. DePas, M.R. Chapman, M. Conover, B.R. Rogers, S.J. Hultgren, and M. Hadjifrangiskou, *The UbiI (VisC) aerobic ubiquinone synthase is required for expression of type 1 pili, biofilm formation, and pathogenesis in uropathogenic Escherichia coli.* Journal of Bacteriology, under revision.

74. Hadjifrangiskou, M., M. Kostakioti, S.L. Chen, J.P. Henderson, S.E. Greene, and S.J. Hultgren, *A central metabolic circuit controlled by QseC in pathogenic Escherichia coli.* Molecular Microbiology, 2011. **80**(6): p. 1516-1529.

75. Barrick, J.E. and R.E. Lenski, *Genome dynamics during experimental evolution.* Nature Reviews Genetics, 2013. **14**(12): p. 827-839.

76. Hand, N.J. and T.J. Silhavy, *Null Mutations in a Nudix Gene, ygdP, Implicate an Alarmone Response in a Novel Suppression of Hybrid Jamming.* Journal of Bacteriology, 2003. **185**(22): p. 6530-6539.

77. Ozsolak, F. and P.M. Milos, *RNA sequencing: advances, challenges and opportunities.* Nature Review Genetics, 2011. **12**(2): p. 87-98.

78. Dai, T., A. Gupta, Y.Y. Huang, M.E. Sherwood, C.K. Murray, M.S. Vrahas, T. Kielian, and M.R. Hamblin, *Blue light eliminates community-acquired methicillin-resistant Staphylococcus aureus in infected mouse skin abrasions.* Photomedicine Laser Surgery, 2013. **31**(11): p. 531-538.

79. Donnelly, R.F., C.M. Cassidy, R.G. Loughlin, A. Brown, M.M. Tunney, M.G. Jenkins, and P.A. McCarron, *Delivery of Methylene Blue and meso-tetra (N-methyl-4-pyridyl) porphine tetra tosylate from cross-linked poly(vinyl alcohol) hydrogels: a potential*

means of photodynamic therapy of infected wounds. Journal of Photochemistry and Photobiology B: Biology, 2009. **96**(3): p. 223-31.

80. *American national standard for safe use of lasers in health care: ANSI Z136.3 – 2011.* Laser Institute of America, 2011. **2011**(American National Standard): p. 1-114.

81. Laboratories, B.R., *BRL pUC host: E. coli DH5α competent cells.* Bethesda Res Lab Focus, 1986. **8**(2): p. 9.

82. Bachmann, B., in *Escherichia coli and Salmonella: Cellular and Molecular Biology*, F.C. Neidhart and R. Curtiss, Editors. 1996, ASM Press. p. 2460-2488.

83. Mulvey, M.A., Y.S. Lopez-Boado, C.L. Wilson, R. Roth, W.C. Parks, J. Heuser, and S.J. Hultgren, *Induction and evasion of host defenses by type 1-piliated uropathogenic Escherichia coli.* Science, 1998. **282**(5393): p. 1494-1497.

84. Totsika, M., S.A. Beatson, S. Sarkar, M.-D. Phan, N.K. Petty, N. Bachmann, M. Szubert, H.E. Sidjabat, D.L. Paterson, M. Upton, and M.A. Schembri, *Insights into a multidrug resistant Escherichia coli pathogen of the globally disseminated ST131 lineage: Genome analysis and virulence mechanisms.* PLoS ONE, 2011. **6**(10): p. e26578.

85. Hayashi, T., K. Makino, M. Ohnishi, K. Kurokawa, K. Ishii, K. Yokoyama, C.-G. Han, E. Ohtsubo, K. Nakayama, T. Murata, M. Tanaka, T. Tobe, T. Iida, H. Takami, T. Honda, C. Sasakawa, N. Ogasawara, T. Yasunaga, S. Kuhara, T. Shiba, M. Hattori, and H. Shinagawa, *Complete genome sequence of enterohemorrhagic Eschelichia coli O157:H7 and genomic comparison with a laboratory strain K-12.* DNA Research, 2001. **8**(1): p. 11-22.

86. Rúgeles, L.C., J. Bai, A.J. Martínez, M.C. Vanegas, and O.G. Gómez-Duarte, *Molecular characterization of diarrheagenic Escherichia coli strains from stools samples and food*

products in Colombia. International journal of food microbiology, 2010. **138**(3): p. 282-286.

87. Levine, M.M., P. Ristaino, G. Marley, C. Smyth, S. Knutton, E. Boedeker, R. Black, C. Young, M.L. Clements, and C. Cheney, *Coli surface antigens 1 and 3 of colonization factor antigen II-positive enterotoxigenic Escherichia coli: morphology, purification, and immune responses in humans.* Infection and Immunity, 1984. **44**(2): p. 409-420.

88. ThorLabs. *Mounted LED specifications*. [cited 2013; Available from: https://http://www.thorlabs.com/newgrouppage9.cfm?objectgroup_id=2692.

89. Allison, K.R., M.P. Brynildsen, and J.J. Collins, *Metabolite-enabled eradication of bacterial persisters by aminoglycosides.* Nature, 2011. **473**(7346): p. 216-20.

90. Hadjifrangiskou, M., A.P. Gu, J.S. Pinkner, M. Kostakioti, E.W. Zhang, S.E. Greene, and S.J. Hultgren, *Transposon mutagenesis identifies uropathogenic Escherichia coli biofilm factors.* Journal of Bacteriology, 2012. **194**(22): p. 6195-6205.

91. Pinkner, J.S., H. Remaut, F. Buelens, E. Miller, V. Aberg, N. Pemberton, M. Hedenstrom, A. Larsson, P. Seed, G. Waksman, S.J. Hultgren, and F. Almqvist, *Rationally designed small compounds inhibit pilus biogenesis in uropathogenic bacteria.* Proc Natl Acad Sci U S A, 2006. **103**(47): p. 17897-902.

92. Wright, K.J., P.C. Seed, and S.J. Hultgren, *Uropathogenic Escherichia coli flagella aid in efficient urinary tract colonization.* Infect Immun, 2005. **73**(11): p. 7657-68.

93. Guckes, K.R., M. Kostakioti, E.J. Breland, A.P. Gu, C.L. Shaffer, C.R. Martinez, S.J. Hultgren, and M. Hadjifrangiskou, *Strong cross-system interactions drive the activation of the QseB response regulator in the absence of its cognate sensor.* Proceedings of the

National Academy of Sciences of the United States of America, 2013. **110**(41): p. 16592-16597.

94. Goila-Gaur, R. and K. Strebel, *HIV-1 Vif, APOBEC, and intrinsic immunity.* Retrovirology, 2008. **5**: p. 51.

95. Bebell, L.M. and A.N. Muiru, *Antibiotic use and emerging resistance: How can resource-limited countries turn the tide?* Global Heart, 2014. **9**(3): p. 347-358.

96. Brooks, B.D. and A.E. Brooks, *Therapeutic strategies to combat antibiotic resistance.* Advanced Drug Delivery Reviews, 2014. **78**: p. 14-27.

97. Roca, I., M. Akova, F. Baquero, J. Carlet, M. Cavaleri, S. Coenen, J. Cohen, D. Findlay, I. Gyssens, O.E. Heure, G. Kahlmeter, H. Kruse, R. Laxminarayan, E. Liébana, L. López-Cerero, A. MacGowan, M. Martins, J. Rodríguez-Baño, J.M. Rolain, C. Segovia, B. Sigauque, E. Taconelli, E. Wellington, and J. Vila, *The global threat of antimicrobial resistance: science for intervention.* New Microbes and New Infections, 2015. **6**: p. 22-29.

98. Thabit, A.K., J.L. Crandon, and D.P. Nicolau, *Antimicrobial resistance: impact on clinical and economic outcomes and the need for new antimicrobials.* Expert Opinion on Pharmacotherapy, 2014. **16**(2): p. 159-177.

99. Uchil, R.R., G.S. Kohli, V.M. Katekhaye, and O.C. Swami, *Strategies to combat antimicrobial resistance.* Journal of Clinical and Diagnostic Research, 2014. **8**(7): p. ME01-ME04.

100. Cook, G.M., C. Greening, K. Hards, and M. Berney, *Chapter One - Energetics of Pathogenic Bacteria and Opportunities for Drug Development*, in *Advances in Microbial Physiology*, K.P. Robert, Editor 2014, Academic Press. p. 1-62.

101. Richter, O.-M.H. and B. Ludwig, *Electron transfer and energy transduction in the terminal part of the respiratory chain — Lessons from bacterial model systems.* Biochimica et Biophysica Acta (BBA) - Bioenergetics, 2009. **1787**(6): p. 626-634.

102. Sazanov, L., *The mechanism of coupling between electron transfer and proton translocation in respiratory complex I.* Journal of Bioenergetics and Biomembranes, 2014. **46**(4): p. 247-253.

103. Aussel, L., F. Pierrel, L. Loiseau, M. Lombard, M. Fontecave, and F. Barras, *Biosynthesis and physiology of coenzyme Q in bacteria.* Biochimica et Biophysica Acta (BBA) - Bioenergetics, 2014. **1837**(7): p. 1004-1011.

104. McNeil, M.B. and P.C. Fineran, *Prokaryotic assembly factors for the attachment of flavin to complex II.* Biochimica et Biophysica Acta (BBA) - Bioenergetics, 2013. **1827**(5): p. 637-647.

105. Herzfeld, K.F., *Theory of light absorption in simple aromatic compounds.* Proceedings of the American Philosophical Society, 1940. **82**(3): p. 359-367.

106. Yagi, K., T. Ozawa, and M. Harada, *Change of absorption spectrum of flavin adenine dinucleotide by its binding with both D-amino acid oxidase apo-protein and benzoate.* Nature, 1959. **184**(4703): p. 1938-1939.

107. Zenichowski, K., M. Gothe, and P. Saalfrank, *Exciting flavins: Absorption spectra and spin–orbit coupling in light–oxygen–voltage (LOV) domains.* Journal of Photochemistry and Photobiology A: Chemistry, 2007. **190**(2–3): p. 290-300.

108. Chandra, R., M. Tiwari, P. Kaur, M. Sharma, R. Jain, and S. Dass, *Metalloporphyrins—Applications and clinical significance.* Indian Journal of Clinical Biochemistry, 2000. **15**(Suppl 1): p. 183-199.

109. Land, E.J., M. Simic, and A.J. Swallow, *Optical absorption spectrum of half-reduced ubiquinone.* Biochimica et Biophysica Acta (BBA) - Bioenergetics, 1971. **226**(2): p. 239-240.

110. Malik, Z., J. Hanania, and Y. Nitzan, *New trends in photobiology bactericidal effects of photoactivated porphyrins — An alternative approach to antimicrobial drugs.* Journal of Photochemistry and Photobiology B: Biology, 1990. **5**(3–4): p. 281-293.

111. Enwemeka, C.S., D. Williams, S.K. Enwemeka, S. Hollosi, and D. Yens, *Blue 470-nm light kills Methicillin-Resistant Staphylococcus aureus (MRSA) in vitro.* Photomedicine and Laser Surgery, 2009. **27**(2): p. 221-226.

112. Yin, R., M. Wang, Y.-Y. Huang, G. Landi, D. Vecchio, L.Y. Chiang, and M.R. Hamblin, *Antimicrobial photodynamic inactivation with decacationic functionalized fullerenes: Oxygen-independent photokilling in presence of azide and new mechanistic insights.* Free Radical Biology and Medicine, 2015. **79**: p. 14-27.

113. Nitzan, Y., M. Gutterman, Z. Malik, and B. Ehrenberg, *Inactivation of Gram-negative bacteria by photosensitized porphyrins.* Photochemistry and Photobiology, 1992. **55**(1): p. 89-96.

114. Anderl, J.N., J. Zahller, F. Roe, and P.S. Stewart, *Role of nutrient limitation and stationary-phase existence in Klebsiella pneumoniae biofilm resistance to ampicillin and ciprofloxacin.* Antimicrobial Agents and Chemotherapy, 2003. **47**(4): p. 1251-1256.

115. Cabeen, M.T., *Stationary phase-specific virulence factor overproduction by a lasR mutant of Pseudomonas aeruginosa.* PLoS ONE, 2014. **9**(2): p. e88743.

116. Kolter, R., D.A. Siegele, and A. Tormo, *The stationary phase of the bacterial life cycle.* Annual Review of Microbiology, 1993. **47**: p. 855-874.

117. Mangan, M.W., S. Lucchini, V. Danino, T.Ó. Cróinín, J.C.D. Hinton, and C.J. Dorman, *The integration host factor (IHF) integrates stationary-phase and virulence gene expression in Salmonella enterica serovar Typhimurium.* Molecular Microbiology, 2006. **59**(6): p. 1831-1847.

118. Mouslim, C. and K.T. Hughes, *The effect of cell growth phase on the regulatory cross-talk between flagellar and Spi1 virulence gene expression.* PLoS Pathogens, 2014. **10**(3): p. e1003987.

119. Navarro Llorens, J.M., A. Tormo, and E. Martínez-García, *Stationary phase in gram-negative bacteria*. Vol. 34. 2010. 476-495.

120. Roop Ii, R.M., J.M. Gee, G.T. Robertson, J.M. Richardson, W.-L. Ng, and M.E. Winkler, *Brucella stationary-phase gene expression and virulence.* Annual Review of Microbiology, 2003. **57**(1): p. 57-76.

121. Wang, J.-H., R. Singh, M. Benoit, M. Keyhan, M. Sylvester, M. Hsieh, A. Thathireddy, Y.-J. Hsieh, and A.C. Matin, *Sigma S-dependent antioxidant defense protects stationary-phase Escherichia coli against the bactericidal antibiotic gentamicin.* Antimicrobial Agents and Chemotherapy, 2014. **58**(10): p. 5964-5975.

122. Balaban, N.Q., K. Gerdes, K. Lewis, and J.D. McKinney, *A problem of persistence: still more questions than answers?* Nat Rev Micro, 2013. **11**(8): p. 587-591.

123. Bush, K., P. Courvalin, G. Dantas, J. Davies, B. Eisenstein, P. Huovinen, G.A. Jacoby, R. Kishony, B.N. Kreiswirth, E. Kutter, S.A. Lerner, S. Levy, K. Lewis, O. Lomovskaya, J.H. Miller, S. Mobashery, L.J.V. Piddock, S. Projan, C.M. Thomas, A. Tomasz, P.M. Tulkens, T.R. Walsh, J.D. Watson, J. Witkowski, W. Witte, G. Wright, P. Yeh, and H.I.

Zgurskaya, *Tackling antibiotic resistance.* Nature reviews. Microbiology, 2011. **9**(12): p. 894-896.

124. Floyd, K.A., J.L. Moore, A.R. Eberly, J.A.D. Good, C.L. Shaffer, H. Zaver, F. Almqvist, E.P. Skaar, R.M. Caprioli, and M. Hadjifrangiskou, *Adhesive fiber stratification in uropathogenic Escherichia coli biofilms unveils oxygen-mediated control of type 1 pili.* PLoS Pathogens, 2015. **11**(3): p. e1004697.

125. Lechner, S., K. Lewis, and R. Bertram, *Staphylococcus aureus persisters tolerant to bactericidal antibiotics.* Journal of molecular microbiology and biotechnology, 2012. **22**(4): p. 235-244.

126. Moy, T.I., A.R. Ball, Z. Anklesaria, G. Casadei, K. Lewis, and F.M. Ausubel, *Identification of novel antimicrobials using a live-animal infection model.* Proceedings of the National Academy of Sciences of the United States of America, 2006. **103**(27): p. 10414-10419.

127. Darby, C.M., A. Venugopal, S. Ehrt, and C.F. Nathan, *Mycobacterium tuberculosis gene Rv2136c is dispensable for acid resistance and virulence in mice.* Tuberculosis (Edinburgh, Scotland), 2011. **91**(5): p. 343-347.

128. Hisert, K.B., M.A. Kirksey, J.E. Gomez, A.O. Sousa, J.S. Cox, W.R. Jacobs, C.F. Nathan, and J.D. McKinney, *Identification of mycobacterium tuberculosis counterimmune (cim) mutants in immunodeficient mice by differential screening.* Infection and Immunity, 2004. **72**(9): p. 5315-5321.

129. Smith, I., C. Nathan, and H.H. Peavy, *Progress and new directions in genetics of Tuberculosis: An NHLBI working group report.* American Journal of Respiratory and Critical Care Medicine, 2005. **172**(12): p. 1491-1496.

130. Tian, J., R. Bryk, M. Itoh, M. Suematsu, and C. Nathan, *Variant tricarboxylic acid cycle in Mycobacterium tuberculosis: Identification of* α*-ketoglutarate decarboxylase.* Proceedings of the National Academy of Sciences of the United States of America, 2005. **102**(30): p. 10670-10675.

131. Lewis, K., *Persister cells, dormancy and infectious disease.* Nat Rev Micro, 2007. **5**(1): p. 48-56.

132. Lewis, K., *Persister Cells.* Annual Review of Microbiology, 2010. **64**(1): p. 357-372.

133. Alves, E., A.C. Esteves, A. Correia, A. Cunha, M.A.F. Faustino, M.G.P.M.S. Neves, and A. Almeida, *Protein profiles of Escherichia coli and Staphylococcus warneri are altered by photosensitization with cationic porphyrins.* Photochemical & Photobiological Sciences, 2015. **14**(6): p. 1169-1178.

134. Croxen, M.A. and B.B. Finlay, *Molecular mechanisms of Escherichia coli pathogenicity.* Nat Rev Micro, 2010. **8**(1): p. 26-38.

135. Völzing, K.G. and M.P. Brynildsen, *Stationary-phase persisters to ofloxacin sustain DNA damage and require repair systems only during recovery.* mBio, 2015. **6**(5): p. e00731-15.

136. White, M.D., K.A.P. Payne, K. Fisher, S.A. Marshall, D. Parker, N.J.W. Rattray, D.K. Trivedi, R. Goodacre, S.E.J. Rigby, N.S. Scrutton, S. Hay, and D. Leys, *UbiX is a flavin prenyltransferase required for bacterial ubiquinone biosynthesis.* Nature, 2015. **522**(7557): p. 502-506.

137. Hellingwerf, K.J., *The molecular basis of sensing and responding to light in microorganisms*. Vol. 81. 2002. 51-59.

138. Braatsch, S., M. Gomelsky, S. Kuphal, and G. Klug, *A single flavoprotein, AppA, integrates both redox and light signals in Rhodobacter sphaeroides.* Molecular Microbiology, 2002. **45**(3): p. 827- 836.

139. Mihara, K.i., O. Hisatiomi, Y. Imamoto, M. Kataoka, and F. Tokunaga, *Functional expression and site-directed mutagenesis of photoactive yellow protein.* The Journal of Biochemistry, 1997. **121**(5): p. 876-880.

140. Mussi, M.A., J.A. Gaddy, M. Cabruja, B.A. Arivett, A.M. Viale, R. Rasia, and L.A. Actis, *The opportunistic human pathogen Acinetobacter baumannii senses and responds to light.* Journal of Bacteriology, 2010. **192**(24): p. 6336-6345.

141. Taylor, B.L. and D.E. Koshland, *Intrinsic and extrinsic light responses of Salmonella typhimurium and Escherichia coli.* Journal of Bacteriology, 1975. **123**(2): p. 557-569.

142. Iseki, M., S. Matsunaga, A. Murakami, K. Ohno, K. Shiga, K. Yoshida, M. Sugai, T. Takahashi, T. Hori, and M. Watanabe, *A blue-light-activated adenylyl cyclase mediates photoavoidance in Euglena gracilis.* Nature, 2002. **415**(6875): p. 1047-1051.

143. Galperin, M.Y., *A census of membrane-bound and intracellular signal transduction proteins in bacteria: Bacterial IQ, extroverts and introverts.* BMC Microbiology, 2005. **5**: p. 35-35.

144. Galperin, M.Y., A.N. Nikolskaya, and E.V. Koonin, *Novel domains of the prokaryotic two-component signal transduction systems.* FEMS Microbiology Letters, 2001. **203**(1): p. 11-21.

145. Masuda, S. and C.E. Bauer, *AppA is a blue light photoreceptor that antirepresses photosynthesis gene expression in Rhodobacter sphaeroides.* Cell, 2002. **110**(5): p. 613-623.

146. Nakasone, Y., T.-a. Ono, A. Ishii, S. Masuda, and M. Terazima, *Temperature-sensitive reaction of a photosensor protein YcgF: Possibility of a role of temperature sensor.* Biochemistry, 2010. **49**(10): p. 2288-2296.

147. Murphy, K.C. and K.G. Campellone, *Lambda Red-mediated recombinogenic engineering of enterohemorrhagic and enteropathogenic E. coli.* BMC Mol Biol, 2003. **4**: p. 11.

148. O'Toole, G.A., L.A. Pratt, P.I. Watnick, D.K. Newman, V.B. Weaver, and R. Kolter, *Genetic approaches to study of biofilms.* Methods Enzymol, 1999. **310**: p. 91-109.

149. Hadjifrangiskou, M. and S.J. Hultgren, *What does it take to stick around?: Molecular insights into biofilm formation by uropathogenic Escherichia coli.* Virulence, 2012. **3**(3): p. 231-233.

150. Kostakioti, M., M. Hadjifrangiskou, and S.J. Hultgren, *Bacterial biofilms: Development, dispersal, and therapeutic strategies in the dawn of the post-antibiotic era.* Cold Spring Harbor Perspectives in Medicine, 2013. **3**(4): p. a010306.

151. Wright, K.J., P.C. Seed, and S.J. Hultgren, *Development of intracellular bacterial communities of uropathogenic Escherichia coli depends on type 1 pili.* Cellular Microbiology, 2007. **9**(9): p. 2230-2241.

152. Terashima, H., S. Kojima, and M. Homma, *Chapter 2, Flagellar motility in bacteria: Structure and function of flagellar motor*, in *International Review of Cell and Molecular Biology*2008, Academic Press. p. 39-85.

153. Lipovsky, A., Y. Nitzan, and R. Lubart, *A possible mechanism for visible light-induced wound healing.* Lasers in Surgery and Medicine, 2008. **40**(7): p. 509-514.

154. Malik, Z., H. Ladan, and Y. Nitzan, *Photodynamic inactivation of Gram-negative bacteria: Problems and possible solutions.* Journal of Photochemistry and Photobiology B: Biology, 1992. **14**(3): p. 262-266.

155. Nitzan, Y., M. Salmon-Divon, E. Shporen, and Z. Malik, *ALA induced photodynamic effects on Gram positive and negative bacteria.* Photochemical & Photobiological Sciences, 2004. **3**(5): p. 430-435.

156. Buonanno, M., G. Randers-Pehrson, A.W. Bigelow, S. Trivedi, F.D. Lowy, H.M. Spotnitz, S.M. Hammer, and D.J. Brenner, *207-nm UV Light - A Promising Tool for Safe Low-Cost Reduction of Surgical Site Infections. I: In Vitro Studies.* PLoS ONE, 2013. **8**(10): p. e76968.

157. Ericson, M.B., A.-M. Wennberg, and O. Larkö, *Review of photodynamic therapy in actinic keratosis and basal cell carcinoma.* Therapeutics and Clinical Risk Management, 2008. **4**(1): p. 1-9.

158. Kligman, D.E. and Y. Zhen, *Intense pulsed light treatment of photoaged facial skin.* Dermatologic Surgery, 2004. **30**(8): p. 1085-1090.

159. Maisels, M.J. and A.F. McDonagh, *Phototherapy for neonatal jaundice.* New England Journal of Medicine, 2008. **358**(9): p. 920-928.

160. Nakonechny, F., M.A. Firer, Y. Nitzan, and M. Nisnevitch, *Intracellular antimicrobial photodynamic therapy: A novel technique for efficient eradication of pathogenic bacteria.* Photochemistry and Photobiology, 2010. **86**(6): p. 1350-1355.

161. Jori, G., M. Camerin, M. Soncin, L. Guidolin, and O. Coppellotti, *Antimicrobial photodynamic therapy: Basic principles*, in *Photodynamic Inactivation of Microbial*

Pathogens: Medical and Environmental Applications, M.R. Hamblin and G. Jori, Editors. 2011, RSC Publishing. p. 1-18.

162. Gasparian, M.E., P.A. Elistratov, S.A. Yakimov, D.A. Dolgikh, and M.P. Kirpichnikov, *An efficient method for expression in Escherichia coli and purification of the extracellular ligand binding domain of the human TGF*β *type II receptor.* Journal of Biotechnology, 2010. **148**(2–3): p. 113-118.

163. Huang, Y.-Y., S.K. Sharma, R. Yin, T. Agrawal, L.Y. Chiang, and M.R. Hamblin, *Functionalized fullerenes in photodynamic therapy.* Journal of Biomedical Nanotechnology, 2014. **10**(9): p. 1918-1936.

164. Ormond, A. and H. Freeman, *Dye sensitizers for photodynamic therapy.* Materials, 2013. **6**(3): p. 817.

165. Oriel, S. and Y. Nitzan, *Photoinactivation of Candida albicans by its own endogenous porphyrins.* Current Microbiology, 2010. **60**(2): p. 117-123.

166. Hamblin, M.R., J. Viveiros, C. Yang, A. Ahmadi, R.A. Ganz, and M.J. Tolkoff, *Helicobacter pylori accumulates photoactive porphyrins and is killed by visible light.* Antimicrobial Agents and Chemotherapy, 2005. **49**(7): p. 2822-2827.

167. Nitzan, Y., Z. Malik, M. Kauffman, and B. Ehrenberg. *Induction of endogenic porphyrin production in bacteria and subsequent photoinactivation by various light sources*. 1997.

168. Andrasik, S.J., *Singlet oxygen generation using new fluorene-based photosensitizers under one- and two-photon excitation*, in *UCF Digital Collections,* 2007, University of Central Florida.

169. Wilkinson, F., W.P. Helman, and A.B. Ross, *Quantum yields for the photosensitized formation of the lowest electronically excited singlet state of molecular oxygen in solution.* Journal of Physical and Chemical Reference Data, 1993. **22**(1): p. 113-262.

170. McEwen, J. *Jablonski diagram*. 2014 [cited 2016; Available from: http://chemwiki.ucdavis.edu/Core/Physical_Chemistry/Spectroscopy/Electronic_Spectroscopy/Jablonski_diagram.

171. *Fluorescence and Phosphorescence*. March 27, 2006 [cited April 28, 2016; Available from: https://physik.unibas.ch/Praktikum/VPII/Fluoreszenz/Fluorescence_and_Phosphorescence.pdf.

172. Kowalczyk, R.M., E. Schleicher, R. Bittl, and S. Weber, *The photoinduced triplet of flavins and its protonation states.* Journal of the American Chemical Society, 2004. **126**(36): p. 11393-11399.

173. Moore, W.M., J.C. McDaniels, and J.A. Hen, *The photochemistry of riboflavin-VI. The photophysical properties of isoalloxazines.* Photochemistry and Photobiology, 1977. **25**(6): p. 505-512.

174. Ronqui, M.R., T.M.S.F. de Aguiar Coletti, L.M. de Freitas, E.T. Miranda, and C.R. Fontana, *Synergistic antimicrobial effect of photodynamic therapy and ciprofloxacin.* Journal of Photochemistry and Photobiology B: Biology, 2016. **158**: p. 122-129.

175. Wang, Y., X. Wu, J. Chen, R. Amin, M. Lu, B. Bhayana, J. Zhao, C.K. Murray, M.R. Hamblin, D.C. Hooper, and T. Dai, *Antimicrobial blue light inactivation of Gram-negative pathogens in biofilms: In vitro and in vivo studies.* Journal of Infectious Diseases, 2016. **213**(9): p. 1380-1387.

176. Perni, S., C. Piccirillo, J. Pratten, P. Prokopovich, W. Chrzanowski, I.P. Parkin, and M. Wilson, *The antimicrobial properties of light-activated polymers containing methylene blue and gold nanoparticles.* Biomaterials, 2009. **30**(1): p. 89-93.

177. Soukos, N.S., S. Som, A.D. Abernethy, K. Ruggiero, J. Dunham, C. Lee, A.G. Doukas, and J.M. Goodson, *Phototargeting oral black-pigmented bacteria.* Antimicrobial Agents and Chemotherapy, 2005. **49**(4): p. 1391-1396.

178. Zolfaghari, P.S., S. Packer, M. Singer, S.P. Nair, J. Bennett, C. Street, and M. Wilson, *In vivo killing of Staphylococcus aureus using a light-activated antimicrobial agent.* BMC Microbiol, 2009. **9**: p. 27.

179. *Healthcare-associated Infections (HAI) Progress Report*. Healthcare-associated Infections 2016 March 3, 2016 [cited April 29, 2016; Available from: http://www.cdc.gov/hai/surveillance/progress-report/.

180. Foxman, B., *Urinary tract infection syndromes: Occurrence, recurrence, bacteriology, risk factors, and disease burden.* Infectious Disease Clinics of North America, 2014. **28**(1): p. 1-13.

181. Behzadi, P., E. Behzadi, H. Yazdanbod, R. Aghapour, M. Akbari Cheshmeh, and D. Salehian Omran, *A survey on urinary tract infections associated with the three most common uropathogenic bacteria.* Mædica, 2010. **5**(2): p. 111-115.